On the left–right asymmetry of the angular distribution of α particles from ternary nuclear fission by polarized neutrons

G. V. Danilyan
Institute of Theoretical and Experimental Physics, 117259 Moscow, Russia

(Submitted 21 September 1999)
Pis'ma Zh. Éksp. Teor. Fiz. **70**, No. 9, 561–564 (10 November 1999)

Some experimental possibilities of establishing the nature of the recently observed *T*-odd angular correlation in ternary fission of ^{233}U by polarized neutrons are discussed. Specifically, investigation of the neutron energy dependence of the correlation coefficient in the ternary fission of ^{239}Pu and ^{235}U could shed light on the problem under discussion. © *1999 American Institute of Physics.*
[S0021-3640(99)00121-8]

PACS numbers: 25.85.Ec, 24.80.+y

T-Odd angular correlation in the ternary fission of ^{233}U has been observed in a basic experiment performed in a polarized cold-neutron beam of the high-flux reactor at the Institute Laue–Langevin by a collaboration of the Institute of Theoretical and Experimental Physics, Tübingen University, Scientific-Research Institute of Nuclear Physics, the Technical University of Darmstadt, the Kurchatov Institute, and the Institute Laue–Langevin:[1]

$$W = \text{const}(1 + D\mathbf{S}\cdot[\mathbf{P}_{LF}\times\mathbf{P}_{\alpha}]), \tag{1}$$

where D is the correlation coefficient, $\mathbf{S}$ is a unit vector in the direction of polarization of the neutrons, and $\mathbf{P}_{LF}$ and $\mathbf{P}_{\alpha}$ are unit vectors in the directions of the momenta of the light fragment and the long-range α particle, respectively.

The measured value of the correlation coefficient D was $3\cdot 10^3$. Actually, $\mathbf{S}$ in the expression (1) should be replaced by a unit vector $\mathbf{I}$ oriented in the direction of polarization of the fissioning nucleus and the coefficient D must be scaled to 100% polarization of the nuclei. The degree of polarization of the compound nucleus produced when unpolarized nuclei capture polarized *s* neutrons is determined by the expressions

$$P_N = +(Pn/3)\{1 + 2/(2J+1)\} \quad \text{for} \quad I = J + 1/2, \tag{2}$$

$$P_N = -(Pn/3) \quad \text{for} \quad I = J - 1/2, \tag{3}$$

where Pn is the degree of polarization of the neutron beam and J is the spin of the target nucleus. The negative sign in Eq. (3) means that the nuclei are polarized in a direction opposite to the direction of polarization of the neutron beam.

The population of the spin states depends on the energy of the neutrons. Therefore the average polarization of the compound nuclei also depends on E_n:

$$\langle P_N \rangle = \{\sigma(+)P_N(+) + \sigma(-)P_N(-)\}/\{\sigma(+) + \sigma(-)\}, \tag{4}$$

where $\sigma(\pm)$ are the corresponding spin partial fission cross sections of the nuclei, which depend on E_n.

Unfortunately, there are no data on $\sigma_+(E_n)$ for ^{233}U target nuclei, and it is impossible to determine the real value of D. Evidently, for $E_n = 0.0017$ eV (20 K) both spin states contribute to the fission cross section, and therefore $D > 3 \cdot 10^{-3}$.

A search for similar effects has been conducted for the decay of polarized neutrons[2] and in the (n, γ_0) reaction.[3] But in both cases only the upper limit on the correlation coefficient was established: $|D| < 10^{-3}$.

Correlations of the type (1) are forbidden only approximately by the invariance of the interactions under time reversal, when the amplitude of the interaction is much less than 1. The strong and electromagnetic interactions of the decay products in the final state can imitate T-odd correlation. Theoretical estimates of the magnitudes of such effects for neutron decay and in the (n, γ) reaction are 10^{-5} in order of magnitude. As far as interaction effects in the final state of the fission process are concerned, because the diversity of final states is large ($\sim 10^{10}$) and the effects need to be summed over all states, it is hardly possible to make a realistic estimate of the magnitude of the effect. Moreover, there is a large difference between neutron decay, where the momenta of the electron and the antineutrino (or proton) enter in the correlation, and the fission process, where the momentum of the light (or heavy) fragment appears in the correlation (1). The possibility of correlation between the momentum of the light fragment and the spin of the nucleus has been pointed out by Vladimirskiĭ and Andreev,[4] who initiated a basic experiment to investigate the nonconservation of spatial parity in binary nuclear fission.[5] It turned out that because of the nonconservation of parity in the weak interaction at the stage of formation of compound nucleus the light fragments (all of them!) are indeed correlated with the spin of the fissioning nucleus:

$$W = \text{const}(1 + \alpha \mathbf{I} \cdot \mathbf{P}_{LF}), \tag{5}$$

where α is of the same order of magnitude ($10^{-4} - 10^{-3}$) as in (n, γ_0) reactions,[6] i.e., the light fragment, irrespective of the value of A and Z and its quantum characteristics, behaves in angular correlations just as a γ ray from a definite transition in a nucleus. This phenomena was explained in Ref. 7 on the basis of the Bohr–Strutinskiĭ theory[8] of the angular distributions of fragments under the additional assumption that in quasistationary transitional states a ''cold,'' strongly deformed, nucleus is pear-shaped and, on account of the correlation of the ''pear'' with the spin of the nucleus, due to an admixture of the opposite parity to the main parity of the quasistationary state, all future light fragments determined by the form of the ''pear'' retain, even at infinity, the initial correlation relative to the direction of polarization of the fissioning nucleus. It is clear that this mechanism also determines all quantum numbers of fragments in the final state in a manner so that summing over final states does not level the correlation. A completely different picture occurs in ternary fission, where at the moment the ''neck'' connecting two fragments ruptures a light charged particle (primarily, an α particle) is also formed. It is difficult to imagine a mechanism that would make all modes of ternary fission

in-phase with one another (a set of quantum states of three particles!), and experiments confirm this. While fragments from ternary fission manifest the same *P*-odd symmetry that is characteristic for binary-fission fragments,[9] no *P*-odd asymmetry has been found in the angular distribution of α particles from ternary fission.[10] This experimental fact is an indirect indication that the correlation (1) in ternary fission is a consequence of interactions in the final state. However, of course, this must be established experimentally.

The interaction in the final state, by definition, should not depend on the initial state, with the exception of a possible spin dependence (magnetic moment dependence) of the fissioning nucleus. Specifically, the correlation coefficient *D*, scaled to 100-percent polarization of the fissioning nucleus, should not depend on the energy of the neutrons giving rise to nuclear fission. But, as already mentioned, the population of the two possible spin states as a result of the capture of *s* neutrons is determined by the energy of the neutrons.

Therefore the investigation of the energy dependence $D(E_n)$ could shed light on the problem under discussion. For this, there are two possibilities: 1) measurement of the correlation coefficient *D* for ^{239}Pu target nuclei at thermal neutron energy and at a 0.3 eV resonance and 2) the same measurements for a ^{235}U target nucleus. In the first case, the spin states $i=0^+$ and $I=1^+$ are occupied when $^{239}\mathrm{Pu}(J=1/2)$ nuclei capture *s* neutrons. The fission cross section in the neutron energy range up to 0.5 eV is determined primarily by the resonance at $E_n=0.297$ eV ($I=1^+$) and negative resonances with spin $I=0^+$. It is obvious that the latter cannot contribute to the correlation (1). Therefore if the correlation (1) is due to an interaction in the final state, then the correlation coefficient *D* should not depend on the neutron energy in the range 0–0.3 eV, since only one spin state can contribute to the correlation, i.e., a possible neutron-energy dependence via the dependence on the spin of the fissioning nucleus is ruled out for ^{239}Pu.

For $^{235}\mathrm{U}(J=7/2)$, the spin states 3 and 4^- are occupied as a result of capture of *s* neutrons, and data on the partial spin fission cross sections are available.[11] Therefore a dependence on the spin (magnetic moment) of the fissioning nucleus can appear in measurements of $D(E_n)$ for neutron energies up to 0.3 eV. This nucleus is also interesting because the average polarization of the fissioning nucleus vanishes at neutron energy ~ 0.3 eV. Obviously, the coefficient *D* should also vanish.

Neutron capture only in the *s* wave has been considered thus far. Even though the capture cross section in the *p* wave is negligibly small, correlations due to the interference of *s* and *p* waves appear in experiments. Specifically, a left–right asymmetry of the angular distribution of fragments from binary fission of nuclei by slow polarized neutrons has been observed:

$$W=\mathrm{const}(1+B\mathbf{S}\cdot[\mathbf{P}_n\times\mathbf{P}_{LF}]), \tag{6}$$

where $\mathbf{P}_n$ is a unit vector in the direction of the momentum of the neutron captured by a nucleus. The asymmetry coefficient *B* is $10^{-4}-10^{-3}$ in order of magnitude, and it depends strongly on the neutron energy. As a result of the different neutron-energy dependence of the partial neutron widths in the *s* and *p* waves, on the average it is proportional to the neutron velocity. The experimental geometry (the measurements were performed in a longitudinally polarized neutron beam, for which the correlatoin (6) vanishes on the average) rules out a direct contribution of the correlation (6) in the measured correlation (1). Moreover, the measurements were performed in a beam of cold neutrons (20 K). For

such neutrons the coefficient B should be several times smaller than for thermal neutrons. For this reason, it is extremely unlikely that the effect observed in ternary fission can be explained by sp interference. Nonetheless, since data on the energy dependence of the coefficient B for binary fission are available for ^{239}Pu and ^{235}U target nuclei (and the sp interference effect should be the same for ternary and binary fission), they can be taken into account when fitting the measurements of the energy-dependence of the coefficient D.

Let us now summarize the discussion. A formally T-odd effect has been observed experimentally in ternary fission of nuclei by polarized neutrons. It could be a manifestation of an admixture of an interaction that is noninvariant under time reversal. However, more likely, it is due to an interaction effect in the final state. It is virtually impossible to estimate theoretically the magnitude of the interaction in the final state or the magnitude of the effect due to the sp interference in the entrance channel because of the difficulty of solving the three-body problem, and with a large diversity of final states as well. The experimental possibilities are also extremely limited. The investigations of the energy-dependence of the effect which were proposed in the present letter could rule out hypotheses of a possible dependence of the effect on the spin of the fissioning nucleus and on the sp interference nature of the observed correlation. If a neutron energy dependence, which would be impossible to explain by interference of s and p waves in neutron capture, is observed in measurements on ^{239}Pu, then evidently it can be asserted that an admixture of an interaction that is noninvariant under time reversal has been observed.

[1] P. Jesinger, G. V. Danilyan, A. M. Gagarski *et al.*, Yad. Fiz. **62**, 1723 (1999) [Phys. Atom. Nucl. **62**, 1608 (1999)].
[2] B. G. Erozolimskiĭ, Yu. A. Mostovoĭ, V. P. Fedunin *et al.*, Yad. Fiz. **28,** 98 (1978) [Sov. J. Nucl. Phys. **28**, 48 (1978)].
[3] M. I. Bulgakov, G. V. Danilyan, A. D. Gulḱo *et al.*, Phys. Lett. B **42**, 351 (1978).
[4] V. V. Valdimirskiĭ and V. N. Andreev, Zh. Éksp. Teor. Fiz. **41,** 663 (1961) [Sov. Phys. JETP **14**, 475 (1962)].
[5] G. V. Danilyan, Usp. Fiz. Nauk **131,** 329 (1980) [Sov. Phys. Usp. **23**, 323 (1980)].
[6] Yu. G. Abov and P. A. Krupchitskiĭ, Usp. Fiz. Nauk **118,** 141 (1976) [Sov. Phys. Usp. **19**, 75 (1976)].; G. V. Danilyan, V. V. Novitskiĭ, V. S. Pavlov *et al.*, JETP Lett. **24**, 344 (1976).
[7] O. P. Sushkov and V. V. Flambaum, Usp. Fiz. Nauk **136,** 3 (1982) [Sov. Phys. Usp. **25**, 1 (1982)].
[8] A. Bohr, in *Proceedings of the International Conference on Peaceful Uses of Atomic Energy*, Geneva (1955), Vol. 2, p. 175; V. M. Strutinskiĭ, Zh. Éksp. Teor. Fiz. **30,** 606 (1956) [Sov. Phys. JETP **3**, 638 (1956/1957)]; At. Énerg. **2**, 508 (1957).
[9] A. V. Belozerov, A. G. Beda, L. N. Bondarenko *et al.*, JETP Lett. **51**, 10 (1990).
[10] A. Ya. Aleksandrovich, G. V. Val'skiĭ, T. K. Zvezdkina *et al.*, Preprint No. 1057, Leningrad Institute of Nuclear Physics (1985).
[11] W. I. Furman, Yu. N. Kopach, A. B. Popov *et al.*, ISINN-6, Dubna, 1998, p. 260.

Translated by M. E. Alferieff

Suppression of incoherent scattering of Mössbauer radiation by nuclei in a reversing magnetic field

A. Ya. Dzyublik*)
Institute for Nuclear Research, 252028 Kiev, Ukraine

(Submitted 21 September 1999)
Pis'ma Zh. Éksp. Teor. Fiz. **70**, No. 9, 565–569 (10 November 1999)

The effect of magnetic field reversal on the incoherent scattering of Mössbauer radiation by nuclei is analyzed. It is shown that this scattering process is suppressed after the field reversal. This effect is analyzed both from the quantum and classical points of view. © *1999 American Institute of Physics.* [S0021-3640(99)00221-2]

PACS numbers: 25.20.Dc

One of the obstacles to the realization of γ-ray lasers on Mössbauer isotopes is the large ratio of the conversion-electron width to the coherent radiation width.[1] For this reason the recent discovery by Shvyd'ko *et al.*[2,3] of a short-time enhancement of the coherent radiation channel of the ^{57}Fe isotope following an abrupt change of the magnetic field direction seems very promising. They had been investigating the time dependence of the Mössbauer transmission through a weak ferromagnetic crystal of $FeBO_3$ after reversal of the field. Immediately after the field reversal a short flash of the transmitted beam intensity was observed, followed by decaying oscillations. The duration of this transient process was of the order of the nuclear lifetime τ_N. Similar reversals have been carried out in many other experiments on Mössbauer absorption by soft ferromagnets placed in an external radio-frequency (rf) magnetic field (see reviews[4–7]). The rf field gives rise to periodic reversals of the crystal magnetization, which lead to periodic jumps of the field at the ^{57}Fe nuclei between two values $+\mathbf{h}_0$ and $-\mathbf{h}_0$. A theory of this effect has been constructed in Refs. 8–13. A rigorous explanation of the transient effect observed by Shvyd'ko *et al.*[2,3] has been given in Ref. 14. In addition, it was predicted that reversal of the magnetic field should lead to suppression of the conversion-electron yield. In the present letter we consider the suppression of the incoherent scattering of γ rays in the same situation and clarify the physical causes of the effect.

Suppose that at $t=0$ the magnetic field at the Mössbauer nucleus in a crystal reverses from $+\mathbf{h}_0$ to $-\mathbf{h}_0$. At $t\to-\infty$ the incident γ ray has wave vector $\mathbf{k}$, polarization $\mathbf{e}_\lambda$, and frequency $\omega=E/\hbar$. In the initial state of the scatterer $|\alpha\rangle$ the nucleus is described by the wave function $\psi^N_{I_gM_g}(t)$, where I is the spin of the nucleus and M is its projection on the direction of $+\mathbf{h}_0$, and the crystal is described by $|\{\nu^0_s\}$, where $\{\nu^0_s\}$ stands for the initial set of phonons. The phononless energy distribution of the incident γ rays is given by

$$w_e^{(0)}(E)=\frac{(\Gamma/2\pi)e^{-2W_e}}{(E-E_0)^2+(\Gamma/2)^2}, \tag{1}$$

where e^{-2W_e} is the Debye–Waller factor of the emitter, and E_0 and Γ are, respectively, the energy and width of the level of the emitting nucleus. In the final state the scatterer is described by $|\beta\rangle=\psi^N_{I_gM'_g}(t)|\{v'_s\}\rangle$, while the γ ray has wave vector $\mathbf{k}'$ and polarization $\mathbf{e}'_{\lambda'}$. We assume the following resonance condition to be fulfilled:

$$E\simeq E_0^+=E'_0+\hbar\alpha_{eg}, \quad \hbar|\alpha_{eg}|\gg\Gamma, \tag{2}$$

where E'_0 is the resonant energy of the absorbing nucleus,

$$\alpha_{eg}=(\gamma_gM_g-\gamma_eM_e)h_0/\hbar, \tag{3}$$

and γ_κ is the gyromagnetic ratio of the nucleus in the ground ($\kappa=g$) or excited ($\kappa=e$) state. In this case only the isolated nuclear transition $M_g\to M_e$ is generated in the field $+\mathbf{h}_0$ and only $-M_g\to -M_e$ in the field $-\mathbf{h}_0$.

The electromagnetic wave scattered into the βth channel by a jth nucleus having initial spin projection $+M_g$ is given (in units $i(2\pi\hbar\omega)^{1/2}$) by (see also[14])

$$\mathbf{E}_{\rm sc}(\mathbf{r},t)^j_{\alpha\to\beta}=\sum_{\lambda'}\mathbf{e}'_{\lambda'}f_{\alpha\beta}(\mathbf{k},\mathbf{e}_\lambda;\mathbf{k}',\mathbf{e}'_{\lambda'})^N_j\frac{1}{r}$$
$$\times\{(1-\theta(t^*))e^{-i\omega' t^*}+\theta(t^*)e^{-i\omega'^-_0 t^*-\Gamma t^*/2\hbar}\}, \tag{4}$$

where $t^*=t-r/c$ is the retarded time, $\omega'^{\pm}_0=E'_0/\hbar\pm(\gamma_gM'_g-\gamma_eM_e)h_0/\hbar$ are the resonant frequencies of the transitions $\pm M_e\to\pm M'_g$ in the field $\mathbf{h}_0$,

$$\theta(x)=\begin{cases}1, & x>0,\\ 0, & x<0,\end{cases} \tag{5}$$

and $f_{\alpha\beta}$ is the scattering amplitude of γ rays by the Mössbauer isotope $+M_g$ in a constant field $\mathbf{h}_0$. In the slow-collision approximation[15] it is given by

$$f_{\alpha\beta}(\mathbf{k},\mathbf{e}_\lambda;\mathbf{k}',\mathbf{e}'_{\lambda'})^N_j=-\langle\{v'_s\}|e^{-i\mathbf{k}'\mathbf{u}_j}|\{v^0_s\}\rangle$$
$$\times\langle\{v^0_s\}|e^{i\mathbf{k}\mathbf{u}_j}|\{v^0_s\}\rangle\frac{c^{-2}\langle e|\hat j^N_{\lambda'}(\mathbf{k}')|g'\rangle^*\langle e|\hat j^N_\lambda(\mathbf{k}')|g\rangle}{E-E_0^+ +i\Gamma/2}, \tag{6}$$

where $\mathbf{u}_j$ is the displacement of the jth nucleus from its equilibrium position, and $\hat j^N_\lambda(\mathbf{k})$ are the Fourier components of the nuclear current density operators (see, e.g., Refs. 10 and 14).

The wave scattered by a nucleus initially in the state $-M_g$ will be[14]

$$\mathbf{E}_{\rm sc}(\mathbf{r},t)^j_{-\alpha\to-\beta}=\sum_{\lambda'}\mathbf{e}'_{\lambda'}f_{-\alpha,-\beta}(\mathbf{k},\mathbf{e}_\lambda;\mathbf{k}',\mathbf{e}'_{\lambda'})^N_j\frac{1}{r}$$
$$\times\{e^{-i\omega' t^*}-e^{-i\omega'^+_0 t^*-\Gamma t^*/2\hbar}\}\theta(t^*), \tag{7}$$

where $f_{-\alpha,-\beta}$ is given by Eq. (6) with e,g replaced by $-e,-g$.

The flux density of γ rays scattered by a nucleus with $\pm M_g$ is

$$j_{\rm sc}(\omega,t)(\pm)=c\sum_{M_g'}\sum_{\{\nu_s'\},\{\nu_s^0\}} g(\{\nu_s^0\})|\mathbf{E}_{\rm sc}(\mathbf{r},t)\pm\alpha\rightarrow\pm\beta|^2, \tag{8}$$

where $g(\{\nu_s^0\})$ is the Gibbs distribution over the initial states of the lattice, and $\mathbf{E}_{\rm sc}(\mathbf{r},t)$ is taken in units $i(2\pi\hbar\omega)^{1/2}$. The corresponding instantaneous differential cross section for scattering of γ rays by the isotope ^{57}Fe with $I_g=1/2$ in an unpolarized target will be

$$\sigma(\omega,t)=\frac{1}{2}(\sigma^{(+)}(\omega,t)+\sigma^{(-)}(\omega,t)), \tag{9}$$

where

$$\sigma^{(\pm)}(\omega,t)=\frac{1}{c}j_{\rm sc}(\omega,t)^{(\pm)}r^2 \tag{10}$$

are the cross sections at nuclei initially in the states $\pm M_g$. The incoherent scattering cross section for the whole target is proportional to (10).

It is useful to introduce the following notation:

$$x=2(E-E_0^+)/\Gamma,\quad \tau=\Gamma t^*/\hbar,\quad x_0=2(E_0-E_0^+)/\Gamma, \tag{11}$$

where x_0 is the detuning parameter and τ is the time in units of the nuclear lifetime $\tau_N=\hbar/\Gamma$. Then substituting (4) and (7) into (8)–(10), we obtain

$$\sigma^{(+)}(\omega,t)\sim\frac{1}{x^2+1}\{(1-\theta(\tau))+e^{-\tau}\theta(\tau)\} \tag{12}$$

and

$$\sigma^{(-)}(\omega,t)\sim\frac{1}{x^2+1}\{(1+e^{-\tau}-2\cos(x\tau/2)e^{-\tau/2}\}\theta(\tau). \tag{13}$$

These cross sections must be averaged over the energy distribution of the incident γ rays:

$$\overline{\sigma^{(\pm)}}(t)=\int_0^\infty w_e(E)\sigma^{(\pm)}(\omega,t)dE. \tag{14}$$

Substitution of (12), (13) into (14) gives the experimentally measured cross sections

$$\overline{\sigma^{(+)}}(t)=\overline{\sigma^{(+)}}\{(1-\theta(\tau))+e^{-\tau}\theta(\tau)\} \tag{15}$$

and

$$\overline{\sigma^{(-)}}(t)=\overline{\sigma^{(+)}}\{1-[\cos(x_0\tau/2)+(2/x_0)\sin(x_0\tau/2)]e^{-\tau}\}\theta(\tau), \tag{16}$$

where $\overline{\sigma^{(+)}}$ is the standard incoherent scattering cross section of γ rays in the stationary case:

$$\overline{\sigma^{(+)}}\sim\frac{1}{x_0^2+4}. \tag{17}$$

From (12), (13) and (15), (16) we see that prior to the field reversal the scattering occurs only at the nuclei $+M_g$. After the reversal these nuclei continue to decay, generating an exponentially damped wave concentrated at the resonant energy ω_0^-, which corresponds to the de-excitation transition $M_e \to M_g'$ in the field $-\mathbf{h}_0$. The $-M_g$ nuclei, on the contrary, begin to absorb the incident radiation only at $t>0$. But their contribution to the radiation yield grows gradually from zero at $t=0$ to $\overline{\sigma}^{(+)}$ at $t \gg \tau_N$. Away from exact resonance ($x_0 \neq 0$) the function $\overline{\sigma}^{(-)}(\tau)$ oscillates with period $\delta\tau = 4\pi/|x_0|$. In the case of exact resonance ($x_0=0$) this cross section becomes a monotonically increasing function of time:

$$\overline{\sigma}^{(-)}(t) = \overline{\sigma}^{(+)}\{1-(1+\tau)e^{-\tau}\}\theta(\tau). \tag{18}$$

In an unpolarized target containing ^{57}Fe isotopes the averaged cross section for exact resonance is

$$\overline{\sigma}(t) = \overline{\sigma}(0)\{1-\tau e^{-\tau}\theta(\tau)\}, \tag{19}$$

where $\overline{\sigma}(0) = \overline{\sigma}^{(+)}/2$ is the value of $\overline{\sigma}(t)$ prior to the reversal.

The function (19) in the interval $0 \leqslant \tau < \infty$ is a sum of monotonically decreasing ($\overline{\sigma}^{(+)}(t)$) and increasing ($\overline{\sigma}^{(-)}(t)$) functions. Therefore it looks like a well with a minimum at the point $\tau=1$, where it equals $0.67\overline{\sigma}(0)$. This means that the incoherent process is suppressed for a time $\sim \tau_N$.

To gain a better understanding of the results, let us model the nucleus by a classical harmonic oscillator interacting with a classical electromagnetic wave. Specifically, we will consider a point particle with charge q and mass m, vibrating with the eigenfrequency $\omega_0(t)$, which coincides with the frequency of transition in the nucleus. For the nuclei with $-M_g$ this eigenfrequency takes the value ω_0^- at $t<0$ and ω_0^+ at $t>0$. For the nuclei with the opposite orientation the respective values are ω_0^+ and ω_0^-. An external electromagnetic wave $\mathbf{E}(t) = \mathbf{E}_0 \cos \omega t$ acts on the oscillator with a force $\mathbf{f}(t) = \mathbf{f}_0 \cos \omega t$, where $\mathbf{f}_0 = q\mathbf{E_0}$. Let the coordinate of the particle along $\mathbf{E}_0$ be $z(t)$. Its vibrations are described by Newton's equation of motion containing both the friction force $-\gamma \dot{z}$ and the radiative reaction, which is proportional to the third derivative of z (Ref. 16). Since the latter leads only to the addition of radiation damping to γ, it is omitted here for brevity. Then the equation of motion in complex form reads (see also Ref. 17)

$$\ddot{z} + \gamma \dot{z} + \omega_0^2(t) z = (f_0/m)e^{i\omega t}, \tag{20}$$

In the quantum case we demand that

$$0 \leqslant |\omega - \omega_0^+| \sim \gamma, \quad \gamma \ll \omega_0^+, |\omega^+ - \omega^-|, \tag{21}$$

that is, only vibrations with the frequency ω_0^+ are resonating with the external force.

First we will consider the oscillator to model a nucleus $-M_g$ which starts to move at ($t>0$), when $\omega(t) = \omega_0^+$. In this case we must solve Eq. (20) with the initial condition $z(0) = \dot{z}(0) = 0$. In the approximation (21) it has the following solution:

$$z(t)^- = A\{e^{i\omega_0^+ t - \gamma t/2} - e^{i\omega t}\}, \tag{22}$$

where the complex amplitude is

$$A=\frac{f_0/2m\omega_0}{\omega-\omega_0^{+}+i\gamma/2}. \tag{23}$$

The similar oscillator for $+M_g$ nuclei at $t<0$ executes forced vibrations with amplitude A and frequency ω. After the reversal ($t>0$), when the frequency of the external force is substantially different from the new eigenfrequency ω_0^{-} of the oscillator, it is then described by Eq. (20) with $f_0\approx 0$. At $t>0$ the solution is

$$z(t)^{+}=Ae^{i\omega_0^{-}t-\gamma t/2}. \tag{24}$$

The classical electromagnetic wave emitted by the vibrating charged particle,

$$\mathbf{E}_{\mathrm{sc}}(\mathbf{r},t)\sim\ddot{\mathbf{z}}(t), \tag{25}$$

depends on the time and frequency as predicted by the quantum results (4) and (7).

Thus the contributions to the scattered radiation from nuclei with different orientations have quite different behavior. While the $+M_g$ nuclei at $t>0$ give rise to a decaying wave with carrier frequency $\omega'^{-}_0 q$, the $-M_g$ nuclei produce both a transient decaying wave with frequency $\omega_0'^{+}$ and a stationary wave with frequency ω'. Accordingly, for the $+M_g$ nuclei the intensity of the scattered radiation is exponentially decreasing at $t>0$, while for the $-M_g$ nuclei it grows during a time of the order of τ_N. The summation of their contributions in unpolarized targets leads to the formation of a ''well'' in the curve describing the time dependence of the incoherent radiation yield. Thus the incoherent channel is suppressed, since the nucleus does not react instantaneously to the change in external conditions. Its response time corresponds to the nuclear lifetime τ_N. It should be noted that this suppression effect is not related to the enhancement of the coherent radiative channel caused by the interference of three coherent scattered waves with frequencies ω, ω^{+}, and ω^{-}.

*)e-mail: dzyublik@kinr.kiev.ua

[1] G. C. Baldwin and J. C. Solem, Rev. Mod. Phys. **53**, 687 (1981).
[2] Yu. V. Shvyd'ko, S. L. Popov, and G. V. Smirnov, JETP Lett. **53**, 231 (1991)).
[3] Yu. V. Shvyd'ko, S. L. Popov, and G. V. Smirnov, J. Phys.: Condens. Matter **5**, 1557 (1993).
[4] L. Pfeiffer, in *Mössbauer Effect Methodology*, Vol. 7, edited by I. J. Gruverman, Plenum Press, New York (1972), pp. 263–298.
[5] J. K Srivastava, in *Advances in Mössbauer Spectroscopy*, edited by B. V. Thosar, P. K. Iengar, J. K. Srivastava, and S. C. Bhargava, Elsevier, Amsterdam (1983), pp. 761–813.
[6] M. Kopcewicz, in *Mössbauer Spectroscopy Applied to Inorganic Chemistry*, Vol. 3, edited by G. J. Long and F. Grandjean, Plenum Press, New York (1989), pp. 243–287.
[7] M. Kopcewicz, Struct. Chem. **2** (105), 313 (1991).
[8] Yu. V. Baldokhin, S. A. Borshch, S. M. Klinger, and V. A. Povitsky, Zh. Éksp. Teor. Fiz. **63**, 708 (1972) [Sov. Phys. JETP **36**, 374 (1972)].
[9] S. R. Julian and J. M. Daniels, Phys. Rev. B **38**, 4394 (1988).
[10] A. Ya. Dzyublik, Phys. Status Solidi B **194**, 699 (1996).
[11] A. Ya. Dzyublik and V. Yu. Spivak, Zh. Éksp. Teor. Fiz. **111**, 1438 (1997) [JETP **84**, 794 (1997)].
[12] A. Ya. Dzyublik and V. Yu. Spivak, Phys. Status Solidi B **209**, 127 (1998).
[13] A. Ya. Dzyublik, V. Yu. Spivak, R. A. Manapov, and F. G. Vagizov, JETP Lett. **67**, 61 (1998).
[14] A. Ya. Dzyublik, J. Phys.: Condens. Matter **11**, 3915 (1999).
[15] G. T. Trammell, Phys. Rev. **126**, 1045 (1962).

[16] J. D. Jackson, *Classical Electrodynamics*, Wiley, New York (1962).
[17] L. D. Landau and E. M. Lifshitz, *Mechanics*, 2nd ed., Pergamon Press, Oxford (1969) [Russian original, Nauka, Moscow (1965)].

Published in English in the original Russian journal. Edited by Steve Torstveit.

Thermalization of neutrons on cold atoms in magnetic traps

D. F. Zaretskiĭ and S. B. Sazonov
Russian Science Center ''Kurchatov Institute'' 123182 Moscow, Russia

(Submitted 16 July 1999; resubmitted 5 October 1999)
Pis'ma Zh. Éksp. Teor. Fiz. **70**, No. 9, 570–572 (10 November 1999)

A new method is proposed for cooling polarized neutrons by thermalizing neutrons in spherical and torroidal magnetic traps with elastic triplet scattering by cold, double spin-polarized, hydrogen atoms.
 [S0021-3640(99)00321-7]

PACS numbers: 28.20.Cz

In the present letter, a method is proposed for cooling polarized neutrons by thermalizing neutrons in a magnetic trap by scattering by cold, double spin-polarized, hydrogen atoms. Up to now, quasistable ensembles of spin-polarized hydrogen atoms have been obtained at very low temperatures (down to $40\,\mu$K[1]) with density $4.5\cdot 10^{18}\,\mathrm{cm}^{-3}$.[2] The lifetimes of such hydrogen reached tens of minutes.[3] Ensembles of double spin-polarized hydrogen atoms with energies down to 10^{-8} eV and densities $10^{18-19}\,\mathrm{cm}^{-3}$ can be produced.

Let polarized neutrons be introduced into a magnetic trap containing double spin-polarized hydrogen atoms. The neutron spins are parallel to the nuclear spin and the electron spin and the neutron energy E_0 is greater than the energy of the atoms. Elastic neutron–atom collisions will cool down or thermalize the neutrons. The neutrons will undergo triplet nuclear scattering and magnetic scattering by the atoms. Moreover, in this case interference of nuclear and magnetic scatterings will make an additional contribution to the scattering cross section. The total scattering cross section σ_s is estimated to be 6.7 b. It is also important that radiative capture of neutrons by protons will not occur in the triplet state. It should be noted that for scattering of neutrons whose spin is parallel to the spin of a double spin-polarized hydrogen atom flippiing of the neutron spin, which would cause a neutron to leave the trap, will not occur because of the conservation of the projection of the total angular momentum.

Let us estimate the cooling of the neutrons as a result of their elastic collisions with atoms over a time of 800 s, close to the neutron lifetime. Let us determine the travel time of a neutron between the $i-1$ and i collisions in terms of the mean-free path length λ, assuming it to be independent of the energy, according to the formula $t_i=\lambda(m/2E_{i-1})^{1/2}$, where E_{i-1} is the energy of a neutron with mass m after the $i-1$ collision. It is known that in an elastic collision with a hydrogen atom a neutron loses, on the average, half its energy. Assuming that the energy of a neutron is 2^K times lower after K collisions with atoms, we shall calculate the thermalization time T as the sum of the t_i. For T and the final neutron energy E_T we obtain, approximately,

$$T = 2.414 t_1 [(E_0/E_T)^{1/2} - 1], \tag{1}$$

$$E_T = E_0 (0.41T/t_1 + 1)^{-2}, \tag{2}$$

where t_1 is the neutron travel time up to the first collision. It is evident that the decrease of the neutron energy depends nonlinearly on the atom density N, since the mean-free path length is determined by the relation $\lambda = (N\sigma_s)^{-1}$. It follows from Eq. (2) that for atom density $N = 10^{18}\,\mathrm{cm}^{-3}$ neutrons with $E_0 = 10^{-6}$ eV can be cooled in a time 800 s to $6 \cdot 10^{-8}$ eV ($t_1 \simeq 108.46$ s).

In a spherical magnetic trap neutrons are confined by the field B of a spherical sextupole, which reflects neutrons with energies $E \leqslant \mu_n B$, where μ_n is the modulus of the neutron magnetic moment. Thus, a 17 T field in a spherical trap can confine neutrons with energies up to 10^{-6} eV.

A system consisting of a toroidal magnetic trap, filled with cold hydrogen atoms, could be preferable for cooling neutrons with higher energies. Such traps are magnetic sextupoles which are formed into a torus. In such setups the velocity of the trapped polarized neutrons along the circular axis of the torus is, in principle, unbounded. It is only important that the component of the velocity normal to the walls of the torus be less than the critical value determined by the confining magnetic field.

As an example we shall consider a toroidal magnetic trap of the type used in the NESTOR design.[4] It consists of a tube with radius $r_0 = 5$ cm that is formed into a ring with radius $R = 50$ cm. Magnetic fields of a special form with intensity B up to 5.6 T confine in it neutrons revolving around the torus with energies up to $2 \cdot 10^{-6}$ eV and velocities $V \leqslant 20$ m/s. The field B and the angular velocity V are related as

$$V = [2(\mu_n/m)B(R+r)r/r_0^2]^{1/2}, \tag{3}$$

where r is the distance from the arbitrary ring-shaped trajectory of a neutron to the circular axis of the torus. Once again, the degree of thermalization and the thermalization time are determined by Eqs. (1) and (2), where we replace t_1 by $t_{11} = t_1$, where t_{11} is the time up to the first collision, which does not depend on the diameter of the torus and is equal to $t_{11} = (N\sigma_s V)^{-1}$. In such a trap, in 800 s neutrons with energy $E_0 = 10^{-6}$ eV can be cooled on hydrogen atoms with density $10^{18}\,\mathrm{cm}^{-3}$ and temperature 10^{-4} K by a factor of 16, just as in a spherical trap, using the magnetic field of the NESTOR setup, which is three times weaker than the field required to confine neutrons with this energy in a spherical trap.

At the same time the neutron cooling by elastic collisions with atoms in a torus will be accompanied by an angular spreading of the neutron beam in the process of scattering. Let us estimate the magnetic field that could prevent neutrons from escaping the trap as a result of scattering. All neutrons with energy E, which have energy $E\cos^2\theta$ after scattering and for which the sine of twice the scattering angle 2θ in the laboratory coordinate system satisfies the inequality

$$E \sin^2 2\theta \leqslant 4\mu_n B, \tag{4}$$

will be reflected from the magnetic barrier and continue moving inside the torus. In other words, neutrons with energy $E \leqslant 4\mu_n B$ for any scattering angle will not be knocked out of the beam. Thus, it follows from Eq. (4) that a 4.5 T field is sufficient to confine 10^{-6} eV neutrons in a beam after scattering. Integrating the angular distribution function

for scattering of neutrons taking account of Eq. (4), we find that the probability of a neutron remaining in the beam after a collision is $W=1-2(1/4-\mu_n B/E)^{1/2}$. We note that the lower the neutron energy, the fewer neutrons will be knocked out of the trap because of scattering. As estimates show, this makes it possible to cool neutrons by the proposed method with smaller losses than in currently used methods. It should be noted that the field of an incomplete sextupole is used in Ref. 4 — the field from the inner side of the torus approaches zero. The field of a complete sextupole is required to confine the scattered neutrons.

A torus with chambers of size L, which are transparent to neutrons and contain cold atoms and are built into the torus, can be used instead of a torus completely filled with hydrogen. The probability of a neutron being scattering by hydrogen atoms in one revolution around the ring of the torus is $p=NL\sigma_s=6.7\cdot 10^{-5}$ (here $L=10$ cm). Thus, before scattering a neutron completes $X=1/p\sim 15000$ revolutions around the ring of the torus. The time up to the first collision will be determined in this case by $t_{11}=2\pi RX/V$. If M chambers with cold atoms are arranged along the perimeter of the torus, then the total thermalization time T from Eq. (1) will be M times shorter, since in this case t_{11} will be replaced by $t_{1M}=t_{11}/M$. Deeper cooling can be attained by increasing the number of chambers.

A scheme consisting of a ''distorted'' torus, in which rounded sections alternate with rectilinear sections, where chambers with atoms are placed, could be preferable for obtaining better matching of the field confining the neutrons and the field confining the atoms. The field on the rectilinear sections should, in the first place, confine atoms and neutrons and, in the second place, prevent neutrons from dispersing as a result of being scattered. For this reason, it should confine neutrons from all sides. The field on the rounded sections should only form the trajectory of the neutrons and just as in Ref. 4 the best field here is a field in the form of an incomplete sextupole, which will prevent neutron losses due to flipping of the neutron spin in the region of zero field on the circular axis of the torus. In addition, the field on the rounded sections should be varied as the energy of the neutrons changes.

Cooled neutrons can be extracted from the trap by using the fact that neutrons with lower energies move along trajectories with a smaller radius. Neutrons with the required energy can be diverted by using a field configuration similar to that in Ref. 4 and periodically switching off the field from the inner side of the torus.

[1] D. G. Fried, T. C. Killian, L. Willmann *et al.*, Phys. Rev. Lett. **81**, 3811 (1998).
[2] H. F. Hess, D. A. Bell, G. P. Kochanski *et al.*, Phys. Rev. Lett. **52**, 1520 (1984).
[3] N. Masuhara, J. M. Doyle, J. C. Sandberg *et al.*, Phys. Rev. Lett. **61**, 935 (1988).
[4] K. J. Kugler, K. Moritz, W. Paul *et al.*, Nucl. Instr. Methods **228**, 240 (1985).

Translated by M. E. Alferieff

On propagation of short pulses in strong dispersion managed optical lines

V. E. Zakharov and S. V. Manakov
Landau Institute of Theoretical Physics, Russian Academy of Sciences, 117334 Moscow, Russia

(Submitted 21 September 1999)
Pis'ma Zh. Éksp. Teor. Fiz. **70**, No. 9, 573–576 (10 November 1999)

We show that the propagation of short pulses in optical lines with strong dispersion management is described by an integrable Hamiltonian system. The leading nonlinear effect is the formation of a collective dispersion which is a result of the interaction of all pulses propagating along the line. © *1999 American Institute of Physics.* [S0021-3640(99)00421-1]

PACS numbers: 42.65.Tg, 42.81.Dp

One of the most important practical applications of nonlinear optics is the theory of propagation optical pulses in nonlinear optical fibers. Due to dispersion, pulses of small amplitude in such a system suffer chromatic spreading, which limits the transmission capacity of a fiber. In 1973 Hasegawa and Tappert[1] proposed to use a focusing nonlinearity for compensation of chromatic spreading. The competion between spreading and nonlinear focusing in a conservative fiber leads to the formation of stationary pulses — optical solitons — which can be used as units of information. The theory of optical solitons and their interactions was developed by Zakharov and Shabat in 1971.[2] Optical solitons have now been proposed for use in dozens of planned large-scale telecommunication systems.

Real optical lines are not conservative. For compensation of the damping one must install a periodic array of amplifiers. Hasegawa and Kodama[3] showed that such ''conventional'' soliton lines inherit the basic features of conservative lines.

A more advanced (see Ref. 4) proposal is to design a line that includes a periodic system of fiber legs with opposite signs of the dispersion in addition to a periodic array of amplifiers. If such a line were linear, the designer could achieve compensation of chromatic spreading. This makes such lines the most promising systems for ultrafast communication. However, to suppress the noise and provide a low-error transmission of information, one should use optical pulses of relatively high amplitude. As a result, in the process of long-distance pulse propagation the nonlinear effects inevitably become important.

The theory of pulse propagation in long periodic structures is a new and interesting chapter of nonlinear physics. In many aspects periodic fibers differ from homogeneous ones. In the latter the dispersion is a smooth function of frequency which can be approximated inside a narrow spectral band by a low-order polynomial. As a result, a pulse

envelope can be described by a partial differential equation of the second or third order, and the pulse interaction is local in time. In this situation, optical solitons propagating without chromatic distortion are the basic objects. Because of the locality of the interaction, the shape of an individual soliton does not depend on the presence of other pulses in the system. We will show in this letter that this is not necessarily true in periodic systems.

We will consider lines in which the local nonlinearity and mean dispersion are much less than the local dispersion. Such lines are characterized by a time τ_0. This is the duration of a pulse that broadens by a factor of two in passing through a fiber leg with constant dispersion. If the pulse is short ($\tau \ll \tau_0$, where τ is the pulse duration), one can speak of strong dispersion management (SDM). In this letter we show that in this limit the line is described approximately by a completely integrable Hamiltonian system.

The leading nonlinear effect is the appearance of a collective average dispersion formed by a whole ensemble of pulses propagating through the line. Since this dispersion is very nonlocal, the pulse envelopes cannot be described by any partial differential equation in coordinate space. The pulses pass through each other without interaction, but the rate of chromatic spreading of an individual pulse depends on the presence of neighboring pulses.

THE THEORY OF SHORT-PULSE PROPAGATION

The basic model for describing dispersion managed fibers is the nonlinear Schrödinger equation with periodic coefficients,

$$i\frac{\partial \Psi}{\partial x} + [d + \Phi'(x)]\Psi_{tt} + R(x)|\Psi^2|\Psi = 0. \tag{1}$$

Here $\Psi(x,t)$ is the envelope of a wave pulse, and $\Phi(x)$ and $R(x)$ are periodic functions of x with the same period 2π. Insofar as $\langle \Phi'(x) \rangle = 0$, d is the average dispersion of the fiber. We assume that

$$|R(x)| \ll |d + \Phi'(x)|. \tag{2}$$

In real transmission lines, this condition is usually satisfied.

Under the assumption (2), Eq. (1) can be replaced with the approximate Gabitov–Turitzyn (GT) model[5–7]

$$i\frac{\partial \chi}{\partial x} = d\omega^2 \chi_\omega - \int G(\Delta)\chi^*_{\omega_1}\chi_{\omega_2}\chi_{\omega_3}\delta_{\omega+\omega_1-\omega_2-\omega_3}\, d\omega_1 d\omega_2 d\omega_3. \tag{3}$$

Here

$$\chi_\omega = \Psi_\omega e^{i\Phi(x)\omega^2}, \quad \Delta = \omega^2 + \omega_1^2 - \omega_2^2 - \omega_3^2,$$

$$G(\Delta) = \frac{1}{2\pi}\int_0^{2\pi} R(x) e^{i\Phi(x)\Delta} dx = J(\Delta\tau_0^2). \tag{4}$$

Here τ_0 is a characteristic parameter of the line, $J(\xi)$ is a function of the dimensionless variable $\xi \sim 1$, and $\Psi_\omega(x)$ is the Fourier transform of $\Psi(x,t)$. In general

$$J(-\xi) = J^*(\xi).$$

In the special case of constant nonlinearity ($R=\text{const}$) and piecewise constant dispersion, one has $J(\xi)=\sin\xi/\xi$.

Taking the inverse Fourier transform of (3) leads to the equation

$$i\frac{\partial\chi}{\partial x}+d\frac{\partial^2\chi}{\partial t^2}+\frac{1}{\tau_0^2}\int F\left(\frac{pq}{\tau_0^2}\right)\chi^*(t+p+q)\,\chi(t+p)\,\chi(t+q)\,dpdq=0. \tag{5}$$

If $s=pq/\tau_0^2>0$, then $F(s)$ is given by the expression.

$$F(s)=\frac{1}{2\pi}\int_0^\infty\{2J^*(z)K_0(\sqrt{2sz})-\pi J(z)N_0(\sqrt{2sz})\}ds. \tag{6}$$

Here $K_0(q)$ is the Bessel function of imaginary argument, and $N_0(q)$ is the Neumann function. For negative s, $F(-s)=F^*(s)$. In the case of strong dispersion $s\ll 1$, one can use asymptotic expansions of the Bessel function at small values of the argument.

Expansion in powers of s leads to the result

$$F=F_0+F_1+F_2+\cdots, \tag{7}$$

$$F_0=\frac{2}{\pi}\int_0^\infty\left[\ln\frac{2}{|s|z}-C\right]\text{Re}\,J(z)dz, \tag{8}$$

$$F_1=\frac{2is}{\pi}\int_{-\infty}^\infty z\left[\ln\frac{2}{|s|z}+1-C\right]\text{Im}\,J(z)dz, \tag{9}$$

$$F_2=\frac{s^2}{4\pi}\int_0^\infty z^2\left[\ln\frac{2}{|s|z}+\frac{3}{2}-C\right]\text{Re}\,J(z)dz. \tag{10}$$

Here C is the Euler constant. Let $\chi=Ae^{i\Phi}$. Plugging $F=F_0$ in (5) and performing the Fourier transform, one obtains a system of equations for A and Φ:

$$\frac{\partial A}{\partial x}=0,\quad \frac{\partial\Phi}{\partial x}=-d\omega^2+\hat{K}(A). \tag{11}$$

Here (see Ref. 8)

$$\hat{K}(A)=\frac{4}{\tau_0^2}\left[fA^2+\int_{-\infty}^\infty\frac{A^2(\omega')-A^2(\omega)}{|\omega'-\omega|}d\omega'\right], \tag{12}$$

$$f=(2\ln\tau_0+C)\,a+b,$$

$$a=\int_0^\infty J(z)dz,\quad b=\int_0^\infty\ln\frac{2}{z}J(z)dz. \tag{13}$$

In order of magnitude

$$K(A)\simeq\frac{4}{\tau_0^2}\ln\frac{\tau_0}{\tau}A^2(\omega). \tag{14}$$

In the limit $\ln \tau_0/\tau \to \infty$ formula (14) is exact. Equations (11) mean that the system (4) is integrable in the limit $\tau_0/\tau \to 0$.

The leading nonlinear effect is the formation of an additional collective dispersion $\hat{K}(A)$. Let the signal $\chi(t)$ be a superposition of a large number of identical pulses with random phases, separated by arbitrary intervals of time:

$$\chi(t) = \sum_{n=1}^{N} \chi_0(t-\tau_n), \quad N \gg 1. \tag{15}$$

Then

$$\chi(\omega) = \chi_0(\omega) \sum_{n=1}^{N} e^{-i(\omega\tau_n - \phi_n)},$$

$$A^2(\omega) = N|A_0(\omega)|^2 = |\chi(\omega)|^2. \tag{16}$$

According to (11) all the pulses in the system suffer the same chromatic spreading and remain identical. The value of spreading is determined by all the pulses present in the line. This is a result of the strong dispersional spreading of each pulse in the fibers of constant dispersion. Due to nonlinearity, this spreading cannot be completely compensated in the next fibers. As a result, each pulse generates long ''tails'' that influence the shapes of the other pulses. In the model developed here, the pulse interaction is very nonlocal — the pulses ''feel'' each other when separated by an arbitrarily long distance. This ultimate nonlocality is a weak point of the simple model developed.

Another weak point of the model is the plethora of soliton solutions. To find such a solution, one can put

$$\Phi(\omega, x) = \lambda x + \Phi_0(\omega),$$

where $\Phi_0(\omega)$ is an arbitrary function of ω and λ is an arbitrary constant.

The amplitude $A(\omega)$ is an arbitrary positive solution of the equation

$$A(\omega)[\lambda + d\omega^2 - \hat{K}(A)] = 0. \tag{17}$$

One can arbitrarily separate the axis $-\infty < \omega < \infty$ into two sets $\Omega_1 \cup \Omega_2$ and put

$$A(\omega) = 0, \quad \omega \in \Omega_1, \quad \lambda + d\omega^2 - \hat{K}(A) = 0, \quad \omega \in \Omega_2. \tag{18}$$

Here (18) is the Fredholm integral equation of the first kind. The system (18) has an infinite number of solutions. To improve the model, one should take into account higher orders of the expansion (7). This is beyond the scope of this article.

We have shown that the propagation of short optical pulses in strong dispersion managed nonlinear systems is quite different from the propagation in ''conventional'' lines with constant dispersion. The interaction of the pulses is very nonlocal — even very distant pulses interact by the formation of a substantial average dispersion. In the leading order the system of pulses is described by an integrable Hamiltonian system. In the framework of this model, solitons do not have a universal form, and their importance

from the practical standpoint is unclear. One can say that in such systems the nonlinearity is purely detrimental. The program for the designer is to make the line as ''linear'' as possible.

One of the authors (S. V. Manakov) is grateful to the Fellowship of the Italian Ministry of Foreign Affairs.

[1] A. Hasegawa and V. Tappert, Appl. Phys. Lett. **23**, 142 (1973).
[2] V. E. Zakharov and A. B. Shabat, Zh. Éksp. Teor. Fiz. **60**, 136 (1971) [Sov. Phys. JETP **33**, 33 (1971)].
[3] A. Hasegawa and Y. Kodama, Opt. Lett. **15**, 1443 (1990); Phys. Rev. Lett. **66**, 161 (1991).
[4] V. E. Zakharov and S. Wabnitz (eds.), *Optical Solitons. Theoretical Challenges and Industrial Perspectives*, Springer, EDP Sciences (1999).
[5] I. Gabitov and S. Turitzin, Opt. Lett. **21**, 327 (1996); JETP Lett. **63**, 814 (1996).
[6] M. Ablovitz and G. Biondini, Opt. Lett. **23**, 1668 (1998).
[7] V. E. Zakharov, ''Propagation of optical pulses in nonlinear systems with varying dispersion,'' *Proceedings of the International School on Optical Solitons*, Le Houches (1998).
[8] I. M. Gel'fand and G. E. Shilov, *Generalized Functions*, Vols. 1–3, Academic Press, New York (1964–1967) [Russian original, Fizmatgiz, Moscow (1958–1959).

Published in English in the original Russian journal. Edited by Steve Torstveit.

Non-Markovian scattering and the condition of applicability for the quasiclassical description of collisions in plasma

S. N. Gordienko

L. D. Landau Institute of Theoretical Physics, Russian Academy of Sciences, 142432 Chernogolovka, Moscow Region, Russia; Russian Science Center ''Kurchatov Institute'' 123182 Moscow, Russia

(Submitted 23 September 1999)
Pis'ma Zh. Éksp. Teor. Fiz. **70**, No. 9, 577–582 (10 November 1999)

It is shown that because of the non-Markovian character of momentum transfer the scattering of a test particle in plasma cannot always be described by a diffusion process. The braking of a particle by plasma occurs in three different stages: short and long times, when scattering is nondiffusive, and intermediate times, when scattering can be described by a diffusion process. The mechanism responsible for nondiffusive scattering at long times results in a new condition of applicability of classical mechanics for describing collisions in plasma $v_T > \hbar^2 \omega_{pe}/m_e e^2 L$, where L is the Coulomb logarithm and e, m_e, and ω_{pe} are, respectively, the electron charge and mass and the plasma frequency. A high-temperature, almost ideal, plasma is an example of a medium where the instantaneous character of collisions makes the classical description applicable even when binary collisions should be described by quantum mechanics (the Born approximation), i.e., the plasma demonstrates the possibility of suppression of quantum effects by collective interaction.
[S0021-3640(99)00521-6]

PACS numbers: 52.20.Hv, 34.10.+x

The assumption that the particle dynamics of plasma is diffusive (in momentum space) is a key point in the derivation of various types of collision integrals for plasma. It seems quite obvious that at times greater than the travel time of a test particle over a distance of the order of the Debye radius the braking process should become Markovian, and the specific nature of Coulomb scattering — momentum transfer in a pair collision decreasing with increasing relative velocity — will ensure a diffusive braking process for an almost ideal plasma. However, multiple Coulomb collisions in a fluctuating plasma microfield have not been studied on the basis of the equations of motion. In the literature the possibility of non-Markovian braking at long times and a ''memory'' mechanism for such a phenomenon were examined, even though it was well known that scattering is nondiffusive at short times.[1]

As a rule, the problem of particle scattering was solved assuming the possibility that

particle collisions in plasma can be reduced to binary collisions after Debye screening of the Coulomb interaction is taken into account.[1–3] The method of Ref. 4, based on a calculation of the distribution function of the transferred momentum in the limit of infinitely large Coulomb logarithm, made it possible to determine the nontrivial physics at small scales, but it turned out to be inadequate for studying the conditions for the applicability of the quasiclassical description in an almost ideal plasma and the possibility of describing braking by a Markovian process.

1. Let us consider a test particle with charge Z_0, mass M, and velocity v along the z axis. The particle moves through a plasma consisting of electrons (charge e and mass m_e) and ions with charges Z and masses m_i. For brevity, we shall assume that the velocity v is much higher than the thermal velocities of the electrons and ions. Then, in accordance with Ref. 4, at times τ such that $\tau < r_D/v$, where r_D is the Debye radius, we find for the distribution function of the momentum change $\Delta\mathbf{p}$ of a test particle in time τ

$$f_\tau(\Delta\mathbf{p}) = \int p(\mathbf{u}) \exp[i(\mathbf{u},\Delta\mathbf{p})] \frac{d\mathbf{u}}{(2\pi)^3}, \tag{1}$$

where $p(\mathbf{u}) = \exp[nU_e(\mathbf{u})]\exp[nU_i(\mathbf{u})]$,

$$U_e = -\frac{2\pi Z_0^2 e^4 \tau}{v} u_z^2 - \frac{\pi Z_0^2 e^4 \tau}{v}(u_x^2+u_y^2)\ln\left(\frac{v^4\tau^2}{Z_0^2 e^4 (u_x^2+u_y^2)}\right),$$

$$U_i = -\frac{2\pi Z_0^2 Z^2 e^4 \tau}{v} u_z^2 - \frac{\pi Z_0^2 Z^2 e^4 \tau}{v}(u_x^2+u_y^2)\ln\left(\frac{v^4\tau^2}{Z_0^2 Z^2 e^4 (u_x^2+u_y^2)}\right).$$

The expression (1) was obtained by calculating the momentum transferred to a test particle on the basis of Newton's second law only.[4] The motion of the test particle was assumed to be rectilinear, which is admissable for times much shorter than free-flight time of the test particle. Since the characteristic function can be represented as a product of characteristic functions, describing the scattering of a test particle by electrons and ions, the scattering by electrons is statistically independent of the scattering by ions. Therefore it is sufficient to study the distribution function of the momentum transferred to electrons:

$$f_\tau^{(e)} = \int \exp(nU_e(\mathbf{u}) - i[\mathbf{u},\Delta\mathbf{p})] \frac{d\mathbf{u}}{(2\pi)^3}, \tag{2}$$

which is what we shall do below. However, we note for completeness that since the distribution function $f_\tau^{(i)}$ of the momentum transferred to ions is determined by a similar expression

$$f_\tau^{(i)} = \int \exp[nU_i(\mathbf{u})/Z - i(\mathbf{u},\Delta\mathbf{p})] \frac{d\mathbf{u}}{(2\pi)^3},$$

the distribution function $f_\tau(\Delta\mathbf{p})$ of the total transferred momentum is given by a convolution of the distribution functions of the momentum transferred to electrons and ions:

$$f_\tau(\Delta\mathbf{p}) = \int f_\tau^{(i)}(\Delta\mathbf{p}-\mathbf{x}) f_\tau^{(e)}(\mathbf{x})\, d\mathbf{x}.$$

2. The function $f_\tau^{(e)}$ can be investigated analytically. After calculations, we find that the indicated distribution function has a Gaussian section

$$f_\tau^{(e)}(\Delta\mathbf{p})=\frac{1}{(2\pi)^{3/2}p_0^2p_1}\exp\left(-\frac{p_z^2}{2p_1^2}-\frac{p_x^2+p_y^2}{2p_0^2}\right), \tag{3}$$

where $p_x^2+p_y^2<2p_0^2\ln(\Lambda/4)$, Λ is determined as the solution of the equation $\Lambda=\ln(2\pi\Lambda n(v\tau)^3)\gg 1$, $p_0^2=2\pi nZ_0^2e^4\Lambda\tau/v$, $p_1^2=2p_0^2/\Lambda$, and a power-law ''tail'' over the transverse momentum transfer

$$f_\tau^{(e)}(\Delta\mathbf{p})=\frac{1}{\pi\sqrt{2\pi}}\exp\left(-\frac{p_z^2}{2p_1^2}\right)\frac{p_1}{(p_x^2+p_y^2)^2} \tag{4}$$

for $p_x^2+p_y^2>2p_0^2\ln(\Lambda/4)$ and $\Delta\mathbf{p}=(p_x,p_y,p_z)$.

The Gaussian part of the distribution function (3) and the power-law asymptotic function (4) are formed by different mechanisms. The Gaussian part is due to multiple scattering with small momentum transfers, i.e., because of scattering by the fluctuation intraplasma electric field, and the power-law tail is due to individual pair collisions with small impact parameters. Thus, in reality, the power-law tail extends not to infinity but only to the maximum possible momentum transfer in a pair collision, i.e., to a value of the order of $p^*\sim 2m_ev$ (if $p^{*2}<2p_0^2\ln(\Lambda/4)$, then the power-law ''tail'' does not occur at all).

We note that the second moment of the transferred momentum, associated with the Gaussian part of the distribution function (3), is

$$\langle(\Delta\mathbf{p})^2\rangle_G=\frac{4\pi nZ_0^2e^4\tau}{v}\ln(2\pi\Lambda n(v\tau)^3). \tag{5}$$

Only a very small fraction of the total number of particles [of the order of $1/\Lambda\ln(\Lambda/4)$] is associated with the power-law ''tail'' of the distribution function, but the contribution of these particles to the second moment is not, generally speaking, small. Thus the second moment, associated with the power-law ''tail,'' is

$$\langle(\Delta\mathbf{p})^2\rangle_t=\frac{4\pi nZ_0^2e^4\tau}{v}\ln\left(\frac{m_e^2v^3}{\pi ne^4Z_0^2\tau\Lambda\ln(\Lambda/4)}\right). \tag{6}$$

3. Let us calculate the distribution function of the transferred momentum for times $\tau\gg r_D/v$. At such times the Debye screening must be taken into account, i.e., for calculations to only logarithmic accuracy it can be assumed that the electric field at a given point is produced only by particles located at distances from this point not exceeding the Debye radius r_D. Simple calculations show that for this it is sufficient to use in Eqs. (1) and (2) instead of the functions U_e and U_i the new functions $U_e^{(D)}$ and $U_i^{(D)}$, given by

$$U_e^{(D)}=-\frac{\pi Z_0^2e^4\tau}{v}(u_x^2+u_y^2)\ln\left(\frac{r_D^2v^2}{Z_0^2e^4(u_x^2+u_y^2)}\right), \tag{7}$$

$$U_i^{(D)}=-\frac{\pi Z_0^2Z^2e^4\tau}{v}(u_x^2+u_y^2)\ln\left(\frac{r_D^2v^2}{Z_0^2Z^2e^4(u_x^2+u_y^2)}\right). \tag{8}$$

The distribution function $f_\tau^{(e)}$ for the momentum transferred to electrons can be calculated explicitly. Thus we obtain

$$f_\tau^{(e)}(\Delta\mathbf{p})=\frac{1}{2\pi p_0^2}\,\delta(p_z)\exp\left(-\frac{p_x^2+p_y^2}{2p_0^2}\right), \tag{9}$$

where $p_x^2+p_y^2<2p_0^2\ln(L/4)$, $L=\ln(2\pi Lr_D^2v\tau)\gg 1$, $p_0^2=2\pi nZ_0^2e^4L\tau/v$, and the power-law ''tail'' over the transverse momentum transfer

$$f_\tau^{(e)}(\Delta\mathbf{p})=\frac{2}{\pi L}\,\delta(p_z)\,\frac{p_0^2}{(p_x^2+p_y^2)^2} \tag{10}$$

for $p^{*2}>p_x^2+p_y^2>2p_0^2\ln(L/4)$, $\Delta\mathbf{p}=(p_x,p_y,p_z)$, and for times $\tau>\tau^*=m_e^2v^3/L\ln(L/4)\pi ne^4Z_0^2$, such that $p^{*2}<2p_0^2\ln(L/4)$, the power-law part of the asymptotic expression (10) is absent.

We specially emphasize that the time τ^* is parametrically less than the free flight time of a test particle in plasma. This guarantees that the approach described above is applicable at such times. The factor $\delta(p_z)$ in Eqs. (9) and (10) is interesting. The appearance of a δ function has a simple physical meaning: Fluctuations of the intraplasma potential exist inside the Debye sphere, and this changes the kinetic energy of a particle and leads to a Gaussian distribution of p_z in Eqs. (3) and (4). However, the fluctuations of the kinetic energy and p_z that are associated with the relief of the intraplasma potential do not grow with increasing time τ for $\tau>r_D/v$, and when they decrease to a level below the transverse fluctuations of the momentum, a corresponding δ function appears in the approximation employed. To calculate the energy losses (friction forces) the fluctuation of not only the electric field but also the polarization electric field, i.e., calculations of a higher order in the coupling constant, must be taken into account.[2]

Calculation of the second moments associated with the Gaussian part of the distribution function (9) and the power-law ''tail'' gives

$$\langle(\Delta\mathbf{p})^2\rangle_G=\frac{4\pi nZ_0^2e^4\tau}{v}\ln(2\pi Lnr_D^2v\tau), \tag{11}$$

$$\langle(\Delta\mathbf{p})^2\rangle_t=\frac{4\pi nZ_0^2e^4\tau}{v}\ln\left(\frac{m_e^2v^3}{\pi nZ_0^2\tau L\,\ln(L/4)}\right), \tag{12}$$

for $r_D/v<\tau<\tau^*$, while for $\tau>\tau^*$

$$\langle(\Delta\mathbf{p})^2\rangle_G=\frac{4\pi nZ_0^2e^4\tau}{v}\ln(2\pi Lnr_D^2v\tau) \tag{13}$$

and $\langle(\Delta\mathbf{p})^2\rangle_t=0$, since the power-law ''tail'' does not arise at all at such times τ.

4. The complete second moment of the transferred momentum is the sum of contributions from the Gaussian part of the distribution function and the power-law ''tail,'' i.e.,

$$\langle(\Delta\mathbf{p})^2\rangle=\frac{4\pi nZ_0^2e^4\tau}{v}\ln\left(\frac{2m_e^2v^6\tau^2}{e^4Z_0^2\ln(\Lambda/4)}\right)\quad\text{for}\quad\tau<r_D/v, \tag{14}$$

$$\langle(\Delta\mathbf{p})^2\rangle = \frac{4\pi n Z_0^2 e^4 \tau}{v} \ln\left(\frac{2m_e^2 v^4 r_D^2}{e^4 Z_0^2 \ln(L/4)}\right) \quad \text{for} \quad r_D/v < \tau < \tau^*, \tag{15}$$

$$\langle(\Delta\mathbf{p})^2\rangle = \frac{4\pi n Z_0^2 e^4 \tau}{v} \ln(2\pi L n r_D^2 v\tau) \quad \text{for} \quad \tau^* < \tau. \tag{16}$$

According to Eqs. (14)–(16), the momentum transfer process can be assumed to be Markovian only for $r_D/v < \tau < \tau^*$. The short-time range $\tau < r_D/v$ is always strongly non-Markovian, and the parameter $M^2\ln(L/4)/m_e^2$ determines the role of non-Markovian effects from the standpoint of the magnitude of the second moment of the transferred momentum at long times $\tau > \tau^*$. We shall not discuss this parameter in greater detail. The non-Markovian behavior is always due to some memory mechanism. The non-Markovian (nondiffusive) nature of scattering at short times, which was discovered in Ref. 1, is due to the fact that particles retain a memory of their travel distance.[1] The non-Markovian nature at long times (16) arises because the Gaussian part of the distribution function retains a memory of the travel time of the particle, and for $\tau > \tau^*$ the Gaussian part ''absorbs'' the power-law tail of the distribution function, which at intermediate times $r_D/v < \tau < \tau^*$ ''conceals'' the non-Markovian character of the scattering of most particles.

It is interesting that the expressions (14)–(16) explicitly demonstrate the collective nature of the argument of the Coulomb logarithm by the presence of $\ln(\Lambda/4)$, $\ln(L/4)$, and L in it (these are parameters and not numbers!), and retaining these factors in the logarithm does not exceed the accuracy.

5. The Gaussian part of the distribution function of the transferred momentum that is responsible for the non-Markovian scattering at long times changes fundamentally the conditions of applicability of the quasiclassical approximation for describing collisions in plasma and other systems of Coulomb particles. Indeed, let $\tau \sim r_D/v$ (the travel time of a test particle through the interaction region). In order for the quasiclassical description to be applicable it is sufficient that pair collisions with sufficiently large momentum transfer p, where $p^2 > 2p_0^2(r_D/v)\ln L(r_D/v)$ (the quantities $p_0^2(\tau)$ and $L(\tau)$ are taken at $\tau = r_D/v$) be describable quasiclassically and that a quasiclassical description be applicable for multiple scattering by the intraplasma field (the Gaussian part of the distribution function) with characteristic momentum transfer $p_0(r_D/v)$. Therefore the nondegeneracy condition $n^{1/3}\hbar/m_e v_T < 1$ and the inequality

$$r_D p_0(r_D/v) > \hbar, \tag{17}$$

replacing the condition $e^2/\hbar v > 1$ arising in the description of the collisions of two Coulomb particles, are sufficient for a quasiclassical description of collisions in plasma. Thus, the condition of applicability of classical mechanics for describing collisions in a nondegenerate, almost ideal, plasma can be written in the form

$$v_T > \frac{1}{L}\frac{\hbar^2}{m_e e^2}\omega_{pe}, \tag{18}$$

where v_T is the thermal velocity of the electrons and ω_{pe} is the plasma frequency. The

new condition (18) for the applicability of classical mechanics to the description of particle collisions in plasma is fundamentally different from the condition $e^2/\hbar v_T > 1$ following from the assumption that the Coulomb interaction in plasma reduces to binary collisions. Indeed, the condition (18) shows that a plasma at high temperatures can be correctly described by the quasiclassical and not the Born approximation, which is of fundamental importance for constructing a diagrammatic technique for Coulomb systems.

Thus, taking account correctly of the multiple character of Coulomb scattering in plasma reveals a fundamentally new physical phenomenon: From the fact that scattering by small angles is multiple scattering, and only scattering by comparatively large angles is determined by pair collisions, the criterion $e^2/\hbar v_T > 1$ for small-angle scattering to be quasiclassical for pair collisions of Coulomb particles has no bearing on the applicability of the quasiclassical approximation to the description of collisions in plasma and is replaced by the condition (18). Indeed, according to Ref. 2, quantum-mechanical effects are immaterial for Coulomb collisions with scattering by an angle much greater than the diffraction angle $\hbar/m_e v_T r_D$. In other words, compared with other states of matter, a plasma manifests a remarkable property: Even though binary collisions should be described at high temperatures in the Born approximation, i.e., they are strongly quantum processes, taking account of the multiple character of the scattering (collective effects) makes the purely classical description of the dynamics correct.

6. It is helpful to illustrate the results of the strict analytical analysis presented above by simple qualitative considerations that reveal the physical meaning of the calculations performed. If a test electron moving with velocity v_T is scattered by a charge e^*, then the condition for the quasiclassical description of such scattering is the inequality $ee^*/\hbar v_T > 1$. If the scattering is due to a single charge e^*, then the latter inequality is an absolute result. However, for a plasma it is also necessary to know which charge should be substituted for e^* in the last inequality, i.e., it is necessary to determine what plays the role of the charge e^* in the case of a multiparticle system. The theory of pair collisions assumes that the charge of a single electron, by which at a given moment a test electron is scattered, should be used for e^*. Taking account of the multiple character of Coulomb collisions in plasma will change this result. Indeed, at a given moment in time a test electron effectively interacts with all particles in a Debye sphere, i.e., with $N_D \sim n r_D^3$ particles. In other words, the entire uncompensated charge of a Debye sphere acts on the test electron. This charge can be estimated according to the fluctuations of the total number of particles in a Debye sphere and is of the order of $e\sqrt{N_D}$. It seems obvious intuitively that in plasma $e^* \sim e\sqrt{N_D}$, and the strict analysis performed above confirms this. This value of e^* makes it possible to obtain Eq. (18) immediately, but without the factor $1/L$ which arises because the ''effective'' charge $e^* \sim e\sqrt{N_D}$ is distributed in space.

I sincerely thank S. I. Anisimov, V. I .Kogan, V. D. Shafranov, and É. I. Yurchenko for their interest in this work and for a discussion of the questions touched upon here.

This work was supported by the Russian Fund for Fundamental Research (Grant No. 98-02-17441) and the Council on the Program for the Support of Leading Scientific Schools (Grant No. 96-15-96448).

[1] V. I. Kogan, Dokl. Akad. Nauk SSSR **135**, 1374 (1960) [Sov. Phys. Dokl. **5**, 1316 (1961)].
[2] D. V. Sivukhin, in *Reviews of Plasma Physics*, Vol. 4, edited by M. A. Leontovich (Consultants Bureau, New York, 1968) [Russian original, Gosatomizdat, Moscow, 1964].
[3] V. D. Shafranov, in *Reviews of Plasma Physics*, Vol. 3, edited by M. A. Leontovich (Consultants Bureau, New York, 1968) [Russian original, Gosatomizdat, Moscow, 1963].
[4] S. N. Gordienko, JETP Lett. **70**, 17 (1999).

Translated by M. E. Alferieff

Effect of oxygen content on the magnetic state of $La_{0.5}Ca_{0.5}MnO_{3-\gamma}$ perovskites

I. O. Troyanchuk,*) D. D. Khalyavin, S. V. Trukhanov, and G. N. Chobot
Institute of Solid State Physics and Semiconductors, Academy of Sciences of Belarus, 220072 Minsk, Belarus

H. Szymczak
Institute of Physics, Polish Academy of Sciences, PL-02-668 Warsaw, Poland

(Submitted 21 September 1999)
Pis'ma Zh. Éksp. Teor. Fiz. **70**, No. 9, 583–587 (10 November 1999)

The magnetization and magnetoresistance are studied in $La_{0.5}Ca_{0.5}MnO_{3-\gamma}$ as a function of oxygen content. It is found that as the oxygen content is decreased, this compound undergoes a sequence of transitions from an antiferromagnetic to a ferromagnetic state ($\gamma \geqslant 0.04$), from the ferromagnetic to a spin-glass state ($\gamma \geqslant 0.14$), and from the spin glass to an inhomogeneous ferromagnetic state ($\gamma \geqslant 0.25$). Strongly reduced samples ($\gamma \geqslant 0.25$) show a large magnetoresistance despite the absence of $Mn^{3+}-Mn^{4+}$ pairs. It is suggested that the oxygen vacancies in the strongly reduced samples ($\gamma \geqslant 0.25$) are long-range ordered.
[S0021-3640(99)00621-0]

PACS numbers: 75.30.Kz, 75.30.Vn, 75.50.Dd

The issue of charge ordering in $Ln_{0.5}A_{0.5}MnO_3$ (Ln=lanthanide, A = alkaline earth element) manganites has attracted considerable attention during the last few years after the discovery of the collosal magneotresistance (CMR) effect, associated with a charge order–disorder transition.[1] In fact, this phenomenon was first studied in $La_{0.5}Ca_{0.5}MnO_3$, by Wollan and Koehler[2] and by Goodenough.[3] The compound $La_{0.5}Ca_{0.5}MnO_3$ undergoes first a ferromagnetic transition at 260 K and then a simultaneous antiferromagnetic and charge-ordering transition at a lower temperature. The magnetic arrangement associated with 1:1 Mn^{3+}/Mn^{4+} order consists of stacked antiferromagnetic octants C and E. The low-temperature crystal structure has been shown to be incommensurate.[4,5]

It is well known that the magnetic ground state of the $LaMnO_{3-\gamma}$ parent compound depends on the oxygen content.[6] This compound shows a concentrational antiferromagnet–ferromagnet transition as the oxygen content increases. In contrast, the compound $La_{0.6}Ba_{0.4}MnO_3$ exhibits a collapse of the long-range ferromagnetic arrangement as the oxygen content decreases.[7] However, to our knowledge it has not yet been determined how the magnetic and transport properties of charge-ordered $Ln_{0.5}A_{0.5}MnO_3$ (Ln=lanthanide) manganites depend on the oxygen content. In this report we present a detailed study of the variation of the magnetic state with oxygen content for the $La_{0.5}Ca_{0.5}MnO_{3-\gamma}$ manganites.

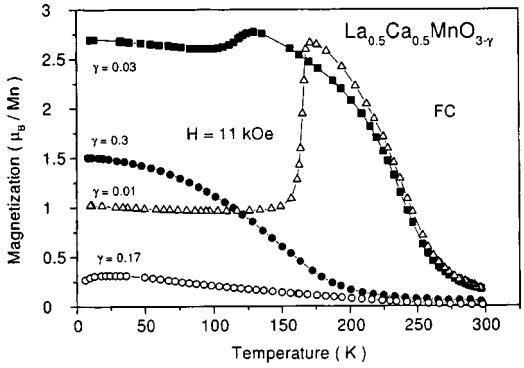

FIG. 1. Magnetization of the $La_{0.5}Ca_{0.5}MnO_{3-\gamma}$ samples as a function of temperature.

The $La_{0.5}Ca_{0.5}MnO_3$ compound was prepared by standard solid-state reaction at $T=1500\,^{\circ}C$ in air. After synthesis the sample was annealed at 900 °C for 100 h in air to obtain the oxygen-saturated compound. The annealed sample was cut into pieces and reduced in silica tubes at 900 °C using metallic tantalum as an oxygen getter. After reduction the change of weight was measured. The starting material $La_{0.5}Ca_{0.5}MnO_3$ is found to be stoichiometric, according to a thermogravimetric study at 1000 °C in flowing hydrogen. The oxygen content of reduced samples was determined from the weight change during reduction. The phase characterization and determination of lattice parameters were performed by powder x-ray diffraction analysis. The electrical resistivity was measured by the dc four-probe method, and the magnetization was determined using a Foner vibrating sample magnetometer.

The $M(T)$ and $M(H)$ curves for the $La_{0.5}Ca_{0.5}MnO_{3-\gamma}$ phases are displayed in Figs. 1 and 2, respectively. The stoichiometric compound exhibits a rise and fall of the magnetization on warming at 180 and 260 K, respectively. In accordance with published data, the anomalous behavior around 180 K is associated with an antiferromagnet–ferromagnet transition, whereas at 260 K there is a Curie point. The anomaly due to the antiferromagnet–ferromagnet transition is much less pronounced for the oxygen-deficit phase with $\gamma=0.03$ (Fig. 1). This phase has a Curie point at 260 K and a magnetic

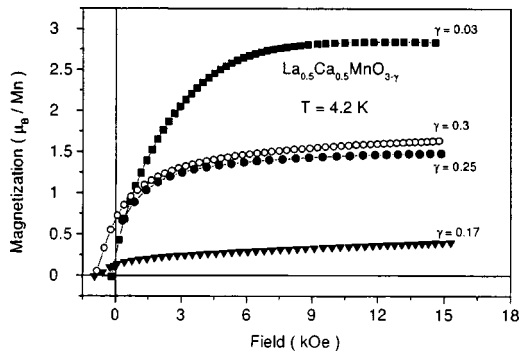

FIG. 2. Magnetization of the $La_{0.5}Ca_{0.5}MnO_{3-\gamma}$ samples as a function of magnetic field.

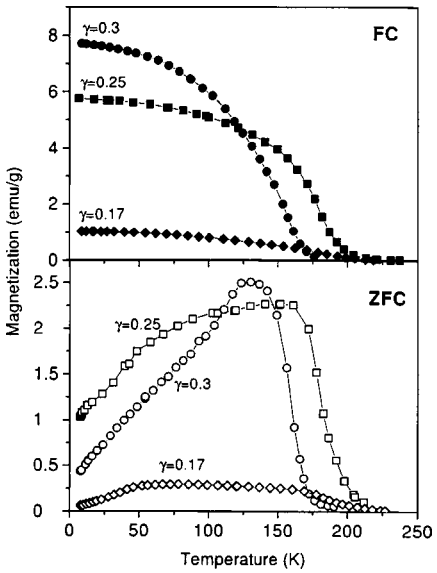

FIG. 3. ZFC and FC magnetizations of $La_{0.5}Ca_{0.5}MnO_{3-\gamma}$ as a function of temperature.

moment of $3.3\mu_B$ per $(Mn^{3+}_{0.5}Mn^{4+}_{0.5})$ unit at 6 K, i.e., slightly smaller than the expected value calculated from the pure ionic model ($3.5\mu_B$). The magnetic behavior of the phases in the oxygen range $0.14 \leqslant \gamma \leqslant 0.2$ is inconsistent with ferromagnetic behavior, because their magnetic moments are much less than those expected for ferromagnetic ordering (Figs. 1 and 2). Both the strong dependence of the magnetization on magnetic field and the broad transition to the magnetically disordered state are consistent with an inhomogeneous low-temperature magnetic state. Surprisingly, the magnetization increases strongly when the content of oxygen vacancies becomes close to $\gamma = 0.25$, i.e., when all the manganese ions adopt a trivalent state (Figs. 1 and 2). However, the magnetic moment at 6 K is only $1.5\mu_B$ per manganese ion, whereas for a ferromagnetically ordered phase the expected value is around $4\mu_B$. Further insight into the magnetic state of oxygen-deficit phases is gained from the zero-field-cooled (ZFC) and field-cooled (FC) magnetization curves recorded in a relatively small (100 Oe) magnetic field (Fig. 3). For the $\gamma = 0.17$ phase we observed first a fast increase of the ZFC magnetization up to 50 K, followed by a region in which the ZFC magnetization depended only slightly on temperature, and finally, at 160–200 K, a region of decreasing magnetization, indicating a transition to a paramagnetic state. By contrast, the FC magnetization demonstrates very weak temperature dependence in the low-temperature range (5–50 K) (Fig. 3), whereas above 50 K the FC magnetization decreases gradually with increasing temperature. Taking into account the magnetic data recorded in a changing magnetic field, one can conclude that such behavior of the ZFC and FC magnetizations could result from large magnetic clusters of magnetic moments becoming gradually blocked with decreasing temperature. Below 50 K the magnetic anisotropy increases strongly, apparently due to magnetic frustration.

The drop in magnetization associated with the transition to the paramagnetic state

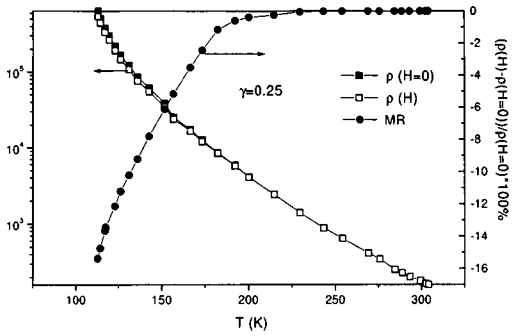

FIG. 4. Resistivity and magnetoresistance of the $La_{0.5}Ca_{0.5}MnO_{2.75}$ sample as a function of temperature.

becomes more pronounced for $La_{0.5}Ca_{0.5}MnO_{2.75}$. This compound undergoes a transition to a magnetically ordered state slightly below 200 K. The difference between the ZFC and FC magnetizations is smaller than that for the $\gamma=0.17$ compound, and the ZFC magnetization does not change below 50 K, thus indicating a decrease of the antiferromagnetic component. A further increase of the oxygen vacancies to $\gamma=0.3$ does not change the magnetic properties appreciably.

All oxygen-deficit compounds ($\gamma \geqslant 0.04$) exhibit semiconductive behavior below the Curie point. The magnetoresistance decreases strongly when the concentrational transition from long-range to short-range magnetic order occurs. The resistivity and magnetoresistance for $\gamma=0.25$ are shown in Fig. 4. This compound exhibits insulating behavior in the entire temperature interval studied. Below the Curie point the magnetoresistance increases strongly, but there is no peak of the magnetoresistance around the Curie point as is observed for the oxidized manganites.

The electrical conductivity and ferromagnetism in the manganites have been explained in terms of the double exchange interaction, with the transfer of an electron from the Mn^{3+} to the Mn^{4+} ions.[8,9] The effect of an applied field is to favor this electron transfer by reducing the spin disorder, leading to a negative magnetoresistance. However, in this model it is impossible to understand the ferromagnetic properties of the manganites without Mn^{4+} ions.[10–12]

Goodenough[12] adduced arguments for the view that the ferromagnetism in the manganite is due not only to double exchange but also to the specific character of the exchange interactions in the Jahn–Teller Mn^{3+} ion system. He proposed that the orbital configuration of the $3d$ electrons removing the static Jahn–Teller distortions depends on the position of the ion nuclei. In this case a dynamic enhancement of the ferromagnetic part of the exchange interactions occurs at the expense of correlation in the orbital orientation of neighboring ions.

Such considerations could explain the ferromagnetic properties of $BiMnO_3$ and $LaMn_{1-x}Ga_xO_3$, in which static Jahn–Teller distortions are removed. It is well known that charge ordering in the manganites favors antiferromagnetic properties.[3,12] However, from our data, increasing the oxygen-vacancy content ($\gamma \geqslant 0.04$) in $La_{0.5}Ca_{0.5}MnO_{3-\gamma}$ leads to a collapse of the ferromagnetic state, in spite of the disappearance of charge order. In our opinion, this fact could be attributed to the strong negative superexchange

interaction between manganese ions surrounded by oxygen vacancies and manganese ions occupying oxygen octahedra. At relatively high concentrations of oxygen vacancies the antiferromagnetic exchange interaction dominates due to the strong negative superexchange interaction Mn^{3+}(coordination number five)$-O^{2-}-Mn^{3+}$(coordination number six). This assumption is in agreement with the antiferromagnetic properties[13] of the perovskite $CaMnO_{2.5}$. In order to explain the large ferromagnetic component of the strongly reduced $La_{0.5}Ca_{0.5}MnO_{3-\gamma}$ ($\gamma \geqslant 0.25$) we have suggested that the oxygen vacancies are distributed regularly over the crystal lattice, forming an oxygen-vacancy superstructure. In this case the positive superexchange interactions between Mn^{3+} ions surrounded by six oxygen neighbors may be dominant, thus leading to ferromagnetic properties of the strongly reduced manganites. According to published data[14,15] the perovskitelike manganites $LnBaMn_2O_{6-\gamma}$ (Ln=La,Y) with oxygen deficit ($\gamma \geqslant 0.5$) exhibit ordering of oxygen vacancies. However, the ferromagnetic component in $YBaMn_2O_{6-\gamma}$ is very weak.[14] Therefore we think that the crystal structures of $LaCaMn_2O_{6-\gamma}$ and $LaBaMn_2O_{6-\gamma}$ are different. Further crystal and magnetic structure refinements are needed for a better understanding of the magnetic properties of the calcium-doped manganites.

The authors acknowledge the financial support of Belarus Fund for Fundamental Research under Project F98-056 and NATO Grant PST. CLG 975703.

*)e-mail: troyan@ifttp.bas-net.by

[1] Y. Tomioka, A. Asamitsu, Y. Moritomo *et al.*, Phys. Rev. Lett. **74**, 5108 (1995).
[2] E. O. Wollan and W. C. Koehler, Phys. Rev. **100**, 545 (1955).
[3] J. B. Goodenough, Phys. Rev. **100**, 564 (1955).
[4] P. G. Radaelli, D. E. Cox, M. Marezio, and S. W. Cheong, Phys. Rev. B **55**, 3015 (1997).
[5] C. H. Chen and S. W. Cheong, Phys. Rev. Lett. **76**, 4042 (1996).
[6] I. O. Troyanchuck, S. N. Pastushonok, A. K. Bogush, and V. I. Pavlov, Phys. Status Solidi A **118**, K111 (1990).
[7] H. L. Ju, J. Gopalakrishnan, J. L. Peng *et al.*, Phys. Rev. B **51**, 6143 (1995).
[8] C. Zener, Phys. Rev. **82**, 403 (1951).
[9] P. G. de Gennes, Phys. Rev. **118**, 141 (1960).
[10] I. O. Troyanchuk, D. D. Khalyavin, E. F. Shapovalova *et al.*, Phys. Rev. B **58**, 2422 (1998).
[11] E. E. Havinga, Philips Res. Rep. **21**, 432 (1966).
[12] J. B. Goodenough, A. Wold, R. J. Arnott, and N. Menyuk, Phys. Rev. **124**, 373 (1961).
[13] K. R. Poeppelmeier, M. E. Leonowicz, and J. M. Longo, J. Solid State Chem. **44**, 89 (1982).
[14] J. A. McAllister and J. P. Attfield, J. Mater. Chem. **8**, 1291 (1998).
[15] V. Caignaert, F. Millange, B. Domengs *et al.*, Chem. Mater. **11**, 930 (1999).

Published in English in the original Russian journal. Edited by Steve Torstveit.

Localization of negatively charged excitons in GaAs/AlGaAs quantum wells

O. V. Volkov, S. V. Tovstonog, and I. V. Kukushkin
Institute of Solid-State Physics, Russian Academy of Sciences, 142432 Chernogolovka, Moscow Region, Russia

K. von Klitzing and K. Eberl
Max-Planck-Institut für Festkörperforschung 70569 Stuttgart, Germany

(Submitted 24 September 1999)
Pis'ma Zh. Éksp. Teor. Fiz. **70**, No. 9, 588–594 (10 November 1999)

The localization of negatively charged excitons on isolated charged donors, located in a barrier at various fixed distances L from the heteroboundary, is investigated in isolated GaAs/AlGaAs quantum wells. The energy shift of the cyclotron replica in the emission spectra of a localized excitonic complex is studied as a function of L. It is shown that in undoped samples charged excitons localize on residual donors at distances $L>350$ Å on account of the formation of D^- complexes at shorter distances. It is established that a cyclotron replica arises with the recombination of an excited state and not the ground state, as previously thought, of an excitonic complex. © *1999 American Institute of Physics.* [S0021-3640(99)00721-5]

PACS numbers: 78.66.Fd, 71.35.Aa

1. Undoped isolated quantum wells are interesting because under photoexcitation conditions electron–hole complexes consisting of several particles bound with one another by Coulomb attraction forces are formed in them. It turns out that in two-dimensional systems with excess electrons or holes the energetically most favorable process is the formation of three-particle complexes (charged excitons or trions) consisting of two electrons and one hole (X^-) or two holes and one electron (X^+), respectively. These formations, which are similar to the hydrogen ions H^- and H_2^+, were predicted by Lampert almost 50 years ago,[1] but reports of their experimental observation have appeared only recently.[2] At the same time, as shown in our works,[3,4] a trion, being a heavy charged particle, is always localized in a Coulomb potential located in a barrier of a charged impurity (the concentration of uncontrollable residual impurities is much higher in an AlGaAs barrier than in a GaAs well). Thus, a more detailed analysis shows trions X^- (X^+) to be excitons bound on a neutral impurity center in a barrier D_b^0X (A_b^0X), where the electron (hole) neutralizing the impurity center is located in a quantum well, just as a photoexcited exciton. In this connection, the key question is the distance at which the impurity centers responsible for localization are located away from the well. For A_b^0X complexes, we used the method of Ref. 4, based on a study of the energy splitting between the main recombination line of a complex and its cyclotron replica,

associated with a transition A_0 into an excited state after a recombination event, to answer this question. It is difficult to use a similar method for D_b^0X complexes because the characteristic energy splittings are small, showing that the impurity center is located faraway. To solve this problem we investigated a specially developed series of samples with a δ layer of donors located in a barrier at a strictly determined distance from the heteroboundary.

Comparing the experimental data with the computational results enabled us to determine more accurately the mechanism leading to the appearance of a cyclotron replica, to study the variation of its properties for various distances L, and to find the characteristic distance to an impurity center in undoped samples. It is shown that since in undoped samples the number of electrons in a well is much higher than the number of impurities located close to the heteroboundary, there exists a critical distance $L=350$ Å, near which donors form D^- complexes and do not effect the excitonic system.

2. We investigated undoped isolated GaAs quantum wells with a $Al_{0.3}Ga_{0.7}As$ barriers, grown by molecular-beam epitaxy (MBE) on an undoped GaAs substrate according to the following scheme: a 3000 Å thick GaAs buffer layer, an undoped GaAs–AlGaAs (30–100 Å) superlattice with a total thickness of 13000 Å , a 200 Å thick GaAs quantum well, a 600 Å thick AlGaAs spacer, and a 100 Å thick protective GaAs layer. In three samples a δ layer of donors (Si) with density $\sim 10^{10}\,\mathrm{cm}^{-2}$ was formed in the spacer at distances $L=150$, 200, and 250 Åfrom the boundary of the well; the fourth structure was left undoped. All structures, including the undoped sample, contained a low-density two-dimensional electronic channel (with carrier density $\sim 10^{10}\,\mathrm{cm}^{-2}$). The characteristic width of the luminescence lines in the structures investigated was 0.1–0.2 meV in a ~ 10 T magnetic field, indicating the structures to be of high quality. The optical excitation of the system was performed with a Ti/Sp laser with photon energy 1.65 eV. A Ramanor U-1000 double monochromator served as the spectral instrument. Combined with a semiconductor detector with charge coupling (CCD), the monochromator gave a resolution of 0.03 meV. The measurements were performed at 1.5 K temperature in magnetic fields 0–11 T.

3. The photoluminescence spectrum measured in a 2.5 T magnetic field for two circular polarizations in a quantum well with $L=250$ Å, is shown in Fig. 1a. In magnetic fields up to 4 T two main lines dominate the spectrum — a free exciton X and the ground state of the excitonic complex D_b^0X — a singlet S_0. The presence of two equivalent electrons in a D_b^0X complex allows a recombination process in which the remaining electron makes a transition into an excited state. In the process, satellites of the ground recombination line, which reflect the spectrum of the excited states of a D_b^0 center (or a free electron in the limiting case of an unbound trion), appear in the emission spectrum. The first, and brightest, satellite SU_1 shown in Fig. 1a is shifted relative to the ground emission line of the complex downwards in energy by an amount approximately equal to one cyclotron energy quantum. This is clearly seen in Fig. 1b, which shows the magnetic-field dependence of the energy of the emission lines under discussion. The cyclotron satellites were investigated in Ref. 5 and used to prove the three-particle nature of the excitonic complex. Up to now the conventional viewpoint has been that the satellites arise as a result of recombination of the ground state of an excitonic complex — a S_0 singlet. However, when interpreting experimental data, such a model encounters serious difficulties, which are presented below. In the first case, the intensity of the S_0 and SU_1

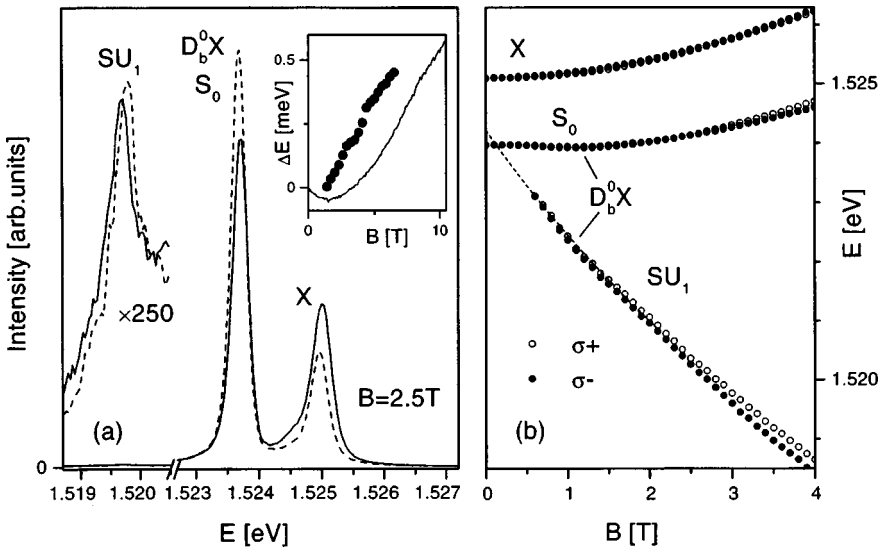

FIG. 1. a) Photoluminescence spectra measured for a quantum well with $L=250$ Å in a 2.5 T magnetic field in σ^- (solid line) and σ^+ (dashed line) polarizations. Inset: The measured energy splitting between the spectral lines in σ^- and σ^+ polarization for D_b^0X (line) and SU_1 (dots) versus the magnetic field. b) Magnetic field dependence of optical transition energies, measured for an undoped quantum well in σ^- (dots) and σ^+ (circles) polarizations.

lines demonstrates a completely different temperature dependence. Thus, as the temperature varies from 1.5 to 20 K, the intensity of the S_0 line decreases by almost an order of magnitude as a result of thermal dissociation of the complex, while the intensity of the SU_1 line decreases only negligibly (see Fig. 4b in Ref. 3). In the second place, if the S_0 and SU_1 lines differ only by the final state of the electron, then they should have the same Zeeman splitting (the energy difference between two circular polarizations). However, as one can easily see from Fig. 1a, in a 2.5 T field this splitting is different not only in magnitude but also in sign, demonstrating fundamentally different magnetic-field dependences, which are shown in the inset. In the third place, the energy difference between the S_0 and SU_1 lines, which should reflect the energy difference between the ground and excited states of the electron remaining after recombination, does not correspond to either the localized-complex model or the free-trion model. Indeed, let us consider the structure of the energy levels of an electron localized in the potential of a charged donor located in the barrier at a certain distance from the heteroboundary. This structure is shown in Fig. 2a. We calculated it using a numerical method similar to that used in Ref. 4 for an acceptor. The spectrum consists of nondegenerate energy levels with a definite projection M of the angular momentum that with increasing magnetic field reach onto linear asymptotic dependences corresponding to Landau levels with the numbers $N=n+(|M|-M)/2$, where $n=0, 1, \ldots$ is the radial quantum number. According to the conventional model, the S_0 and SU_1 lines correspond to a final state with $M=0$ (D_0) and $n=0$, 1, respectively. For a free electron the energy difference between them should be $\hbar\omega_c$. However, for an electron localized on a donor the difference is always greater than $\hbar\omega_c$. In the limit $B\to 0$ the energy splitting is equal to the localization energy of the

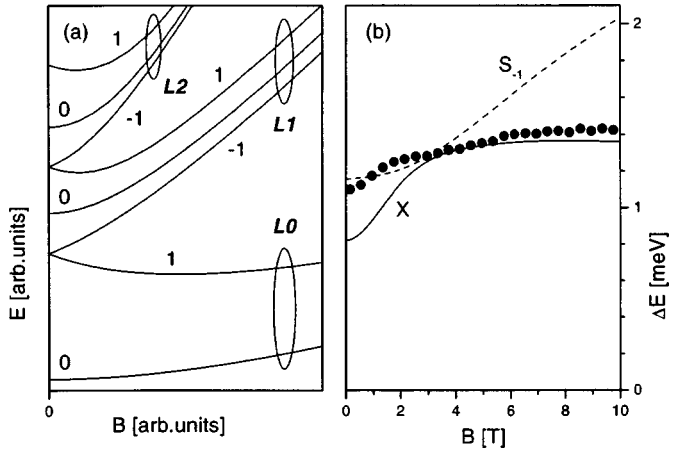

FIG. 2. a) Electron energy level diagram calculated for a donor located at a distance $L=100$ Å from the well. States with angular momentum $M=0, \pm 1$, forming the first three Landau levels $L0,1,2$, are shown. b) Magnetic-field dependence of the binding energy of an excitonic complex (energy difference of an exciton and ground state S_0), measured (dots) in a quantum well with $L=250$ Å and computed theoretically (solid line). The dashed line shows the field dependence of the energy difference between the excited S_{-1} and ground S_0 states of an excitonic complex.

complex. The dependence of this energy on the distance L, measured for all experimental samples, is shown at the bottom of Fig. 3a. As one can see, in an undoped sample, corresponding to the point $L=350$ Å (for reasons presented below), the intercept is negative. This is also clearly seen in Fig. 1b, which shows the extrapolation of the field dependence (as $B\rightarrow 0$) of the energy of a SU_1 transition measured for an undoped sample.

Thus, the experimental data show that the initial state for a cyclotron replica SU_1 is not the ground state of a singlet S_0 but rather a state with higher energy. In addition, these excited states of the excitonic complex do not appear in the luminescence spectra (Fig. 1a), since additional spectral lines, besides the free-exciton line, are not observed above the ground recombination line S_0. In addition, the result that the localization energies are negative makes it necessary to assume that the final state is also an excited state of the donor. To check this we developed a numerical method, based on a 4×4 Luttinger Hamiltonian,[6] that takes account of the complicated structure of the valence band and the three-dimensional character of the particle motion in the well. The matrix elements of the Hamiltonian were calculated in the cylindrical gauge similarly to Ref. 7, but in contrast to this and other calculations we expressed the three-dimensional basis functions as products of the numerical solutions obtained for one-dimensional differential equations by the relaxation method.[8] The three-particle wave function was written in a basis consisting of products of single-particle functions. An improved variant of a procedure for selecting basis functions, as described in Ref. 9, was used to decrease the computational time for diagonalization. A standard set of the band parameters of the materials, which is used in Ref. 7, was taken. To check the computational method we calculated the field dependence of the binding energy of the ground state of a complex S_0, which can easily be measured as the difference of the energies of the recombination lines of an exciton X and a complex

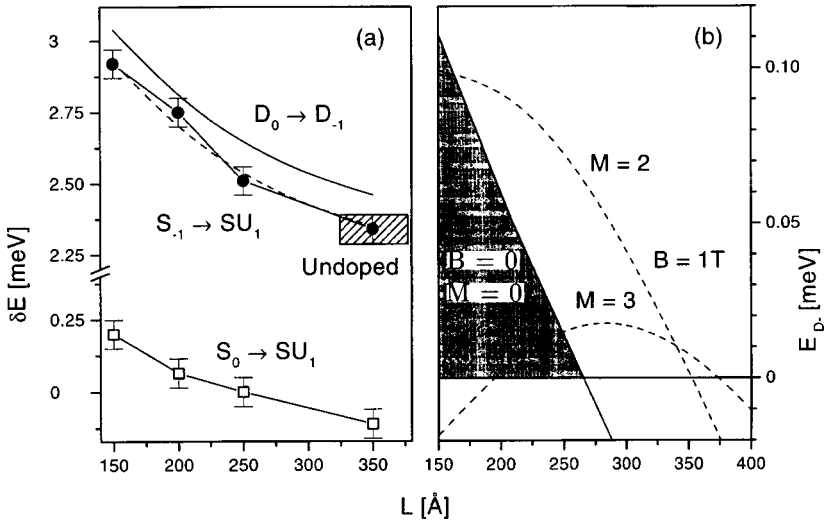

FIG. 3. a) Localization energy δE of charged excitons versus the distance L from the donor to the heteroboundary, measured for all experimental samples. The values of δE obtained from the splitting between the ground state S_0 of a complex and the cyclotron replica SU_1 are shown by squares, and the values obtained from the splitting between the excited state S_{-1} and the replica SU_1 are shown by dots. The solid line shows the theoretical dependence $\delta E(L)$ calculated for the energy difference between the states of an electron on a donor with angular momenta $M=-1$ and 0. b) Binding energy of the second electron on a donor (D^- center) versus the distance L from the donor to the heteroboundary, calculated for magnetic fields $B=0$ (solid line) and $B=1$ T (dashed line).

S_0. The result is compared in Fig. 2b with the experimental points. The good agreement between the computed and measured binding energies demonstrates that the method works. We also calculated the energy of the complex for different values of the total angular momentum $J=M+S$, equal to the sign of the orbital angular momentum M of the complex and the spin angular momentum $S=\pm 3/2$ of a hole. It turned out that the first excited state of the system after the singlet S_0 with $M=0$ and the triplet T_1 with $M=1$[10] is a singlet S_{-1} with $M=-1$ and the required properties. Indeed, in accordance with the law of conservation of angular momentum this state can recombine only with a donor state with $M=-1$ (D_{-1}), which is an excited state (Fig. 2a). The energy difference between the state S_{-1} and the ground state S_0 is shown in Fig. 2b (dashed line). As one can see, this state is close in energy to an exciton and is probably an intermediate metastable state in the process of energy relaxation of hot electrons into the S_0 state. It is quite long-lived, since relaxation into the state S_0 involves a change in the angular momentum. Although it is not stable with respect to decay into an electron and an exciton, its appearance in the recombination spectra is quite likely, just as the high-energy cyclotron replicas[3] associated with recombination from high-lying excited states of a complex.

To show that the state S_{-1} is indeed the initial state for the SU_1 line, we compared the splitting expected in this case between the SU_1 line and the ground recombination

line S_0 with the experimentally observed splitting, using the following method. Since the S_0 line corresponds to the recombination process $S_0 \rightarrow D_0 + h\nu_1$ and the SU_1 line corresponds to the process $S_{-1} \rightarrow D_{-1} + h\nu_2$, we have $\Delta E_D = \Delta E_S + (h\nu_1 - h\nu_2)$, where ΔE_D and ΔE_S are the energy differences for states with $M = -1$ and 0 for a donor and a singlet complex, respectively. We determined the right and left-hand sides of this inequality as a function of the magnetic field B for all experimental samples and then fit the formula $\Delta E(B)^2 = (\alpha B)^2 + \delta E^2$ to them, thereby determining the localization energy δE as a function of distance to the donor. The results are shown in Fig. 3a, where the solid line is the computational result for a donor and the filled circles were obtained by analyzing the experimental data taking account of the correction by ΔE_S. As one can see from the figure, the proposed model describes the experimental data much better than the assumption that the replica SU_1 arises as a result of recombination of S_0 (squares in Fig. 3a). The remaining systematic error of 0.1 meV seems to be due to the inaccuracy of the numerical model and was taken into account when fitting the theoretical dependence (shown by the dashed curve in Fig. 3a) to the experimental data. From the localization energy measured in an undoped sample we estimated according to the theoretical dependence used for the fit, the characteristic distance L to the donor realized in this structure (hatched rectangle in Fig. 3a). It is evident that the characteristic distance is $L \approx 350$ Å, and the localization energy is $\delta E \approx 2.3$ meV. The fact that δE is much greater than the binding energy of an exciton on a donor (1.2 meV) means that it is impossible to observe a trion in unlocalized form. Under these conditions an increase of temperature will result most likely in efficient dissociation of an exciton and a neutral donor rather than ionization of a complex with formation of a free trion and a charged impurity. This is precisely the behavior we observed in our experiment.[3]

Our results raise the question of why we can determine a concrete, nonzero, threshold quantity L_{cr} with a uniform distribution of residual impurities in an undoped sample (the characteristic volume donor density in the barrier is $N_D \sim 10^{15}\,\mathrm{cm}^{-3}$) and we do not see large broadening of the S_0 and SU_1 lines caused by a strong dependence of the binding energy on the distance for small L? Our explanation is that in undoped quantum wells the density of residual closely-spaced ($L < L_{cr}$) donors is much lower ($n_D = N_D L_{cr} \sim 10^9\,\mathrm{cm}^{-2}$) than the density of two-dimensional electrons, and these charged impurity centers capture two electrons each, forming a D^- complex.[11] Because of the Pauli principle the binding energy of an exciton on a D^- complex is negative, and therefore excitons are localized only on donors located on the D^- stability boundary, where the localization energy, which decreases with increasing L, is maximum. Since for large $L > L_{cr}$ the localization energy of an exciton is a weakly varying function of L, the broadening of the lines S_0 and SU_1 is also weak. To check this we calculated the dependence of the binding energy of a second electron in D^- as a function of L. The results are shown in Fig. 3b. It is evident that in a zero magnetic field the D^- stability boundary passes at a distance ≈ 265 Å from the well, in complete agreement with the calculations in Ref. 11. In a 1 T magnetic field this distance increases to 375 Å , which agrees well with our result for an undoped quantum well.

This work was supported by the Russian Fund for Fundamental Research and the ''Physics of Solid-State Nnanostructures'' program.

[1] M. A. Lampert, Phys. Rev. Lett. **1**, 450 (1950).
[2] K. Kheng, R. T. Cox, Y. M. d'Aubique *et al.*, Phys. Rev. Lett. **71**, 1752 (1993); A. J. Shields, J. L. Osborne, M. Y. Simmons *et al.*, Phys. Rev. B **52**, R5523 (1995).
[3] O. V. Volkov, V. I. Zhitomirskiĭ, I. V. Kukushkin *et al.*, JETP Lett. **66**, 766 (1997).
[4] O. V. Volkov, I. V. Kukushkin, K. von Klitzing *et al.*, JETP Lett. **68**, 236 (1998).
[5] G. Finkelstein, H. Shtrikman, and I. Bar-Joseph, Phys. Rev. B **53**, 12593 (1996).
[6] J. M. Luttinger, Phys. Rev. **102**, 1030 (1956).
[7] G. E. W. Bauer and T. Ando, Phys. Rev. B **38**, 6015 (1988).
[8] O. V. Volkov, V. E. Zhitomirskii, I. V. Kukushkin *et al.*, Phys. Rev. B **56**, 7541 (1997).
[9] D. M. Whittaker and A. J. Shields, Phys. Rev. B **56**, 15185 (1997).
[10] A. J. Shields, M. Pepper, M. Y. Simmons *et al.*, Phys. Rev. B **52**, 7841 (1995).
[11] H. L. Fox and D. M. Larsen, Phys. Rev. B **51**, 10709 (1995).

Translated by M. E. Alferieff

Oscillations of the thermodynamic properties of a one-dimensional mesoscopic ring caused by Zeeman splitting

M. V. Moskalets
pr-t Il'icha 93-a, kv. 48, Khar'kov, 310020 Ukraine

(Submitted 19 May 1999; resubmitted 24 September 1999)
Pis'ma Zh. Éksp. Teor. Fiz. **70**, No. 9, 595–600 (10 November 1999)

It is shown that the interrelationship of spin splitting in a magnetic field and spatial quantization in a one-dimensional ballistic ring coupled with a reservoir results in mesoscopic oscillations of a new type which vanish with increasing temperature. The period of such oscillations is inversely proportional to the density of states in the spin subsystem in the ring. © *1999 American Institute of Physics.*
[S0021-3640(99)00821-X]

PACS numbers: 73.23.Ra, 71.70.Ej

The oscillations of the thermodynamic[1] and the kinetic[2] properties of doubly-connected samples (rings) at low temperatures as a function of the magnetic flux with period equal to the magnetic flux quantum $\Phi_0 = h/e$ is a fundamental effect in mesoscopic physics, and it is a manifestation of the Aharonov–Bohm (AB) effect[3] in solids. In thermodynamics this effect leads to the existence of thermodynamically equilibrium (persistent) currents in normal (nonsuperconducting) rings. Such currents were predicted theoretically in Refs. 4 and 5 and observed experimentally in Refs. 6–8. Persistent currents are due to the AB effect in systems with a discrete spectrum. As the temperature increases, the persistent current vanishes when the temperature exceeds the characteristic splitting between the energy quantization levels of electrons in the ring.[1]

An important property of a persistent current is the parity effect,[9–12] which is that the properties of the current depend on the parity of the number of particles N_0 in the ground state for spinless electrons or on N_0 modulo 4 for electrons with spin. This effect occurs for isolated rings and for rings coupled with an electron reservoir.[11,13,14] Specifically, for an even number of electrons with spin in the ground state the period of the AB oscillations is equal to the magnetic flux quantum, while the period for odd N_0 is $\Phi_0/2$.

Although a magnetic flux formally acts only on the charge degree of freedom of a system of electrons, because of parity the spin subsystem also strongly influences the AB oscillations, an effect which is especially strong when the interelectronic interaction is taken into account.[1] Specifically, such an influence results in the existence of fractional AB oscillations with period Φ_0/N_0 in isolated systems with a small number of electrons $N_0 \geqslant 1$.[15,12,16] In systems with a large number of particles, in the general case fractional oscillations do not occur,[16] but the interaction with a spin subsystem can decrease the period of the AB oscillations by a factor of 2 or 4.[14]

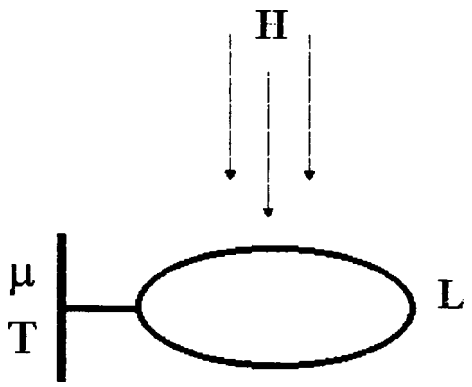

FIG. 1. One-dimensional ring of length L in a perpendicular magnetic field H. The ring is weakly coupled with an electron reservoir with chemical potential μ and temperature T.

Thus, the action on a spin subsystem will ultimately be manifested in a persistent current. The interaction with a magnetic field producing a magnetic flux in a ring lifts the spin degeneracy, and as will be shown in the present letter it results in the existence of a new type of mesoscopic oscillations in a ring coupled with a reservoir. Specifically, as the intensity of the magnetic field varies, the state of the electronic system oscillates (with a period in terms of the magnetic flux much greater than Φ_0) between a state characteristic for rings with even N_0 and a state characteristic for odd N_0 (see Ref. 14). These states differ qualitatively from one another. Specifically, as already noted, the fundamental period of the AB oscillations is Φ_0 in the first case and $\Phi_0/2$ in the second case.

Let us consider a one-dimensional ballistic ring (Fig. 1) with length L, weakly coupled with an electron reservoir with chemical potential μ and temperature T low enough so that inelastic processes in the ring can be neglected. A magnetic field H, corresponding to magnetic flux $\Phi = HL^2/4\pi$ through the ring, is applied perpendicular to the plane of the ring. We shall assume that the chemical potential of the electron reservoir does not depend on the magnetic field and is the same for electrons with opposite spins. Assuming the number N_e of particles in the ring to be large, we can linearize the electron spectrum near the Fermi points and describe the interacting electrons on the basis of a Luttinger-liquid model.[17] Then the Lagrangian L_{LL} in the boson form for an electron system has the form[18]

$$L_{LL} = \frac{\hbar v_p}{2g_\rho}\left\{\frac{1}{v_\rho^2}\left(\frac{\partial\theta_\rho}{\partial t}\right)^2 - \left(\frac{\partial\theta_\rho}{\partial x}\right)^2\right\} + \frac{\hbar v_\sigma}{2g_\sigma}\left\{\frac{1}{v_\sigma^2}\left(\frac{\partial\theta_\sigma}{\partial t}\right)^2 - \left(\frac{\partial\theta_\sigma}{\partial x}\right)^2\right\}, \tag{1}$$

where x is the coordinate along the ring, t is the time, and v_i and g_i are the Haldane parameters ($i = \rho, \sigma$). The indices ρ and σ mark quantities describing the charge and spin degrees of freedom. We take account of the interaction with the magnetic field and particle exchange with the reservoir by means of the following Lagrangian:

$$L_{\text{int}} = \frac{2\hbar}{L}\pi^{1/2}\left\{\frac{\partial\theta_\rho}{\partial t}\left[\frac{k_{j\rho}}{4} + \frac{\Phi}{\Phi_0}\right] + \frac{\partial\theta_\sigma}{\partial t}\frac{k_{j\sigma}}{4}\right\} + \frac{g}{2}\beta H\frac{N_\sigma}{L} + \mu\frac{N_\rho}{L}. \tag{2}$$

Here $k_{j\rho}$ and $k_{j\sigma}$ are topological numbers determined by the parity of the numbers $N_{e\uparrow}$ and $N_{e\downarrow}$ of electrons with a definite spin projection in the ring;[11,14] g is the gyromagnetic ratio for electrons in the ring; $\beta = e\hbar/(2m)$ is the Bohr magneton. The numbers of charge and spin excitations in the ring are the same, correspondingly, $N_\rho \equiv N_e = N_{e\uparrow} + N_{e\downarrow}$ and $N_\sigma = N_{e\uparrow} - N_{e\downarrow}$. In our case the interaction with a uniform magnetic field H actually reduces to the AB interaction[1] [first term in Eq. (2)] and a Zeeman interaction [second term in Eq. (2)], which does not depend on the orbital motion. We note that for a nonuniform magnetic field the Zeeman interaction results in an effective spin-orbit interaction.[19]

We shall now calculate the magnetic field dependent part $\Delta\Omega(H)$ of the thermodynamic potential of the electrons in the ring. It is known[11] that in the ballistic case this dependence is determined by the contribution of the zeroth modes of the bosonic fields. We shall assume that for $H=0$ the ground state is nonmagnetic: $N_{0\sigma}=0$. Calculations similar to those presented in Ref. 14 give

$$\Delta\Omega(H) = -T\ln(Z), \tag{3}$$

where

$$\begin{aligned} Z = \Big\{ & \theta_3(2\phi, q_\rho^4)\,\theta_3(0, q_\sigma^4)\,\theta_3(2\delta_\mu, q_{0\rho}^4)\,\theta_3(2\delta_z, q_{0\sigma}^4) \\ & + \theta_2(2\phi, q_\rho^4)\,\theta_2(0, q_\sigma^4)\,\theta_2(2\delta_\mu, q_{0\rho}^4)\,\theta_2(2\delta_z, q_{0\sigma}^4) \\ & + \theta_3\left(\left(2\phi + \frac{1}{2}\right), q_\rho^4\right)\theta_3\left(\frac{1}{2}, q_\sigma^4\right)\theta_3\left(\left(2\delta_\mu + \frac{1}{2}\right), q_{0\rho}^4\right)\theta_3\left(\left(2\delta_z + \frac{1}{2}\right), q_{0\sigma}^4\right)\Big\}. \end{aligned}$$

Here

$$\theta_2(v,q) = 2\sum_{n=0}^{\infty} q^{(n+1/2)^2}\cos\left(2\pi\left(n+\frac{1}{2}v\right)\right), \quad \theta_3 = (v,q) = 1 + 2\sum_{n=1}^{\infty} q^{n^2}\cos(2\pi n v)$$

is the Jacobi theta function;[20]

$$q_{\rho(\sigma)} = \exp\left(-\frac{T}{2T^*_{\rho(\sigma)}}\right); \quad q_{0\rho(\sigma)} = \exp\left(-\frac{\pi^2 T}{8T_{0\rho(\sigma)}}\right),$$

where

$$T^*_{\rho(\sigma)} = \frac{\hbar v_{\rho(\sigma)} g_{\rho(\sigma)}}{\pi L}, \quad T_{0\rho(\sigma)}\frac{\pi\hbar v_{\rho(\sigma)}}{g_{\rho(\sigma)}L}; \quad \phi = \frac{\Phi}{\Phi_0}\ \mathrm{mod}1;$$

$$\delta_\mu = \frac{\mu}{4T_{0\rho}}\ \mathrm{mod}1; \quad \delta_z = \frac{g\beta H}{8T_{0\sigma}}\ \mathrm{mod}1.$$

The expression (3) was obtained for an odd number $N_{0\uparrow(\downarrow)}$ of electrons with a definite spin projection in the ground state ($T=0$, $H=0$, $\delta_\mu=0$). For an even number $N_{0\uparrow(\downarrow)}$ the formal substitution $\phi \to \phi + 0.5$ must be made in the expression (3). Comparing the

expression (3) with the expressions presented in Ref. 14 it can be concluded that as a function of the parameter δ_z we obtain an expression describing a system with an even number of particles in the ground state ($\delta_z=0$) as well as an expression describing a system with odd N_0 ($\delta_z=1/4$).

It is obvious that the magnetic field enters in two ways in the expression for $\Delta\Omega$. First, it enters via the parameter ϕ, which gives rise to the conventional AB oscillations (with a period in terms of the magnetic flux Φ_0) in an isolated ring ($N_e=\text{const}$) and in a ring coupled with a reservoir ($\mu=\text{const}$). Second, it enters via the parameter δ_z, which also results in oscillations of the thermodynamic potential in a magnetic field. In the present letter we analyze oscillations of the second type. We note that in the present model such oscillations exist only in the $\mu=\text{const}$ regime and they are absent for an isolated ring.

Physically, the oscillations under study are due to the following. As the magnetic field increases, for electrons with a definite spin projection spin splitting results in a monotonic shift of the spatial quantization levels in the ring relative to a fixed chemical potential μ. Ultimately, this increases the number of electrons with spin projection along the field in the ground state of the ring and decreases the number of electrons with the opposite spin projection, i.e., the number of excitations in the ground state becomes different from zero, $N_{0\sigma}\neq 0$. The number of charge excitations $N_{0\rho}$ in the ground state remains unchanged. For this reason, the Coulomb blockade effect,[21] which is important for mesoscopic systems and is due to a small electrostatic capacitance of the system, has no effect on the oscillations under study.

Let us now determine the period of the oscillations which are due to the Zeeman effect. Since the function $\theta_2(v,q)$ is periodic with period 2 as a function of the first argument and the period of the function $\theta_3(v,q)$ is 1 with respect to v, we conclude from the expression (3) that the period of the oscillations under study is

$$\Delta\left(\frac{g}{2}\beta H\right)=4T_{0\sigma}. \tag{4}$$

The quantity $4T_{0\sigma}$ determines the energy required to increase the number of spin excitations in the ring. Thus, in a model of noninteracting electrons ($g_\rho=g_\sigma=2$; $v_\rho=v_\sigma=v_F$, where v_F is the Fermi velocity) we have $T_{0\sigma}=T_{0\rho}=\Delta_F/4$, where Δ_F is the splitting between the energy levels of electrons near the Fermi energy (for $H=0$). Thus, taking account of the chiral and spin degeneracies, the period (4) of the oscillations corresponds to a change in the number of spin excitations by 4.

Next, let us calculate the persistent current $I=-\partial\Omega/\partial\Phi$ in the ring. When differentiating with respect to Φ, the parameter δ_z can be assumed to be constant, since the corresponding period [see Eq. (4)] scaled to the magnetic flux (for noninteracting electrons)

$$\Delta\Phi=\Phi_0\frac{2}{g}\frac{m}{m^*}\frac{N_0}{4}$$

(where m^* is the electron effective mass) is much greater than the period Φ_0 of the AB oscillations. The change in δ_z accompanying a change in Φ gives corrections of the order of $1/N_0$, which can be neglected. Thus, in the mesoscopic limit $N_0\gg 1$ in a one-

dimensional ring the Zeeman effect does not distort the AB oscillations, but it leads to a periodic variation of the amplitude of such oscillations as a function of the magnetic field. We present an expression for the sum of the amplitudes of all odd harmonics $I_1 = I(\phi = \frac{1}{4})$. We note that I_1 for $T \gg T_\rho^*$ is actually the amplitude of the first harmonic of the current:

$$I_1 = \frac{T}{\Phi_0} \frac{F\left(\frac{1}{4}, q_\rho\right)}{Z\left(\phi = \frac{1}{4}\right)} \theta_3\left(\frac{1}{2}, q_\rho^4\right) \theta_2(0, q_\sigma^4)\, \theta_2(2\delta_\mu, q_{0\rho}^4)\, \theta_2(2\delta_z, q_{0\sigma}^2), \tag{5}$$

where

$$F(\nu, q) = 2\pi \sum_{n=1}^{\infty} (-1)^n \frac{\sin(2\pi n \nu)}{\sinh(n \ln(1/q))}.$$

The asymptotic representation of I_1 in the limit $T \to 0$ and at high temperatures for the model of noninteracting electrons are as follows:

$$I_1 / I_0 = \begin{cases} -\dfrac{1 - \exp\left(-\dfrac{\Delta_F}{T}\left(\dfrac{1}{4} - \left|\delta_z\right|\right)\right)}{1 + \exp\left(-\dfrac{\Delta_F}{T}\left(\dfrac{1}{4} - \left|\delta_z\right|\right)\right)}, & T \ll \dfrac{\Delta_F}{2\pi^2}, \quad \delta_m = 0, \quad |\delta_z| < \dfrac{1}{2}, \\ -\dfrac{16\pi T}{\Delta_F} \exp\left(-\dfrac{2\pi^2 T}{\Delta_F}\right) \cos(2\pi\delta_\mu) \cos(2\pi\delta_z), & T \gg \dfrac{\Delta_F}{2\pi^2}, \end{cases} \tag{6}$$

where $I_0 = e v_F / L$.

It follows from the expressions presented that the quantity I_1 for $\delta_z = \pm 1/4$ vanishes and the period of the AB oscillations decreases by a factor of 2. This is due to the change in the number of spin excitations in the ring by 1 (compared with $\delta_z = 0$). In this case the numbers of electrons with the opposite direction of the spin have a different parity, which, as is well known,[1,14] gives rise to a period of $\Phi_0/2$ for the AB oscillations. At the same time, I_1 changes sign for $\delta_z = 1/2$ as a result of a change in the number of spin excitations in the ring by 2. Figure 2 shows I_1 (curve *1*) as a function of the magnetic field (the parameter δ_z). The figure also shows the analogous dependence (curve *2*) for the sum of the amplitudes I_2 of the even harmonics. We note that as temperature increases, $T \gg T_{0\sigma}$, and quantization of the spectrum of the spin subsystem becomes immaterial, the oscillations under study vanish.

In summary, for sufficiently strong magnetic fields the spin splitting can result in an additional (by π) change in the phase of the AB oscillations or in a decrease in the period of the oscillations by a factor of 2. Let us estimate the characteristic change ΔH of the magnetic field [see expression (4)] for which this effect can be observed. A persistent current has been observed experimentally in ballistic rings produced in a two-dimensional electron gas in a GaAsAs/GaAs heterostructure.[8] In this case $L \approx 10^{-5}$ m

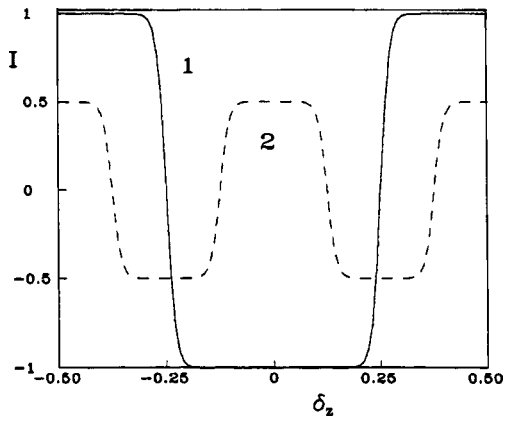

FIG. 2. Sum of the amplitudes of odd I_1 (*1*) and even I_2 (*2*) harmonics of the persistent current in units of $I_0 = ev_F/L$ versus the magnetic field (the parameter δ_z) for noninteracting electrons. $T/\Delta_F = 0.01$, $\delta_\mu = 0$.

and $v_F = 2.6 \times 10^5$ ms^{-1}. Assuming the gyromagnetic ratio $g = 2$, in the model of noninteracting electrons we obtain $\Delta H = 1.8$ T, which corresponds to $\delta_z = 1$. We note that the period of the AB oscillations is $\Delta H_{AB} \approx 5 \times 10^{-4}$ T.

In the present letter we studied the influence of the Zeeman effect on the thermodynamic properties of a uniform ballistic ring coupled with a reservoir and containing interacting electrons in a perpendicular magnetic field. It was shown that spin splitting causes the properties of the ring to oscillate with a nonuniversal period in terms of the magnetic flux period. This period is proportional to the product of the magnetic flux quantum $\Phi_0 = h/e$ and the number N_0 of particles in the ring. This effect introduces an additional phase change in the AB oscillations as a function of the magnetic field as a result of a change in the number of spin excitations in the ring.

[1] A. A. Zvyagin and I. V. Krive, Fiz. Nizk. Temp. **21**, 687 (1995) [Low Temp. Phys. **21**, 533 (1995)].
[2] S. Washburn and R. A. Webb, Adv. Phys. **35**, 375 (1986).
[3] Y. Aharonov and D. Bohm, Phys. Rev. **115**, 484 (1959).
[4] I.O. Kulik, JETP Lett. **11**, 275 (1970).
[5] M. Büttiker, Y. Imry, and R. Landauer, Phys. Lett. A **96**, 365 (1983).
[6] L. P. Levy, G. Dolan, J. Dunsmuir, and H. Bouchiat, Phys. Rev. Lett. **64**, 2074 (1990).
[7] V. Chandrasekhar, R. A. Webb, M. J. Brady *et al.*, Phys. Rev. Lett. **67**, 3578 (1991).
[8] D. Mailly, C. Chapelier, and A. Benoit, Phys. Rev. Lett. **70**, 2020 (1993).
[9] A. J. Leggett, in *Granular Nanoelectronics*, edited by D. K. Ferry, J. R. Barker, C. Jacoboni, NATO ASI, Ser. B, vol .**251** (Plenum, New York, 1991) p. 297.
[10] F. V. Kusmartev, JETP Lett. **53**, 28 (1991).
[11] D. Loss, Phys. Rev. Lett. **69**, 343 (1992).
[12] N. Yu and M. Fowler, Phys. Rev. B **45**, 11795 (1992).
[13] M. V. Moskalets, Eur. Phys. J. B **7**, 645 (1999).
[14] M. V. Moskalets, Physica E **4**, 17 (1999).
[15] F. V. Kusmartsev, J. Phys.: Condens. Matter **3**, 3199 (1991).
[16] F. V. Kusmartsev, J. E. Weisz, R. Kishore, and M. Takahashi, Phys. Rev. B **49**, 16234 (1994).
[17] F. D. M. Haldane, J. Phys. C **14**, 2585 (1981).
[18] C. L. Kane and M. P. A. Fisher, Phys. Rev. B **46**, 15233 (1992).
[19] D. Loss and P. M. Goldbart, Phys. Rev. B **45**, 13544 (1992).

[20] H. Bateman, *Higher Transcendental Functions*, edited by A. Erdélyi (McGraw-Hill Book Company, Inc., New York, 1953).
[21] D. V. Averin and K. K. Likharev, in *Mesoscopic Phenomena in Solids*, edited by B. Altshuler, P. A. Lee, and R. A. Webb (Elsevier, Amsterdam, 1991).

Translated by M. E. Alferieff

Fermion zero modes on vortices in chiral superconductors

G. E. Volovik

Helsinki University of Technology, Low Temperature Laboratory, FIN-02015 HUT, Finland; Landau Institute of Theoretical Physics, Russian Academy of Sciences, 117334 Moscow, Russia

(Submitted 30 September 1999)
Pis'ma Zh. Éksp. Teor. Fiz. **70**, No. 9, 601–606 (10 November 1999)

The energy levels of fermions bound to the vortex core are considered for the general case of chiral superconductors. There are two classes of chiral superconductivity: in the class I superconducting state the axisymmetric singly quantized vortex has the same energy spectrum of bound states as in an *s*-wave superconductor: $E=(n+1/2)\omega_0$, with integral n. In class II the corresponding spectrum is $E=n\omega_0$ and thus contains a state with exactly zero energy. The effect of a single impurity on the spectrum of bound states is also considered. For class I the spectrum acquires the doubled period $\Delta E=2\omega_0$ and consists of two equidistant sets of levels, in accordance with A. I. Larkin and Yu. N. Ovchinnikov, Phys. Rev. B **57**, 5457 (1998). For the class II states the spectrum is not influenced by a single impurity if the same approximation is applied.
[S0021-3640(99)00921-4]

PACS numbers: 74.20.Mn, 74.60.Ge

INTRODUCTION

Low-energy fermions bound to the vortex core play the main role in the thermodynamics and dynamics of the vortex state in superconductors and Fermi superfluids. The spectrum of the low-energy bound states in the core of the axisymmetric vortex with winding number $m=\pm 1$ in the isotropic model of *s*-wave superconductors was obtained in the microscopic theory by Caroli, de Gennes and Matricon:[2]

$$E_n=\omega_0\left(n+\frac{1}{2}\right). \tag{1}$$

This spectrum is twofold degenerate due to spin degrees of freedom. The integral quantum number n is related to the angular momentum of the fermions, $n=-mL_z$. The level spacing is small compared to the energy gap of the quasiparticles outside the core, $\omega_0 \sim \Delta^2/E_F \ll \Delta$. Therefore, in many physical cases the discreteness of n can be neglected and one can apply the quasiclassical approach to calculate the energy spectrum. Using this simplified approach, one finds that the spectrum crosses zero energy as a function of continuous angular momentum L_z. Thus one has fermion zero modes. The fermions in

this 1D ''Fermi liquid'' are chiral: the positive-energy fermions have a definite sign of the angular momentum L_z. In the general case of arbitrary winding number m, the number of fermion zero modes, i.e., the number of branches crossing the zero level, equals $-2m$ (see Ref. 3). This represents an analog of the well-known index theorem of relativistic quantum field theory.

At low temperature $T \sim \omega_0$ the discrete nature of the spectrum becomes important. The quantization of the zero modes was obtained within the quasiclassical approach using the Bohr–Sommerfeld scheme.[4] However, the term 1/2 in Eq. (1), which came from the phase shift, was missing in this approach and was restored only on the basis of general symmetry arguments in Ref. 5. Here we extend the quasiclassical approach and obtain an exact quantization rule. We find that in respect to the phase shift the superconducting/superfluid states can be divided into two classes: In the states of class I the spectrum of bound states in the $m = \pm 1$ vortices is the same as in Eq. (1). In the states of class II the corresponding spectrum is:

$$E_n = \omega_0 n. \tag{2}$$

It contains the state with $n = 0$, which has exactly zero energy. The representatives of this class are the superfluid ^{3}He–A, where the existence of the zero-energy bound state was first calculated by Kopnin and Salomaa in a microscopic theory,[6] and possibly the layered superconductor Sr_2RuO_4, in which chiral p-wave superconductivity is suggested.[7]

Using the quasiclassical approach, we also consider how the spectrum changes under the influence of a single impurity in the vicinity of the vortex core. We find that the Larkin–Ovchinnikov result obtained for the s-wave vortex[1,8] is valid only for the class I superconducting states.

QUASICLASSICAL APPROACH TO BOUND STATES IN THE VORTEX CORE

In this approach, developed in Refs. 3, 9, and 4, the fast radial motion of the fermions in the vortex core is integrated out, and one obtains only the slow motion corresponding to the fermion zero modes. Since many properties of the fermion zero modes do not depend on the exact structure of the order parameter and vortex core, we consider for simplicity the following pairing states:

$$\text{spin singlet:} \quad \mathbf{\Delta} = \Delta(\mathbf{r})(\hat{p}_x + i\hat{p}_y)^N \hat{p}_z^{l-|N|}, \quad \text{odd } l, \tag{3}$$

$$\text{spin triplet:} \quad \mathbf{\Delta} = \sigma_z \Delta(\mathbf{r})(\hat{p}_x + i\hat{p}_y)^N \hat{p}_z^{l-|N|}, \quad \text{even } l. \tag{4}$$

Here $\hat{\mathbf{p}}$ is the direction of the quasiparticle momentum, N and $l \geqslant |N|$ are integers, and σ_z is the Pauli matrix for conventional spin. Chiral superconductors are characterized by a nonzero value of the index N, which in our simple case represents the projection of the orbital angular momentum l of the Cooper pair along the z axis. For example, an s-wave superconductor has numbers $N = l = 0$ in Eq. (3), while the triplet p-wave ($l = 1$) superconductor, with an order parameter of the ^{3}He–A type, is specified by the numbers $|N| = l = 1$ in Eq. (4). The index N is also the topological invariant in momentum space which is responsible for the Chern–Simons terms in the 2D superfluids/superconductors (see Refs.10–12), and for this reason it is well-defined even in cases when the momentum l and its projection are undefined.

We assume the following structure of the order parameter in the core:

$$\Delta(\mathbf{r}) = \Delta(r) e^{im\phi}, \tag{5}$$

where z, r, ϕ are the coordinates of a cylindrical coordinate system with the z axis along the vortex line.

The Bogoliubov–Nambu Hamiltonian for quasiparticles is given by

$$\mathcal{H}_{\mathbf{p}} = \begin{pmatrix} \dfrac{p^2 - p_F^2}{2m_e} & \Delta \\ \Delta^* & -\dfrac{p^2 - p_F^2}{2m_e} \end{pmatrix}. \tag{6}$$

In the quasiclassical approach it is assumed that the characteristic size ξ of the vortex core is much larger than the wavelength: $\xi p_F \gg 1$. In this quasiclassical limit the description in terms of trajectories is most relevant. The trajectories are almost straight lines. The low-energy trajectories are characterized by the momentum $\mathbf{q}$ of the incident quasiparticle on the Fermi surface, i.e., with $|\mathbf{q}| = p_F$, and the impact parameter b. Let us consider for simplicity the 2D or layered superconductors, so that $\mathbf{q} = p_F(\hat{\mathbf{x}} \cos\theta + \hat{\mathbf{y}} \sin\theta)$. Then, after substituting $\Psi \to e^{i\mathbf{q}\cdot\mathbf{r}}\Psi$ and $\mathbf{p} \to \mathbf{q} - i\nabla$ and expanding in small ∇, we obtain the quasiclassical Hamiltonian for the fixed trajectory $\mathbf{q}, b$:

$$\mathcal{H} = -i\tau_3 \mathbf{v}_F \cdot \nabla + \Delta(r)[\tau_1 \cos(N\theta + m\phi) - \tau_2 \sin(N\theta + m\phi)], \quad \mathbf{v}_F = \frac{\mathbf{q}}{m_e}. \tag{7}$$

We have omitted the spin indices, since they are not important for the spectrum in the superconducting states under consideration.

Since the spatial derivative is along the trajectory, it is convenient to choose the coordinate system as follows: $s = r\cos(\phi - \theta)$ is the coordinate along the trajectory, and $b = r\sin(\phi - \theta)$ (see, e.g., Ref. 6). In this system the Hamiltonian is

$$\mathcal{H} = -iv_F \tau_3 \partial_s + \tau_1 \Delta(r) \cos(m\tilde{\phi} + (m+N)\theta) - \tau_2 \Delta(r) \sin(m\tilde{\phi} + (m+N)\theta), \quad \tilde{\phi} = \phi - \theta. \tag{8}$$

The dependence of the Hamiltonian on the direction θ of the trajectory can be removed by the following transformation:

$$\Psi = e^{i(m+N)\tau_3\theta/2}\tilde{\Psi}, \tag{9}$$

$$\tilde{\mathcal{H}} = e^{-i(m+N)\tau_3\theta/2}\mathcal{H}e^{i(m+N)\tau_3\theta/2} = -iv_F\tau_3\partial_s + \Delta(\sqrt{s^2+b^2})(\tau_1 \cos m\tilde{\phi} - \tau_2 \sin m\tilde{\phi}), \tag{10}$$

$$\tan\tilde{\phi} = \frac{b}{s}. \tag{11}$$

Now θ enters only the boundary condition for the wave function, which according to Eq. (9) is

$$\tilde{\Psi}(\theta + 2\pi) = (-1)^{m+N}\tilde{\Psi}(\theta). \tag{12}$$

With respect to this boundary condition, there are two classes of vortices: with odd and even $m+N$. The quantum spectrum of fermions in the core is essentially determined by this condition. Let us consider vortices with $m=\pm 1$.

The quasiclassical Hamiltonian in Eq. (10) is the same as for the *s*-wave vortex and can thus be treated in the same manner as in Ref. 3. The state with the lowest energy corresponds to trajectories that cross the center of the vortex, i.e., with $b=0$. Along this trajectory, one has $\sin\tilde{\phi}=0$ and $\cos\tilde{\phi}=\mathrm{sign}\, s$. In this case Eq. (10) becomes supersymmetric,

$$\tilde{\mathcal{H}}=-iv_F\tau_3\partial_s+\tau_1\Delta(|s|)\mathrm{sign}\, s \tag{13}$$

and thus contains an eigenstate with zero energy. Including all the transformations, we write the corresponding eigenfunction as

$$\Psi_0(s,\theta,b=0)=e^{ip_Fs}e^{i(m+N)\tau_3\theta/2}\begin{pmatrix}1\\-i\end{pmatrix}\psi_0(s),$$

$$\psi_0(s)=\exp\left(-\int^s ds'\,\mathrm{sign}\, s'\frac{\Delta(|s'|)}{v_F}\right). \tag{14}$$

When b is small the third term in Eq. (10) can be considered as a perturbation, and this gives the energy levels in terms of b and thus in terms of the angular momentum $L_z=p_Fb$:

$$E(L_z,\theta)=-mL_z\omega_0,\quad \omega_0=\frac{\int_{-\infty}^{\infty}ds|\psi_0(s)|^2\dfrac{\Delta(|s|)}{p_F|s|}}{\int_{-\infty}^{\infty}ds|\psi_0(s)|^2}. \tag{15}$$

The next step is the quantization of motion in the θ,L_z plane. Since the angle and momentum are canonically conjugate variables, the quantized energy levels are obtained from the quasiclassical energy in Eq. (15), if L_z is considered as an operator. The Hamiltonian

$$H(\theta)=im\omega_0\partial_\theta \tag{16}$$

has the eigenfunctions $e^{-iE\theta/m\omega_0}$. The boundary condition (12) gives the following quantization of the energy levels for $m=\pm 1$ vortices:

$$E_n=n\omega_0 \text{ for odd } N;\quad E_n=\left(n+\frac{1}{2}\right)\omega_0 \text{ for even } N. \tag{17}$$

EFFECT OF A SINGLE IMPURITY

As distinct from the Andreev scattering in the vortex core, which leads to bound states, a microscopic impurity leads to conventional elastic scattering, in which the momentum **q** of the quasiparticle changes and thus a transition between different trajectories occurs. In the limit of low energy of the quasiparticle the impact parameter b of the scattered particle is close to zero and thus is smaller than the distance R from the impurity to the center of the vortex, which is of the order of ξ. If we assume that the impurity is of atomic size, then the scattering of a low-energy quasiparticle occurs only between two

trajectories which cross simultaneously the vortex center and the impurity. Thus we are interested in the matrix element between the states with $\theta=\theta_{\rm imp}$ and $\theta=\pi+\theta_{\rm imp}$ (Ref. 8). In the general case this coupling has the form

$$\mathcal{H}_{\rm imp}=2\lambda e^{i\gamma}\psi(\pi+\theta_{imp})\,\psi^*(\theta_{\rm imp})+2\lambda e^{-i\gamma}\psi^*(\pi+\theta_{\rm imp})\,\psi(\theta_{\rm imp}). \tag{18}$$

Together with the free Hamiltonian in Eq. (16) this gives the following Schrödinger equation for the motion in θ-space:

$$im\omega_0\frac{\partial\psi}{\partial\theta}+2\lambda e^{i\gamma}\delta(\theta-\theta_{\rm imp})\,\psi(\pi+\theta_{\rm imp})+2\lambda e^{-i\gamma}\delta(\theta-\pi-\theta_{\rm imp})\,\psi(\theta_{\rm imp})=E\psi(\theta), \tag{19}$$

with the boundary condition

$$\psi(\theta+2\pi)=\pm\psi(\theta). \tag{20}$$

Here the signs $-$ and $+$ are for the $|m|=1$ vortex in the class I and class II superconducting states, respectively. The solution of these equations give the energy eigenvalues:

$$\cos\frac{\pi E}{\omega_0}=\frac{2\omega_0\lambda}{\omega_0^2+\lambda^2}\sin(m\gamma), \quad |m|=1, \quad \text{class I}, \tag{21}$$

$$\sin\frac{\pi E}{\omega_0}=\frac{2\omega_0\lambda}{\omega_0^2+\lambda^2}\cos\gamma, \quad |m|=1, \quad \text{class II}. \tag{22}$$

For the class I superconducting states, Eq. (21) is similar to Eq. (2.10) of Ref. 8, obtained for the *s*-wave case: in the presence of an impurity the spectrum has the doubled period $\Delta E=2\omega_0$ and consists of two equidistant sets of levels. These two sets transform into each other under the symmetry transformation $E\to -E$, which is the analog of CPT symmetry.

For the class I states, Eq. (22) also gives two sets of levels with alternating shift. Here, however, the two sets are not mutually symmetric with respect to $E=0$. This contradicts the CPT symmetry of the system. The only way to reconcile Eq. (22) with this symmetry is to assume that because of the CPT symmetry either (i) there is no coupling between the two trajectories, or (ii) the phase of the coupling is fixed, $\gamma=\pi/2$. Then the energy levels are $E_n=n\omega_0$, i.e., the same as without impurities. Thus the same CPT symmetry that is responsible for the eigenstate with $E=0$ provides rigidity of the spectrum.

Now we shall show that in the simplest model of the impurity potential $H_{\rm imp}=U\tau_3\delta(\mathbf{r}-\mathbf{R})$ the coupling between opposite trajectories does indeed disappear for the superconducting states of class II. Let us consider the lowest-energy trajectories; they cross the center of the vortex, and as a result, $\delta(\mathbf{r}-\mathbf{R})=\delta(s-R)\,\delta(\theta-\theta_{\rm imp})/R$. The matrix element in Eq. (14) between two wave functions corresponding to opposite trajectories, i.e., for which the angles θ differ by π, is proportional to

$$\lambda e^{i\gamma}\sim\frac{U}{R\xi}e^{2ip_FR}\exp\left(-\frac{2}{v_F}\int_0^R dr\,\Delta(r)\right)(1\quad i)[\tau_3 e^{i(m+N)\tau_3\pi/2}]\begin{pmatrix}1\\-i\end{pmatrix}. \tag{23}$$

vFrom the spinor structure it follows that the impurity scattering between the opposite trajectories disappears, $\lambda = 0$, for vortices with even $m+N$. Thus in the superconducting states of class II the spectrum of fermions in the $m = \pm 1$ vortices is not influenced by a single impurity.

CONCLUSION

The phase $(m+N)\tau_3\theta/2$ in Eq. (9) plays the role of the Berry phase. It shows how the wave function of the quasiparticle changes when the trajectory is rotated by an angle θ. This Berry phase is instrumental for the Bohr–Sommerfeld quantization of the energy levels in the vortex core. It chooses between the two possible quantizations consistent with the CPT symmetry of states in superconductors: $E_n = n\omega_0$ and $E_n = (n+1/2)\omega_0$.

The same phase is also important for the effect of a single impurity on the spectrum of bound states. We have found that if the spectrum in the pure superconductor is $E_n = (n+1/2)\omega_0$, an impurity splits it into two series according to the Larkin–Ovchinnikov prescription.[1,8] However, if the initial spectrum is $E_n = n\omega_0$ (an example is the $m = \pm 1$ vortex in a chiral p-wave superconductor, where $N=1$), then the impurity does not change this spectrum. This rigidity of the spectrum must be taken into account when the effect of randomness due to many impurities is considered and a new level statistics for the fermionic spectrum in the core is introduced.[13] The existence of the level with exactly zero energy can substantially change the estimate[14] of the fractional charge carried by the vortex core in chiral superconductors.

I am indebted to P. Wiegmann, whose remark on the Berry phase was extremely fruitful, and to M. Feigel'man and N. Kopnin for numerous discussions.

[1] A. I. Larkin and Yu. N. Ovchinnikov, Phys. Rev. B **57**, 5457 (1998).
[2] C. Caroli, P. G. de Gennes, and J. Matricon, Phys. Lett. **9**, 307 (1964).
[3] G. E. Volovik, JETP Lett. **57**, 244 (1993).
[4] N. B. Kopnin and G. E. Volovik, Phys. Rev. Lett. **79**, 1377 (1997); Phys. Rev. B **57**, 8526 (1998).
[5] T. Sh. Missirpashaev and G. E. Volovik, Physica B **210**, 338 (1995).
[6] N. B. Kopnin and M. M. Salomaa, Phys. Rev. B **44**, 9667 (1991).
[7] M. Rice, Nature (London) **396**, 627 (1998); K. Ishida, H. Mukuda, Y. Kitaoka *et al.*, Nature (London) **396**, 658 (1998).
[8] A. A. Koulakov and A. I. Larkin, Phys. Rev. B **59**, 12021 (1999).
[9] M. Stone, Phys. Rev. B **54**, 13222 (1996).
[10] G. E. Volovik and V. M. Yakovenko, J. Phys.: Condens. Matter **1**, 5263 (1989).
[11] G. E. Volovik, JETP Lett. **66**, 522 (1997).
[12] T. Senthil, J. B. Marston, and M. P. A. Fisher, Phys. Rev. B **60**, 4245 (1999).
[13] M. V. Feigel'man and M. A. Skvortsov, Phys. Rev. Lett. **78**, 2640 (1997).
[14] J. Goryo, http://xxx.lanl.gov/abs/cond-mat/9908113; G. E. Volovik, *AIP Conference Proceedings*, Vol. 194, edited by G. G. Ihas and Y. Takano, Gainesville, Fla. (1989), pp. 136–146.

Published in English in the original Russian journal. Edited by Steve Torstveit.

Photoinduced magnetism of ballistic nanostructures

L. I. Magarill and A. V. Chaplik
Institute of Semiconductor Physics, Siberian Branch of the Russian Academy of Sciences, 630090 Novosibirsk, Russia

(Submitted 21 September 1999; resubmitted 7 October 1999)
Pis'ma Zh. Éksp. Teor. Fiz. **70**, No. 9, 607–612 (10 November 1999)

It is predicted that a constant magnetization appears in certain nanostructures under stationary illumination. Under certain conditions, determined by the symmetry of the system, a magnetic moment appears (or an existing moment changes) even if the incident wave is linearly polarized. © *1999 American Institute of Physics.*
[S0021-3640(99)01021-X]

PACS numbers: 75.70.−i, 73.23.Ad

The magnetic properties of low-dimensional structures in the ballistic regime have been repeatedly discussed in the literature. A recent review is devoted to the orbital contribution to the magnetization of such objects.[1] This review also contains a detailed bibliography concerning this question. The problems arising here involve quite difficult (as a rule, numerical) calculations, since finite samples are being considered, and the result depends strongly on the shape of the boundary. To date, calculations have been performed strip and circular billiards[2] and a two-dimensional quantum dot with a parabolic confinement potential.[3] Orbital magnetism of nanotubes has been calculated in Ref. 4, and the present authors have clarified the role of the spin-orbit interaction (SOI) in the magnetization of nanotubes.[5] The question of persistent currents in quantum rings is also closely related with the problem of the magnetization of nanostructures; interest in this question has been revived by the experiments of Ref. 6 with a single semiconductor ring in a ballistic regime. We also note that substantial progress has been made in the technique for performing measurements of the magnetization of 2D electronic systems,[7] which makes an experimental check of the calculations performed timely.

All works mentioned above concern the calculation of the thermodynamically equilibrium magnetic moment. In the present letter we call attention to the possibility that under certain conditions a stationary but nonequilibrium magnetization appears under the action of an electromagnetic wave incident on a nanostructure. At least for circularly polarized light, the mechanism of the effect discussed is completely obvious: The absorption of such a photon is accompanied by transfer of mechanical and therefore magnetic moments to the system. It is less obvious that under certain conditions, associated with the symmetry properties of the system, a linearly polarized wave also gives rise to the appearance of a constant magnetic moment (or changes an existing magnetization). As examples we consider a quantum dot with a parabolic potential, a one-dimensional quantum ring, and a nanotube.

Our aim is to calculate the constant component of the nonequilibrium photoinduced magnetic moment (PIMM) of a system in the field of a monochromatic electromagnetic wave. We shall use the dipole (i.e., nonrelativistic) approximation and we shall find the magnetization induced by the *electric* vector of a high-frequency field. In the absence of a constant magnetic field (and, of course, excluding the ferromagnetic situation) the magnetic moment of a system without illumination is zero. We shall seek an effect that is linear in the intensity J of the electromagnetic wave incident on the system.

QUANTUM DOT WITH A PARABOLIC POTENTIAL

Let the 2D electrons move in the potential

$$U_{\text{eff}}=\frac{m}{2}(\omega_x^2x^2+\omega_y^2y^2). \tag{1}$$

Then the problem posed can be solved exactly if the electric field of the wave is spatially uniform. Irrespective of the illumination intensity, the answer is found to be linear in J and can be found either classically or in the quadratic Kubo response technique or by solving exactly the Schrödinger equation with time (an oscillator with a moving suspension point). In the latter case we have in mind a well-known property of a system of n particles moving in a general parabolic potential and interacting with another according to an arbitrary law that depends only on the pair distances between particles (see Ref. 8). When a uniform electric field is imposed on such a system, the motion of the center of mass completely separates from the internal degrees of freedom, and the external electric field enters only in combination with the coordinate $\mathbf{R}_c$ of the center of mass. Correspondingly, the total multiparticle wave function decomposes into factors $\Psi=\psi(\mathbf{R}_c)\Phi(\boldsymbol{\rho}_k)$, where $\boldsymbol{\rho}_k$ are relative coordinates. The function ψ corresponds to a particle with mass nm and total charge ne in the same parabolic potential and a uniform ac electric field. For identical particles $\psi(\mathbf{R}_c)$ is symmetric in an obvious manner with respect to all permutations, so that the Pauli principle holds because of the function Φ and the spin factor. The magnetic moment operator of the system, being a quadratic form of the momenta and coordinates, likewise decomposes into contributions from the center of mass and the internal degrees of freedom, but the induced part of the moment, proportional to the squared external field and of interest to us, is related only with the motion of the center of mass. Thus the problem reduces to a single-particle problem for an effective particle with the total mass and charge.

Introducing the phenomenological relaxation time (''friction'' in the classical approach), it is easy to obtain a formula for the constant magnetic moment of a quantum dot:[1)]

$$M=\frac{ne^3\omega}{2m^2c}\,\frac{\mathrm{Im}[E_{0x}^*E_{0y}(\omega_x^2+(\nu-i\omega)^2)(\omega_y^2+(\nu+i\omega)^2)]}{[(\omega_x^2-\omega^2+\nu^2)^2+4\nu^2\omega^2][(\omega_y^2-\omega^2+\nu^2)^2+4\nu^2\omega^2]}. \tag{2}$$

Here $\mathbf{E}_0$ is the complex amplitude of the electric field of the wave, ν is the relaxation frequency, and m is the number of electrons in the dot. It is interesting to note that the anisotropy of the potential of the dot ($\omega_x\neq\omega_y$) makes the effect under discussion possible even if the wave is linearly polarized:

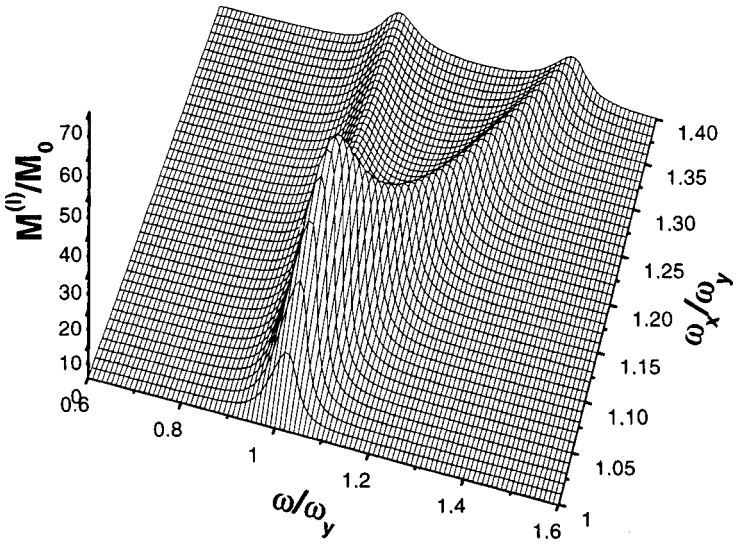

FIG. 1. The induced magnetic moment versus the frequency of the wave and the degree of anisotropy of the quantum dot. $M_0 = ne^3E_0^2\sin(2\theta)/2m^2c\omega_y^3$, $\nu/\omega_y = 0.1$.

$$M^{(l)} = \frac{ne^3E_{0x}E_{0y}\omega^2\nu}{m^2c}\,\frac{\omega_x^2-\omega_y^2}{[(\omega_x^2-\omega^2+\nu^2)^2+4\nu^2\omega^2][(\omega_y^2-\omega^2+\nu^2)^2+4\nu^2\omega^2]}. \quad (3)$$

This possibility is evident from purely symmetry considerations. The axial induced magnetic moment vector is constructed from the stiffness tensor of the parabolic quantum dot $K_{ij} = \partial^2 U_{eff}/\partial x_i \partial x_j$ and the electric field vector of the wave: $M_i^{(l)} \sim e_{ijk}K_{jm}E_{0m}E_{0k}$, where e_{ijk} is an absolutely antisymmetric unit pseudotensor. There is a characteristic polarization dependence of $M^{(l)}$ of the form $\sin(2\theta)$, where θ is the angle between the electric field vector $\mathbf{E}_0$ of the wave and the x axis. The moment $M^{(l)}$ depends nonmonotonically on the degree of anisotropy. A three-dimensional plot of $M^{(l)}(\omega, \omega_x)$ with ω_y = const is presented in Fig. 1. The magnetization is small for both small and large anisotropy. In the latter case the moment decreases because the average impact parameter is small (strongly elongated quantum dot).

For an isotropic dot ($\omega_x = \omega_y = \omega_0$), as is evident a priori, the magnetization is proportional to the degree of circular polarization $P_c = 2\,\mathrm{Im}(E_{0x}^* E_{0y})/|\mathbf{E}_0|^2$ and is given by the expression

$$M^{(c)} = P_c\,\frac{ne^3\omega|\mathbf{E}_0|^2}{4m^2c}\,\frac{1}{(\omega_0^2-\omega^2+\nu^2)^2+4\nu^2\omega^2}. \quad (4)$$

For purely circular polarization $P_c = \pm 1$ under resonance conditions $\omega = \omega_0 \gg \nu$ we obtain hence a physically transparent result: The magnitude of the PIMM is equal to the effective Borh magneton $e\hbar/2mc$ multiplied by the number of photons absorbed in time $1/2\nu$, and the sign is determined by the sign of the circular polarization. We also note that the induced moment is related only with the induced part of the solution of the equations of motion (in the quantum approach — the same for the Heisenberg coordinate opera-

tors). For this reason, the partial magnetization of an electron does not depend on its energy (i.e., on the initial conditions), and the result is proportional to the total number of particles in the dot and does not depend on temperature and, generally, on the form of the initial distribution function. Of course, such universality of the result is valid only for the parabolic model of a quantum dot.

NANOTUBE AND A 1D CIRCULAR RING

Here and in the next section the interaction with an electromagnetic field is treated as a small perturbation and the Kubo formulism is used to find the quadratic response. It is obvious that in this approximation a constant component can arise in the induced magnetic moment. We note an obvious analogy between our situation and the photogalvanic effect (PGE) in media without a center of inversion: The constant current is proportional to the light intensity.[10,11] However, in contrast to the PGE, the absence of a center of inversion in the system is not necessary for a PIMM to arise.

For a circularly polarized wave propagating along the axis of a nanotube the PIMM is given by the formula

$$M^{(\pm)}=\sum_l M_l^{(\pm)}=\mp\frac{e}{2mc}\sum_l \frac{Q_l^{(\pm)}}{2\nu\Delta_l^{(\pm)}}, \tag{5}$$

$$Q_l^{(\pm)}=\frac{e^2E_0^2\Delta_l^{(\pm)}}{8mB}\sum_{p_z}\frac{[f(\varepsilon_{p_z,l})-f(\varepsilon_{p_z,l\pm1})]\nu}{(\Delta_l^{(\pm)}-\omega)^2+\nu^2}\equiv\frac{e^2E_0^2\Delta_l^{(\pm)}}{8mB}\frac{(n_l-n_{l\pm1})\nu}{(\Delta_l^{(\pm)}-\omega)^2+\nu^2}, \tag{6}$$

where $\varepsilon_{p_z,l}=p_z^2/2m+Bl^2$ is the energy spectrum of an electron on the surface of the nanotube, p_z is the momentum along the axis of the tube, $l=0,\ \pm1,\ \pm2,\ \ldots.$ is the azimuthal quantum number, $B=1/2mR^2$ is the rotational quantum, R is the tube radius, $f(\varepsilon)$ is the Fermi function, and $\Delta_l^{(\pm)}=\varepsilon_{p_z,l\pm1}-\varepsilon_{p_z,l}\equiv B(1\pm2l)$, and $\hbar=1$ in what follows. Thus, in the present case of a simple energy spectrum the answer can be expressed in terms of the population n_l of the subbands. For a quantum ring the answer differs only by the absence of integration over p_z. The result has the same form (6), where now n_l is the occupation number of the l-th level of the ring. Once again, for a resonance on the transition $l\to l\pm1$ the partial contribution to the PIMM is $M_l^{(\pm)}\propto Q_l^{(\pm)}/\nu$ ($Q_l^{(\pm)}$ is the partial contribution determined by Eq. (6) to absorption on this transition). If a constant magnetic field directed along the z axis is applied to the tube (or ring), then the expressions (5) and (6) for the PIMM remain valid. Here it is only necessary to interpret ε_{l,p_z} as the spectrum of an electron in the presence of a magnetic field $\varepsilon_{l,p_z}=p_z^2/2m+B(l+\Phi)^2$, where Φ is the magnetic flux through the cross section of the tube in units of the flux quantum. It is easy to prove that the induced magnetic moment (just as the equilibrium moment) is periodic in Φ with period 1. The relation

$$M^{(-)}(-\Phi)=-M^{(+)}(\Phi) \tag{7}$$

also holds.

SPIN-ORBIT INTERACTION (SOI) IN A NANOTUBE

A special situation arises when a linearly polarized wave is incident on a nanotube placed in a longitudinal magnetic field, if the vector $\mathbf{E}_0$ is parallel to the axis of the

cylinder. The selection rules for dipole transitions in this case give $\Delta p_z=0$, $\Delta j=0$, $\mu\to-\mu$, where j is the half-integral z projection of the total angular momentum, and the quantum number $\mu=\pm1$ labels two spin-split branches of the electron energy spectrum.[5,12] Thus, only spin-flip transitions are possible, just as in the corresponding planar problem with a wave incident in a direction along the normal. If the magnetic field $\mathbf{H}$ also lies in the plane of the 2D electrons, then a PGE arises:[13] A constant current flows in the directions $\mathbf{n}\times\mathbf{H}$ and $\mathbf{E}_0(\mathbf{E}_0\cdot(\mathbf{n}\times\mathbf{H}))$ ($\mathbf{n}$ is the normal to the plane of the system). However, this current vanishes in the absence of Zeeman splitting (the g factor is zero). For a nanotube (for purely topological reasons) with $\mathbf{E}_0\parallel\mathbf{H}\parallel z$ the azimuthal photogalvanic current contributes to the magnetic moment of the system even for $g=0$.

We shall treat the spin-orbit interaction in the Rashba model.[14,15] The Hamiltonian for the electrons on the surface of a cylinder taking account of the SOI has the form[5] (cylindrical coordinates with the z axis along the axis of the cylinder are used)

$$\hat{H}_0=\frac{\hat{p}_z^2+(\hat{p}_\varphi+\Phi/R)^2}{2m}+\alpha[\hat{\sigma}_z(\hat{p}_\varphi+\Phi/R)-\hat{\Sigma}\hat{p}_z)],\quad \hat{\Sigma}=\begin{bmatrix}0 & ie^{-i\varphi}\\ -ie^{i\varphi} & 0\end{bmatrix}.$$

Here $\hat{p}_\varphi=-i(1/R)\partial/\partial\varphi$. In Ref. 5 the wave functions and the spectrum of the corresponding Schrödinger equation are also presented. Using these results and the quadratic Kubo formula, we find an expression for the PIMM in our situation:

$$M=\sum_{j,p_z}M_{j,p_z}=-\frac{e}{2mc}\sum_{j,p_z}Q_{j,p_z}\,\frac{1}{2\nu}\,\frac{4\lambda_j(1-\Lambda)^2}{\Delta_{j,p_z}},\tag{8}$$

where Q_{j,p_z} is the contribution to absorption on the transition $j,p_z,\mu=-1\to j,p_z,\mu=1$:

$$Q_{j,p_z}=\frac{2e^2E_0^2B^3\lambda_j^2\Lambda^2(1-\Lambda)^2}{m\omega^2}\,\frac{(f(\varepsilon_{j,p_z,-1})-f(\varepsilon_{j,p_z,1}))\,\nu(\omega^2+\Delta_{j,p_z}^2+\nu^2)}{[(\Delta_{j,p_z}^2-\omega^2+\nu^2)^2+4\nu^2\omega^2]\Delta_{j,p_z}}.\tag{9}$$

Here $\varepsilon_{j,p_z,\mu}=p_z^2/2m+B[\lambda_j^2+(1-2\Lambda)/4+\mu\sqrt{\lambda_j^2(\Lambda-1)^2+p_z^2R^2\Lambda^2}]$, $\lambda_j=j+\Phi$, $\Lambda=2m\alpha R$(α – effective SOI constant), and $\Delta_{j,p_z}=\varepsilon_{j,p_z,1}-\varepsilon_{j,p_z,-1}$ is the transition energy.

In conclusion, we shall estimate the PIMM for a parabolic quantum dot. From Eq. (4), the PIMM for an individual quantum dot under resonance conditions is

$$M=n\mu_B\frac{e^2}{\hbar c}\,\frac{m_0}{m}\,\frac{\pi J}{\hbar\omega_0 m\nu^2},\tag{10}$$

where $\mu_B=e\hbar/2m_0c$ is the Bohr magneton. For reasonable values of the parameters $\hbar\omega_0=1$ meV, $1/\nu=10$ ps, $n=10$, and illumination intensity $J=1$ W/cm^2 we have $M\approx35\mu_B$. The sensitivity of the measurement method used in Ref. 7 is $\sim10^{10}\mu_B$. Therefore the effect is quite measurable for a sample with an array containing 10^9-10^{10} quantum dots.

This work was supported by the Russian Fund for Fundamental Research (Grant No. 99-02-17127), the ''Physics of Solid-State Nanostructures'' program, and NWO.

[1)]Taking account of electron scattering correctly is a separate and very difficult problem. Without pretending to solve it, we confine our attention in the present letter to a well-known (in the literature; see, for example, Ref. 9) device: The electric field of the wave is switched on adiabatically according to an exponential law, and in the final formulas its decrement is identified with the reciprocal of the relaxation time.

[1] K. Richter, D. Ullmo, and R. A. Jalabert, Phys. Rep. **276**, 1 (1996).
[2] E. Gurevich and B. Shapiro, J. Phys. I France **7**, 807 (1997).
[3] V. A. Geĭler, V. A. Margulis, and I. V. Chudaev, Zh. Éksp. Teor. Fiz. **109**, 762 (1996) [JETP **82**, 409 (1996)].
[4] H. Ajiki and T. Ando, Solid State Commun. **102**, 135 (1997).
[5] L. I. Magarill and A. V. Chaplik, Zh. Éksp. Teor. Fiz. **115**, 1478 (1999) [JETP **88**, 815 (1999)].
[6] D. Mailly, C. Chapellier, and A. Benoit, Phys. Rev. Lett. **70**, 2020 (1993).
[7] I. Meinel, D. Grundler, S. Bargstadt-Franke *et al.*, Appl. Phys. Lett. **70**, 3305 (1997).
[8] A. O. Govorov and A. V. Chaplik, JETP Lett. **52**, 31 (1990); Zh. Éksp. Teor. Fiz. **99**, 1853 (1991) [Sov. Phys. JETP **72**, 1037 (1991)].
[9] Yu. A. Il'yanksiĭ and L. V. Keldysh, *Interaction of Electromagnetic Radiation with Matter* (Moscow State University Press, Moscow, 1989) p. 85.
[10] V. I. Belinicher and B. I. Sturman, Usp. Fiz. Nauk **130**, 415 (1980) [Sov. Phys. Usp. **23**, 133 (1980)].
[11] E. L. Ivchenko and G. E. Pikus, in *Semiconductor Physics*, edited V. M. Tushkevich and V. Ya. Frenkel (Consultants Bureau, New York, 1986) p. 427.
[12] L. I. Magarill, D. A. Romanov, and A. V. Chaplik, Zh. Éksp. Teor. Fiz. **113**, 1411 (1998) [JETP **86**, 771 (1998)].
[13] L. I. Magarill, Fiz. Tverd. Tela (Leningrad) **32**, 3359 (1990) [Sov. Phys. Solid State **32**, 2064 (1990)].
[14] Yu. A. Bychkov and É. I. Rashba, JETP Lett. **39**, 78 (1984).
[15] E. I. Rashba and V. I. Sheka in *Landau Level Spectroscopy*, edited by G. Landwehr and E. I. Rashba (Elsevier, New York, 1991) p. 178.

Translated by M. E. Alferieff

Excitonic state in quantum wells formed from ''above-barrier'' electronic states

E. A. Mulyarov
Institute of General Physics, Russian Academy of Sciences, 117942 Moscow, Russia

N. N. Sibel'din,*) M. L. Skorikov, and V. A. Tsvetkov
P. N. Lebedev Physics Institute, Russian Academy of Sciences, 117924 Moscow, Russia

B. Etienne
Laboratoire de Microstuctures et de Microelectronique, 92225 Bagneux, France

(Submitted 7 October 1999)
Pis'ma Zh. Éksp. Teor. Fiz. **70**, No. 9, 613–619 (10 November 1999)

Lines corresponding to localized excitonic states formed from ''above-barrier'' electron and/or hole states (specifically, excitation lines of excitons formed by an electron localized in a QW and a free heavy hole) have been observed in the photoluminescence excitation spectra of $GaAs/Al_{0.05}Ga_{0.95}As$ structures with quantum wells (QWs), each containing one single-particle size-quantization level for charge carriers of each type. A computational method is proposed that permits finding the binding energy and wave functions of excitons in QWs taking the Coulomb potential into account self-consistently. The computed values of the excitonic transition energies agree quite well with the experimental results. © *1999 American Institute of Physics.*
[S0021-3640(99)01121-4]

PACS numbers: 71.35.Cc, 78.66.Fd

The excitonic states in quantum wells (QWs) formed from size-quantized single-particle electron and hole states are described well in a quasi-two-dimensional model under certain conditions.[1,2] In this case the electron and hole motion in a transverse (perpendicular to the walls of the QWs) direction is essentially uncorrelated and is determined primarily by the potential relief of the heterostructure, while the Coulomb interaction responsible for the character of the particle motion in the plane of the QWs has almost no effect on the transverse component of the motion. At the same time, it has been shown in a number of works that a different situation is possible, where the Coulomb interaction plays a large or even the main role in the transverse motion of the particles forming an exciton. Examples of such excitonic states are excitons with a light hole[3] and almost three-dimensional excited excitonic states[4] in QWs of strained InGaAs/GaAs heterostructures, excitonic states in spin superlattices,[5] and others.

It should be noted that the existence of excitonic states, whose localization in a QW is due to the influence of interparticle interaction on the transverse motion, is a general property of structures with QWs, though the physical conditions for the formation of such

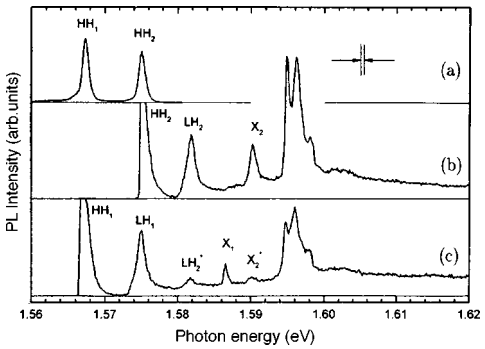

FIG. 1. Photoluminescence spectra (excitation by radiation with $\hbar\omega = 1.65$ eV) (a) and photoluminescence excitation spectra of narrow (b) and wide (c) QWs in the absence of a magnetic field.

states and these states themselves are quite diverse. Specifically, these could be states localized in QWs that correspond to excitons consisting of particles one or both of which were not bound in the QW in the absence of the Coulomb interaction (''above-barrier'' electrons and holes).

In the present work excitonic states were investigated experimentally and theoretically in ''classical'' type-I GaAs/AlGaAs structures with shallow QWs, each containing a single-particle size-quantization level for particles of each type (electrons, heavy and light holes). On account of the simplicity of their single-particle electronic spectrum, such structures are most convenient for observing additional excitonic states localized in QWs. The observation of lines corresponding to these excitonic states in the photoluminescence excitation spectra is the main experimental result of this work. The excitonic transition energies calculated in a self-consistent model agree quite well with the experimental data.

The experiments were performed on samples of a $GaAs/Al_{0.05}Ga_{0.95}As$ structure grown by molecular-beam epitaxy. The structure contained two GaAs QWs, 40 Å and 30 Å wide, separated by a 600 Å thick AlGaAs barrier. The excitonic states were investigated by photoluminescence (PL) spectroscopy and PL excitation (PLE) spectroscopy at 2 K temperature in magnetic fields up to 5.5 T oriented either perpendicular or parallel to the layers of the structure. The sample was excited by radiation from a Ti-sapphire laser, whose tuning range permitted photoexcitation of charge carriers into a size-quantization level in a QW and into above-barrier states in the continuum. The radiation of the sample was analyzed by a high-transmission monochromator and detected with a cooled photomultiplier.

The PL and PLE spectra in the absence of a magnetic field are shown in Fig. 1. Two recombination radiation lines of excitons with a heavy hole from wide (HH_1) and narrow (HH_2) QWs in the structure can be seen in the PL spectrum (Fig. 1a) (the index 1 marks lines associated with electronic transitions in a wide QW and the index 2 is for a narrow QW). To investigate the PLE spectra, the spectral position of the output slit of the monochromator was fixed approximately at the center of the long-wavelength wing of one of the PL lines: HH_1 or HH_2. As a result, when measuring the energy of the excitation photon, the PLE spectrum of either the wide (Fig. 1c) or narrow (Fig. 1b) QW was recorded.

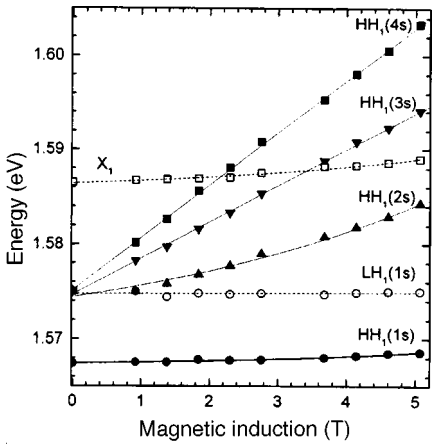

FIG. 2. Energy position of the lines of heavy (HH_1) and light (H_1H_2) excitons in the PLE spectrum of a wide QW versus the magnetic induction.

The excitation lines of excitons with heavy (HH) and light (LH) holes, corresponding to the matching pairs of size-quantization levels of the noninteracting particles (electrons and heavy or light holes), are observed in the PLE spectrum of each well. In addition, in the PLE spectra of both wells quite strong X lines (X_1 — in the spectrum of a wide well and X_2 in the spectrum of a narrow well) and an intense triplet in the range 1.594–1.599 eV are seen in the barrier layer at energies less than the band gap, and relatively weak lines LH_2^* and X_2^* are also seen in the spectrum of the wide QW.

In a magnetic field oriented perpendicular to the layers of the structure, lines corresponding to excited states of magnetoexcitons appear in the PLE spectra. Figure 2 shows the dependences of the spectral position of the lines HH_1, LH_1, and X_1 and the transition energies into the excited $2s$, $3s$, and $4s$ states of excitons with heavy holes in a wide QW as a function of the magnetic induction. Extrapolating these dependences for excited s states (thin solid lines) to zero field, it is possible to determine the energies of transitions into excited states of excitons with heavy holes in the absence of a magnetic field and hence to estimate their binding energy. A similar construction was made for excitonic transitions in a narrow well. As a result, the binding energies of excitons formed from an electron and a heavy hole in a wide and narrow QWs were found to be 7.2 meV and 6.4 meV, respectively.

The diamagnetic shifts of the X_1 and X_2 lines in a transverse field ($\simeq$2.4 meV and $\simeq$2.6 meV B=5.06) are much larger than for the HH_1 and HH_2 lines ($\simeq$1.2 meV and $\simeq$1.4 meV at B=5.06 T), respectively, but much less than for the lines of the excited states of excitons with heavy holes (Fig. 2). This shows that the X lines correspond to states which are more weakly bound than an exciton with a heavy hole in the ground state but more strongly than its excited states. In a B=5.06 T magnetic field parallel to the layers of the structure, the diamagnetic shifts of the lines HH_1 and HH_2 are $\simeq$0.7 meV, and the shifts for the X_1 and X_2 lines are, respectively, $\simeq$1.8 meV and $\simeq$2.3 meV. An appreciable decrease of the diagmagnetic shifts of the lines HH_1 and HH_2 with a change in the magnetic field orientation agrees with the circumstance that excitons with a heavy hole in both wells are

quasi-two-dimensional and their Bohr radii in the plane of the QWs are much greater than the width of the wells. While the weak dependence of the diamagnetic shifts of the X lines on the field orientation shows that in the plane of the QWs the extent of the wave functions of particles in the states corresponding to these lines is approximately the same as in the transverse direction. On this basis we infer that the lines X_1 and X_2 are due to excitation of excitons formed from a particle of the same sign (electron) in a size-quantization level in the QW and a free ''above-barrier'' particle of opposite sign which is ''pulled'' into the region of the well by a strong Coulomb attraction.

Finally, the origin of the lines LH_2^* and X_2^* in the PLE spectrum of the wide well, which according to their spectral position exactly coincide with the lines LH_2 and X_2, respectively, in the PLE spectrum of the narrow well but have almost an order of magnitude lower intensities seems to be associated with the resonance excitation of light excitons in a wide QW accompanying the absorption of the recombination radiation of heavy excitons of the narrow well. As one can see from Fig. 1, the energies of these transitions in the structure investigated are virtually identical.

Let us now consider the excitonic states in a QW, taking the Hamiltonian of the electron–hole pair (with a zero magnetic field) in the effective mass approximation

$$\hat{H}=\hat{H}_e(z_e)+\hat{H}_h(z_h)+\hat{H}_\rho(\rho)+V(z_e,z_h,\rho)+E_g^{\mathrm{bar}}, \tag{1}$$

where $\hat{H}_{e(h)}$ is the Hamiltonian of the transverse motion of an electron (hole) taking account of only the heterostructure (step) potential, $\hat{H}_\rho$ is the kinetic energy operator for relative motion in the plane of the well, V is the Coulomb potential, $z_{e(h)}$ is the coordinate of the electron (hole) in the transverse direction, ρ is the distance between them in the plane of the well, and E_g^{bar} is the band gap in the barrier.

We shall assume that the wave function of the exciton can be represented in the form

$$\Psi(\mathbf{r}_e,\mathbf{r}_h)=\psi_e(z_e)\psi_h(z_h)\phi(\rho). \tag{2}$$

Then, multiplying the Schrödinger equation $\hat{H}\Psi=E\Psi$ successively by $\psi_h(z_h)\phi(\rho)$, $\psi_e(z_e)\phi(\rho)$, and $\psi_e(z_e)\psi_h(z_h)$ and integrating over the coordinate pairs (z_h,ρ), (z_e,ρ), and (z_e,z_h), respectively, we obtain a system of three equations of the form

$$(\hat{H}_e+\langle V\rangle_{h,\rho})\psi_e=E_e\psi_e, \quad (\hat{H}_h+\langle V\rangle_{e,\rho})\psi_h=E_h\psi_h, \quad (\hat{H}_\rho+\langle V\rangle_{e,h})\phi=E_\rho\phi, \tag{3}$$

where

$$E_e=E-\langle\hat{H}_h\rangle_h-\langle\hat{H}_\rho\rangle_\rho, \quad E_h=E-\langle\hat{H}_e\rangle_e-\langle\hat{H}_\rho\rangle_\rho, \quad E_\rho=E-\langle\hat{H}_e\rangle_e-\langle\hat{H}_h\rangle_h. \tag{4}$$

The averages $\langle\ldots\rangle_{i,j}$ and $\langle\ldots\rangle_i$ in Eqs. (3) and (4) signify quantities averaged over the corresponding single-coordinate wave functions. Solving the system of one-dimensional equations (3) self-consistently, we can find the exact wave function of an exciton of the form (2) and the energy E of an excitonic transition. As the zeroth approximation for $\psi_e(z_e)$ and $\psi_h(z_h)$ we can take the single-particle wavefunctions of an electron and a hole bound in a QW or give arbitrarily the initial functions with the required symmetry. Successive approximations are performed until the difference in the values of E determined by Eqs. (4) fall within the computational error limits. We note that in the first two equations (3), describing the motion of an electron and a hole in a direction transverse to

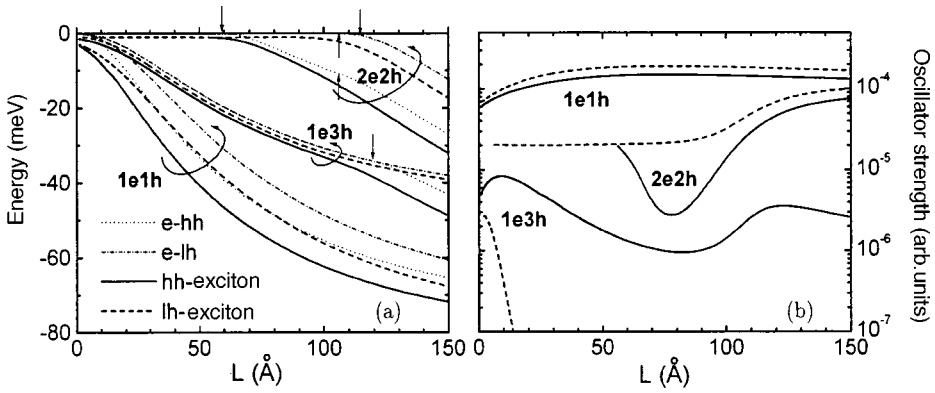

FIG. 3. Energies (a) and oscillator strengths (b) of excitonic transitions as a function of the quantum well width L and the transition energies between size-quantization levels of noninteracting electrons and holes (e–hh and e–lh) in a QW (a). The arrows mark the values of L for which the single-particle bound states of an electron ($\uparrow$) or hole ($\downarrow$) in a QW vanish; the parts of the curves lying to the left of the corresponding arrows show the behavior of the remaining size-quantization level.

the plane of the QW, besides the heterostructural potential there also enter $\langle V\rangle_{e,\rho}$ and $\langle V\rangle_{h,\rho}$ corresponding to the electron–hole interaction. The long-range character of the terms $\langle V\rangle_{e,\rho}$ and $\langle V\rangle_{h,\rho}$ results in the appearance of a variety of additional excitonic bound states in the QWs.

Figure 3 shows the energies (minus the band gap in the barrier layer $E_g^{\mathrm{bar}}=1.6006$ eV) and the oscillator strengths of $1s$-type excitonic transitions for type-I GaAs/AlGaAs structure with a 50.3 meV deep QW for electrons and a 30.8 meV deep QW for holes. As one can see from this figure, excitonic transitions are possible between bound states in the QW in the absence of a Coulomb interaction (the electronic state $1e$ and the hole states $1hh$ and $1lh$) and between states for whose localization a single heterostructural potential is inadequate. As an example, the third size-quantization level for a heavy hole ($3hh$) ceases to exist (it is expelled from the well) with QW width $L\leqslant 120$ Å (marked by the arrow on the curve of the energy of the $1e$–$3hh$ interband transition), while for the light hole ($3lh$) it ceases to exist for $L=200$ Å . Nonetheless, the excitonic states $1e3hh$ and $1e3lh$, corresponding to an electron in the first and, correspondingly, a heavy and light holes in the third size-quantization levels, exist right up to $L=0$. It is also evident that for any QW width transitions are possible into an excitonic state $2e2lh$ [constructed on the antisymmetric wave functions $\psi_e(z_e)$ and $\psi_h(z_h)$] for which with $L<150$ Å both electronic and hole size-quantization levels are initially absent. Such a state is of a particularly excitonic nature: Its energy is virtually independent of L, and the QW itself in this case plays the role of a flat defect, which destroys the translational invariance and localizes an exciton in the transverse direction. As calculation shows, for the experimentally investigated QWs with $L=30$ Å and 40 Å other excited states (for example, $1e5hh$, $1e7hh$, and $3e1lh$), whose binding energies are less than 1 meV and whose characteristic size in the QW plane is hundreds of Å , also exist; however, the oscillator strengths for transitions into the states are several orders of magnitude lower than for the transitions enumerated in Fig. 3, and they are not observed in the optical spectra. The transition into the state $1e3lh$ also has a low oscillator strength, since the wave functions

TABLE I. Excitonic transition energies (minus the band gap 1600.6 meV of the barrier) in isolated QWs with $L=40$ and 30 Å .

	Experiment		Theory	
L, Å	line	energy (meV)	state	energy (meV)
40	HH_1	−33.3	$1e1hh$	−33.6
30	HH_2	−25.5		−25.3
40	LH_1	−25.6	$1e1lh$	−25.7
30	LH_2	−18.8		−18.6
40	X_1	−14.1	$1e3hh$	−14.1
30	X_2	−10.4		−10.0
40			$2e2lh$	−0.9
30				−0.9

of the electron and light hole are almost orthogonal because of the small difference between their effective masses.

We note that the offset of the band gap (81.1 meV) at the heteroboundary and its distribution between the conduction band and the valence band (62% and 38%, respectively), which were used in the calculation, were found by comparing the theoretically computed and experimentally obtained energies of interband transitions between size-quantized states of electrons and heavy holes in each QW. The effective masses were taken in the strong quantization limit:[6] $m^z_{hh(lh)}=-(\gamma_1\mp 2\gamma_2)^{-1}$ and $m^\rho_{hh(lh)}=(\gamma_1 \pm \gamma_2)^{-1}$ with the parameters of bulk GaAs $\gamma_1=6.790$, $\gamma_2=1.924$, and $m_e=0.0665$[7] (in units of the free-electron mass). Since the Al content in the barrier is low, we neglected the difference between these parameters in the GaAs and AlGaAs layers. No adjustable parameters were used in the calculation of the excitonic states.

The energies corresponding to the position of the excitonic lines in the PLE spectra and the theoretically computed energies of the excitonic transitions in 30 and 40 Å wide QWs are presented in Table I. It is evident that the spectral positions of the lines X_1 and X_2 agree well with the computed $1e3hh$ transition energies for both wells. Equally good agreement is also observed for transitions into the ground states of excitons with light and heavy holes.

Additional investigations are required to explain the origin and spectral position of the components of the triplet, one of which is, evidently, a line of a free exciton in the barrier layer (with binding energy $\simeq 5$ meV[8]). We note that the $2e2lh$ states obtained in the model of an isolated QW for wide and narrow wells extend deep into the barrier (their rms extent in the transverse direction is about 200 Å), and in reality they should interact very strongly both with one another and with the volume exciton in the barrier separating the wells. The calculations show that the tunneling coupling between the wells leads to the formation of two high-lying excitonic states in the investigated structure with light and heavy holes with binding energies 1.35 meV and 2.3 meV, respectively, and localized predominantly in the barrier. The first one forms as a result of the interaction of almost resonant states $2e2lh$ in the wide and narrow wells (the upper level is expelled into the continuum as a result of the splitting). The second state is also of a similar nature,

even though in the isolated wells with $L<55$ Å the state $2e2hh$ is unbound because of the large difference between the effective masses of the electron and heavy hole. At the same time, delocalized (volume) excitonic states, which can appear in the optical spectra as a result of resonances in the above-barrier reflections, fall into the same energy range. The fact that on account of the large spatial extent the high-lying states are very sensitive to the field of the surface charges, which is always present in the interior volume of the structure, must also be taken into account.

In closing, we note the following. In the present letter quite shallow QWs in structures with a low Al content in the barrier layers were investigated. However, it is obvious that the role of the Coulomb interaction of an electron and a hole in the formation of bound states in a QW, especially important for the states with energies close to the top of the QW, will be manifested irrespective of the depth of the well. In structures with deeper wells this effect will be less distinct because of the presence of a larger number of size-quantization levels.

We thank L. V. Keldysh, V. D. Kulakovskiĭ, and V. V. Kapaev for helpful discussions. This work was supported by the Russian Fund for Fundamental Research (Projects Nos. 99-02-16367 and 97-02-17600), the ''Physics of Solid-State Nanostructures'' (97-1050 and 97-1072) and ''Fundamental Spectroscopy'' (08.02.73) programs, and the Program for Support of Scientific Schools (95-15-96341 and 96-15-96476), and by INTAS.

*)e-mail: sibeldin@sci.lebedev.ru

[1] G. Bastard, E. E. Mendez, L. L. Chang, and L. Esaki, Phys. Rev. B **26**, 1974 (1982).
[2] R. L. Greene, K. K. Bajaj, and D. E. Phelps, Phys. Rev. B **29**, 1807 (1984).
[3] A. V. Kavokin, M. A. Kaliteevski, S. V. Goupalov *et al.*, Phys. Rev. B **54**, R11078 (1996).
[4] V. D. Kulakovskii, A. Forchel, K. Pieger *et al.*, Phys. Rev. B **50**, 7467 (1994).
[5] J. Warnock, B. T. Jonker, A. Petrou *et al.*, Phys. Rev. B **48**, 17321 (1993).
[6] G. E. W. Bauer and T. Ando, Phys. Rev. B **38**, 6015 (1988).
[7] L. W. Molenkamp, R. Eppenga, G. W. Hooft *et al.*, Phys. Rev. B **38**, 4314 (1988).
[8] S. Adachi, J. Appl. Phys. **58**, R1 (1985).

Translated by M. E. Alferieff

Anomalous electric conductivity of lithium under quasi-isentropic compression to 60 GPa (0.6 Mbar). Transition into a molecular phase?

V. E. Fortov, V. V. Yakushev, K. L. Kagan, I. V. Lomonosov, V. I. Postnov, and T. I. Yakusheva

Institute of Chemical Physics, Russian Academy of Sciences, 142432 Chernogolovka, Moscow Region, Russia

(Submitted 7 October 1999)
Pis'ma Zh. Éksp. Teor. Fiz. **70**, No. 9, 620–624 (10 November 1999)

The electric conductivity of lithium compressed by dynamic methods by a factor of ~3 to 60 GPa pressure is measured. It is shown that the anomalous, by more than an order of magnitude with respect to the value under normal condition, decrease of electric conductivity under the experimental conditions is due primarily to the change in the interatomic distance. The results obtained can be explained on the basis of the hypothesis that a molecular structure is formed in the lithium at high pressure. © *1999 American Institute of Physics.*
[S0021-3640(99)01221-9]

PACS numbers: 62.50.+p, 72.15.Eb, 71.20.Dg

Investigations at high pressure play an important role in understanding the fundamental properties of matter. The conventional point of view is that as density and pressure increase, structural phase transformations occur in a solid, a closest-packed phase with the maximum coordination number appears, insulators become conductors, and ionization by pressure occurs in extreme states of matter. Under normal conditions lithium possesses an ordered body-centered cubic (bcc) structure, metallic sheen and conductivity, and it is a typical metal. However, quantum-mechanical calculations[1] show that under pressure the nuclei of the alkali metal lithium form bound pairs, leading to the appearance of structures similar to condensed molecular phases of hydrogen and, most likely, similar with respect to their electronic properties to narrow-gap semiconductors. It is expected that the bcc structure of lithium, which is stable under ordinary conditions, transforms near 50 GPa into an orthorhombic structure and then at ~100 GPa into a molecular structure.

The first, recent experiments on the static compression of lithium in diamond anvils[2,3] have revealed a number of interesting optical anomalies, but they do not contain measurements of the electrical conductivity — the basic indicator of metal–insulator transitions.

Our objective in the present investigation is to measure the electrical conductivity of lithium under quasi-isentropic loading up to 60 GPa, attained by special explosive dynamic-pressure generators. In one series of experiments we employed multistep quasi-

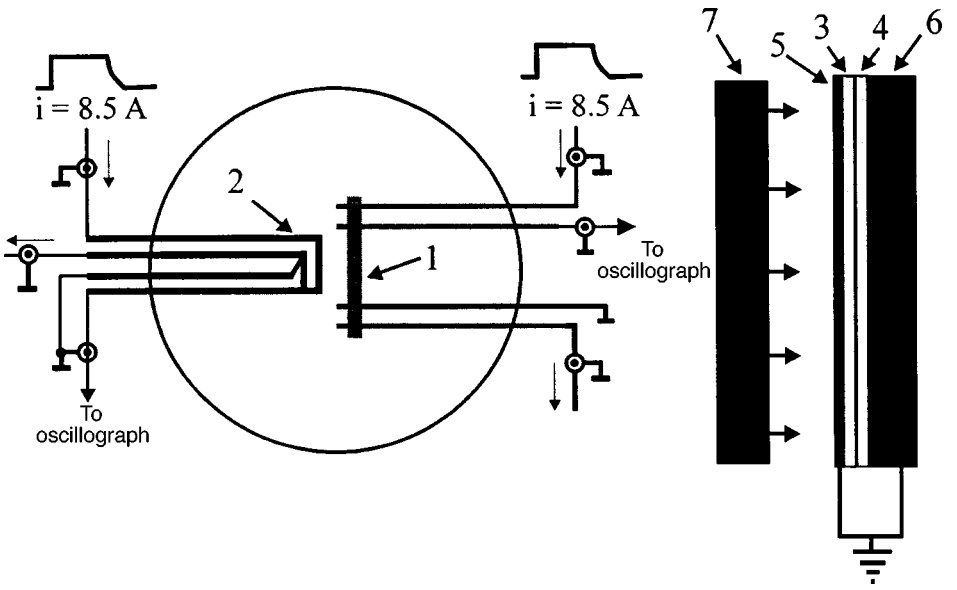

FIG. 1. Diagram of the experiments.

isentropic compression specially produced by a sequence of shock waves that makes it possible to decrease substantially the final temperature of the material and, correspondingly, to reach higher densities compared with compression using a single shock wave.[4] For example, the estimated change in temperature of lithium behind a single wave of amplitude 60 GPa is approximately 5200 K, while the quasi-isentropic compression regime realized in our experiments gives 660 K with the same pressure.

An even larger decrease of the entropy and temperature of compressed lithium was achieved in a different series of experiments as a result of smearing of the shock fronts in a medium with anomalous dynamic compressibility (quartz glass). For definite assumptions in calculations of the temperature and density of the compressed material, we considered this loading regime to be isentropic.

We note that under the conditions of the dynamic experiments performed, the characteristic spatial and temporal scales substantially decrease the probability of diffusion and chemical processes occurring in the experimental samples as compared with experiments in diamond anvils.

The general layout of the experiments and the construction of the measuring cell for obtaining quasi-isentropic compression of lithium samples are shown in Fig. 1. In the experiments, two independent measuring channels were used. Power to the channels was supplied by a pulsed generator, making it possible to produce in low-resistance loads square current pulses of magnitude 8.5 A. A lithium sample 1 in the form of 150–200 μm thick foil and a piezoresistive manganin pressure gage 2 were placed between the layers 3 and 4 of low-density polyethylene (0.928 g/cm^3), each about 1 mm thick. The pressure gage and the experimental sample were inserted into the measuring circuits in a four-point scheme, which ruled out any influence due to the resistance of the contacts and input leads. The apparatus also included an 80 mm in diameter and 2 mm thick,

Kh18N10T steel, base 5 and a 6 mm thick copper reflector plate 6. Preliminary experiments established that under our experimental conditions polyethylene is a good insulator (the resistivity exceeds $10^5\ \Omega \cdot \mathrm{cm}$). The apparatus was assembled in an argon atmosphere with all gaps filled with vacuum grease. At the final phase the plates 5 and 6 were tightened together with bolts. The electric signals were recorded with a Tektronix TDS-744A digital oscillograph in the frequency band 0–1 GHs with a 2 ns sampling time.

Dynamic loading of a sample was performed by a series of shock waves circulating between the base 5 and the reflector 6. The series of shock waves was initiated by the impact of a steel plate 7 accelerated to the required velocity by special explosive devices. Heat effects during dynamic compression of the samples were further decreased by additionally introducing two fused-quartz plates into the experimental cell. For example, in the experiment described below the layers in the direction from the base to the reflector possessed the following thicknesses: polyethylene — 0.55 mm; quartz — 2.0 mm; polyethylene — 0.4 mm; lithium — 150 μm; polyethylene — 0.9 mm. quartz — 1 mm. The idea of these experiments was to use the anomalous compressibility of quartz below the elastic limit[5,6] and the kinetic laws of its transition into the plastic state, which cause the shock front to become smeared and, correspondingly, lead to virtually isentropic compression. This method is described in detail in Ref. 7 for the example of silicate glass, which possesses close dynamic properties. We note that according to our data quartz can be used for isentropization not only of the direct but also the reflected compression waves right up to ~ 70 GPa.

The thermodynamic properties of lithium (temperature, sound velocity, and so on) under dynamic loading conditions were determined using a semiempirical multiphase equation of state[8] on the basis of the measured pressure, since numerical simulation of the process of multiple shock compression showed complete agreement between the pressures calculated by solving the problem of the decay of a discontinuity and the experimental values. To describe the low-temperature states correctly, the model of Ref. 8 was modified to a full Debye model of a crystal,[9] and the Debye function was approximated analytically. The change in the thickness of the lithium samples under pressure, resulting in a corresponding correction of the resistivity ratio ρ/ρ_{293}, was also taken into account in analyzing the experimental data.

The result of a typical experiment on the measurement of the electrical conductivity of lithium under a multistep quasi-isentropic compression to final pressure ~ 60 GPa is presented in Fig. 2 in the form of a time-dependence of the ratio of the instantaneous resistance R of the sample to its initial value R_{293} at room temperature. The figure also shows the profile of the pressure p obtained with a manganin gauge. It is evident that the pressure grows in steps corresponding to reflections of a shock wave from the plates 5 and 6. The resistivity of lithium grows synchronously with the pressure. Seven jumps can be resolved in the curve $R(t)$. Figure 3 shows in a similar manner the results of an experiment in which lithium was loaded according to a curve close to an isentrope from the initial state at liquid-nitrogen temperature. As noted above, in this experiment the pressure jumps are not shock waves.

The experimental results are shown in Fig. 4 in the form of curves of the resistivity of lithium versus the density. In the experiment with isentropic compression from the initial temperature 77 K, lithium was in the solid phase at all pressures realized. The computed temperatures for this case are plotted along the abscissa at the top of the plot.

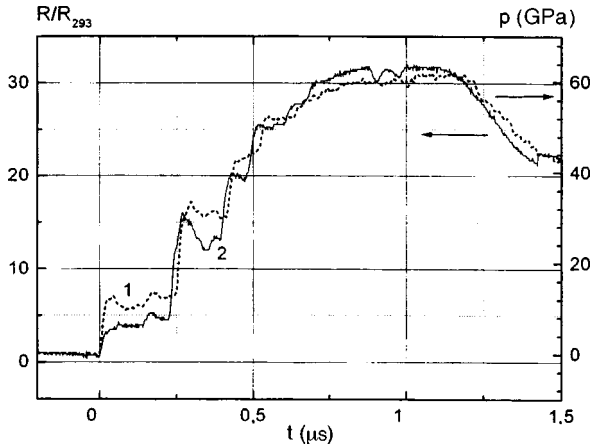

FIG. 2. Experimental pressure profile (curve 1) and the corresponding time dependence of R/R_{293} of a lithium sample under conditions of multistep shock compression.

It is evident that the maximum temperature with lithium density 1.42 g/cm^3 (compression by a factor of 2.7) and pressure $\sim$60 GPa is only 190 K. Nonetheless, the resistivity of lithium is 13 times higher than under normal conditions, and the main increase in ρ is observed in the density range 1.2–1.4 g/cm^3. A similar conclusion can also be drawn from the experiment with multiple shock compression. The corresponding values of ρ/ρ_{293} are plotted as squares with the computed temperatures of the sample indicated above each square. In this arrangment lithium melts in the first shock wave, and under further compression it remains in the liquid state, but even in this case its resistivity increases progressively under compression.

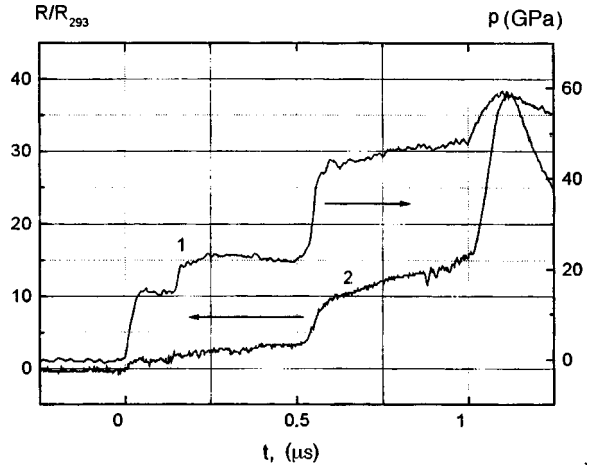

FIG. 3. Experimental pressure profile (curve 1) and the corresponding time-dependence of R/R_{293} of a lithium sample under conditions of isentropic compression with initial temperature 77 K.

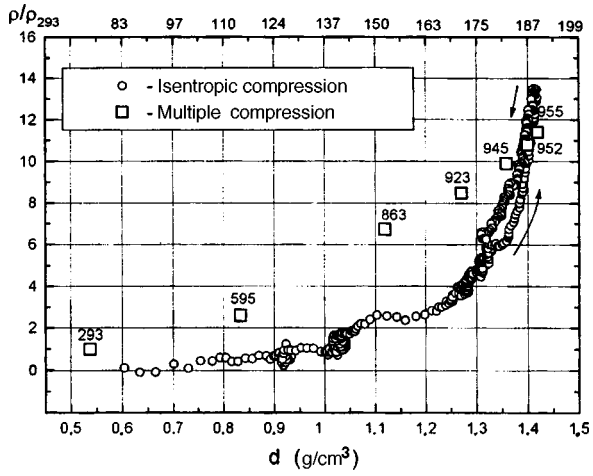

FIG. 4. Experimental curve of the resistivity of lithium versus the density.

We note that the sharp increase in ρ/ρ_{293} observed at densities 1.2–1.4 g/cm^3 for crystal and liquid heated lithium cannot be explained by temperature effects and is primarily due to the change in density, i.e., the interatomic distance. Therefore our data show that lithium — the first metal in the periodic system of elements which has a single valence electron — can no longer be regarded as a simple metal at high pressures. The character of the variation of the electrical conductivity in the experiments performed confirms the concept[1] that under compression lithium approaches a molecular structure. Apparaently, it will be possible to obtaing more definite quantitative results about this phenomenon from similar experiments at lower temperatures and higher pressures as well as by investigating other alkali metals.

We thank N. Ashcroft for stimulating discussions.

[1] J. B. Neaton and N. W. Ashcroft, Nature (London) **100**, 141 (1999).
[2] A. L. Ruoff and Y. Mori, in *Abstracts of International Conference on High Pressures in Science and Technology* (AIRAPT-17), Honolulu (1999), p. 75.
[3] V. V. Struzhkin, M. Somayazulu, R. J. Hemley *et al.*, ibid, p. 76.
[4] Ya. B. Zel'dovich and Yu. P. Raĭzer, *Physics of Shock Waves and High-Temperature Hydrodyamic Phenomena*, Vols. 1 and 2, translation of 1st Russian edition (Academic Press, New York, 1966, 1967) [Russian original, 2nd edition, Nauka, Moscow, 1966].
[5] J. Wackerle, J. Appl. Phys. **33**, 922 (1962).
[6] H. Sigiura, K. Kondo, and A. Sawaoka, J. Appl. Phys. **52**, 3375 (1981).
[7] V. I. Postnov, S. S. Nabatov, A. A. Shcherban', and V. V. Yakushev, Zh. Tekh. Fiz. **57**, 1181 (1987) [Sov. Phys. Tech. Phys. **32**, 694 (1987)].
[8] A. V. Bushman, G. I. Kanel', A. L. Ni, and V. E. Fortov, *Thermal Physics and Dynamics of Intense Pulsed Interactions* (OIKhF SSSR, Chernogolovka, 1988).
[9] L. D. Landau and E. M. Lifshitz, *Statistical Physics* (Pergamon Press, New York) [Russian original, Nauka, Moscow, 1995).

Translated by M. E. Alferieff

Ferroelectric phase transition in Langmuir–Blodgett films of copper phthalocyanine

S. G. Yudin, L. M. Blinov, N. N. Petukhova, and S. P. Palto
Institute of Crystallography, Russian Academy of Sciences, 117333 Moscow, Russia

(Submitted 11 October 1999)
Pis'ma Zh. Éksp. Teor. Fiz. **70**, No. 9, 625–631 (10 November 1999)

A ferroelectric phase transition is observed in Langmuir–Blodgett films prepared from substituted copper phthalocyanine molecules. The linear and nonlinear dielectric properties of the films and the switching of their spontaneous polarization are investigated in the temperature range of the phase transition. The observed features can be explained by the Landau–Ginzburg model of a first-order phase transition. © *1999 American Institute of Physics.* [S0021-3640(99)01321-3]

PACS numbers: 77.80.Bh, 77.84.Jd, 68.18.+p

Fundamentally new possibilities for investigating ferroelectricity appeared from the moment the first ferroelectric Langmuir–Blodgett films (LB) based on the well-known copolymer vinylidene fluoride with trifluoroethylene (PVDF–TFE).[1,2] It became possible to talk about proper two-dimensional ferroelectricity.[3]

In the present letter we report the observation of ferroelectric properties in a fundamentally new object — LB films of substituted copper phthalocyanine (CPC). A characteristic feature of this observation is that the disk-shaped molecules of the metallic complexes of phthalocyanines (including CPC) are centrosymmetric (D_{4h} symmetry), and one would think that they cannot form a ferroelectric structure. In this connection, lead phthalocyanine (LPC), in films of which interesting electric anomalies (specifically, switching of conductivity) that can be explained by the induction of a polar phase by an external electric field, have been observed, is not an instructive example.[4] In the LPC molecule, the lead atom, which is too large, protrudes out of the plane of the macroring for steric reasons, thereby removing the center of inversion by lowering the symmetry of the molecule to D_4 and creating an electric dipole perpendicular to this plane. The results of the present investigations convincingly show the presence of switchable spontaneous polarization and a phase transition into a nonpolar (paraelectric) phase in alkyl-substituted CPC films obtained by the LB method.[5] This is a second example of ferroelectricity in LB films, but in the new system, in contrast to PVDF–TFE films,[1–3] we seem to be dealing with an improper mechanism of ferroelectricity.

The structural formula of the compound investigated is displayed in Fig. 1. The details of the preparation of films of this compound and investigations of their structure by the STM method have been published in Ref. 6. Here we note that in the present work LB films consisting of 10 monomolecular layers, prepared by the standard LB method at 20 °C and surface pressure $\pi = 18$ mN/m using *Z*-type transfer,[7] are investigated. The

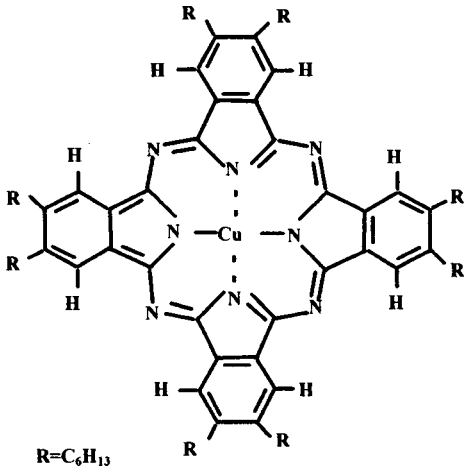

FIG. 1. Structural formula of the molecule.

thickness of the films (20 ± 2 nm) was measured according to the optical density with calibration by an Autoprobe Park Scientific Instruments atomic-force microscope operating in the contact-free mode.[8]

For electric measurements, a 1 mm wide aluminum electrode was deposited on a 20×20 mm substrate in a 10^{-5} torr vacuum. Three similar aluminum electrodes were deposited on top of the film.

The arrangement for temperature investigations is shown in Fig. 2. The temperature of the sample was varied in the range from -20 to $+40\,^{\circ}$C in a thermostat using Peltier devices and a platinum resistance thermometer. The measuring system consists of a set of virtual devices (generator, synchronous detector, digital oscillograph, and others), implemented in a PhysLab program.[9]

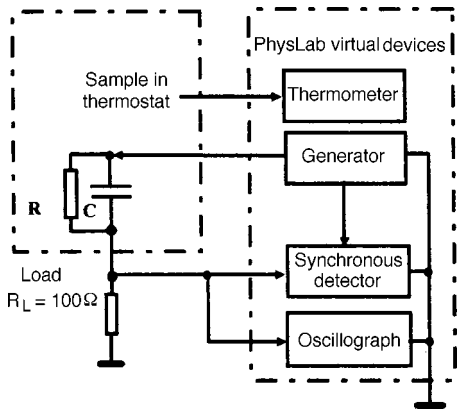

FIG. 2. Diagram of the experimental apparatus. The sample is presented in the form of an equivalent circuit with resistance R and capacitance C.

For dielectric measurements, a sinusoidal voltage from a generator is applied to the sample, and a synchronous detector is used to record the amplitude and phase relations of the current response. In the present work we employ a sinusoidal voltage with frequency 1 kHz and amplitude 500 mV. The PhysLab synchronous detector makes it possible to perform not only simultaneous detection of the real and imaginary components of the current at the fundamental frequency but also simultaneous detection of the corresponding components on other harmonics. We used the last property to investigate the temperature behavior of the nonlinear part of the electric susceptibility characteristic for ferroelectric phase transitions.

In accordance with the equivalent circuit for the sample presented in Fig. 2, the current in the circuit is determined by the relation

$$I = I_R + I_C = \frac{U}{R} + \frac{d(CU)}{dt}, \tag{1}$$

where I_R and I_C are, respectively, the active and reactive components of the current; R is the Ohmic resistance of the sample; and, U is the voltage on the sample. In Eq. (1) the capacitance of the sample cannot be removed from the derivative operator, since for nonlinear dielectrics it is a function of voltage. Taking this into consideration, the capacitive component of the current can be represented in the form

$$I_C = C(U)\frac{dU}{dt} + U(t)\frac{dC(U)}{dt}$$

$$\cong \left(C_0 + U(t)\frac{dC}{dU} \right) \frac{dU}{dt} + U(t)\frac{dC}{dU}\frac{dU}{dt} = C_0\frac{dU}{dt} + 2U(t)\frac{dC}{dU}\frac{dU}{dt}, \tag{2}$$

where $C_0 = C(U=0)$. In Eq. (2) we employed the weak field dependence of the capacitance for low voltages on the sample, retaining only two terms in the Taylor series. If a sinuosoidal field $U(t) = U_0 \sin(\omega t)$ is applied to the sample, the relation (1), taking account of Eq. (2), becomes

$$I = \frac{U_0}{R}\sin(\omega t) + \omega U_0 C_0 \cos(\omega t) + \omega U_0^2 \sin(2\omega t)\frac{dC}{dU}. \tag{3}$$

It is easy to see that phase-sensitive detection at the fundamental frequency makes it possible to measure the first two terms, which are proportional to the conductance and capacitance of the sample. These components can be easily distinguished by synchronous detection, since they are shifted in phase by 90° relative to one another. The third term reflects the nonlinear contribution and is observed at higher harmonics.

To observe switching of the spontaneous polarization we shall employ Mertz's well-known method, where in the same arrangment as in Fig. 2 a voltage with a triangular form is applied to the sample and current pulses containing the characteristic contribution from the polarization-switching current is recorded with a virtual digital oscillograph.

Figure 3 shows the temperature dependences of the capacitive and active components of the currents, which are proportional to the real part of the permittivity and the conductance of the sample, respectively. On cooling from $+15$ to $+5°$ C sharp growth of these quantities, which reach their maximum values $+5°$ C, is observed. Even sharper

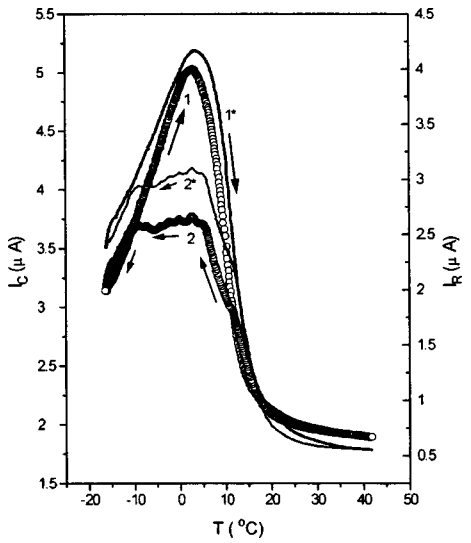

FIG. 3. Temperature dependences of the capacitive I_C (curves 1 and 2) and active I_R (curves 1′ and 2′) components of the effective current with a sinusoidal voltage $U=U_0\sin(2\pi ft)$ ($f=1000\,Hz$, $U_0=500$ mV) applied to the sample. The arrows show the direction of temperature variation.

changes are observed on heating from $-20\,^{\circ}$C to $+40\,^{\circ}$C: The capacitance changes by a factor of 3, and the conductance changes by almost a factor of 10. Thus a quite distinct phase transition is observed.

The observation of switching currents, which arise at temperatures below $+25\,^{\circ}$C (Fig. 4) and are characteristic for ferroelectrics, is important. Indeed, at $+30\,^{\circ}$C the current response to a triangular voltage ($f=700$ Hz, $U_0=6$ V) consists of square pulses, which is a typical capacitance contribution in samples of linear dielectrics. Below $20\,^{\circ}$C the situation changes sharply. Distinct current pulses with duration $dt\cong 100$ μs arise against the background of a capacitive contribution and a conduction current that arises. The amplitude of the pulses increases as temperature decreases to $+4\,^{\circ}$C. The polarization-switching currents remain right down to the lowest temperatures achieved in the experiment, but at temperatures below $+10\,^{\circ}$C they are largely masked by the rapidly rising contribution from the conduction current, which is seen even at $T=10\,^{\circ}$C (Fig. 4). The switchable polarization reaches 3×10^{-4} C/m^2 at $10\,^{\circ}$C. The coercive field increases as the temperature decreases and corresponds to 1 V of applied voltage at $T=10\,^{\circ}$C. On the basis of the 20-nm film thickness the coercive field is estimated to be 5×10^8 V/m.

Even though a distinct amplitude hysteresis of the permittivity ϵ is observed, its temperature hysteresis is weak. This makes it difficult to determine the order of the phase transition from the temperature variation of ϵ. Important additional information about the character of the phase transition can be obtained from data on the nonlinearity of the permittivity measured on the third harmonic. According to the phenomenological Landau–Ginzburg model,[10] the contribution of the a proper ferroelectric (or improper ferroelectric with polarization proportional to the structural order parameter) due to the polarization P, to the free energy density can be represented in the form

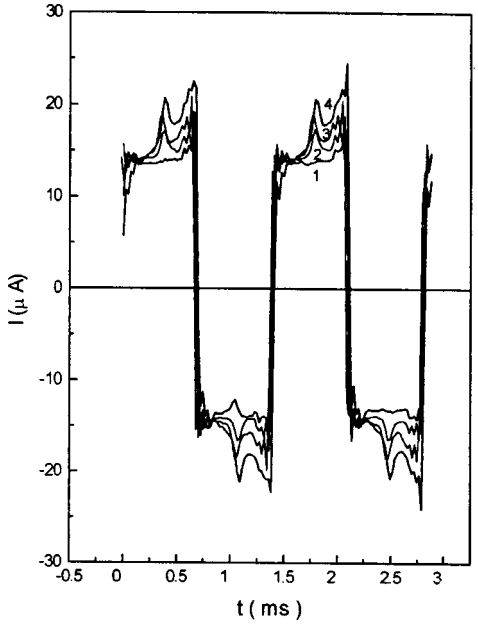

FIG. 4. Current oscillograms for various temperatures with a triangular voltage with amplitude $U_0=6$ V applied to the sample. Curves: 1 — $T=30$ °C, 2 — $T=15$ °C, 3 — $T=12$ °C, 4 — $T=10$ °C.

$$F=\frac{1}{2}\alpha P^2+\frac{1}{4}\beta P^4+\frac{1}{6}\gamma P^6-EP, \quad \alpha=\alpha_0(T-T_0), \tag{4}$$

where α_0, β, and γ are the temperature-independent Landau coefficients and T_0 is the Curie temperature. We note that for $\beta>0$, $\gamma\geqslant 0$ the free energy (4) describes a second-order phase transition, and for $\beta<0$, $\gamma>0$ it describes a first-order phase transition.

Minimizing the free energy (4), it is easy to find an equation of state in an electric field:

$$E=P[\alpha_0(T-T_0)+\beta P^2+\gamma P^4]. \tag{5}$$

To obtain the nonlinear contribution, determined by the last term in Eq. (3), we must find the field derivative of the electric susceptibility χ, which is determined from Eq. (5) by differentiating with respect to the polarization:

$$\chi^{-1}=\alpha+3\beta P^2+5\gamma P^4. \tag{6}$$

The derivative of interest to us is obtained by repeated differentiation of Eq. (6):

$$\frac{d\chi}{dE}=-\chi^3(6\beta P+20\gamma P^3). \tag{7}$$

In Eq. (7) the polarization depends on the field in accordance with the equation of state (5), but for weak fields (below the coercive field), which correspond to the experiment, it is convenient to represent the polarization approximately as

$$P \cong P_s + E_\chi, \tag{8}$$

where P_s is the spontaneous polarization, differing from zero only in the ferroelectric phase.

Substituting the expression (7), using Eq. (8), into Eq. (3) we obtained the nonlinear contributions to the fifth harmonic:

$$I_{2\omega} = -2\left\{\chi^3[3\beta P_s + 10\gamma P_s^3] + 15\frac{U_0^2}{d^2}\chi^5\gamma P_s\right\} S\omega\frac{U_0^2}{d^2}\sin 2\omega t, \tag{9}$$

$$I_{3\omega} = 3\chi^4[\beta + 10\gamma P_s^2] S\omega\frac{U_0^3}{d^3}\cos(3\omega t) + \frac{15}{2}\gamma\chi^6 S\omega\frac{U_0^5}{d^5}\cos(3\omega t), \tag{10.1}$$

$$I_{4\omega} = 15\chi^5\gamma P_s S\omega\frac{U_0^4}{d^4}\sin(4\omega t), \tag{10.2}$$

$$I_{5\omega} = -\frac{5}{2}\gamma\chi^6 S\omega\frac{U_0^5}{d^5}\cos(5\omega t), \tag{10.3}$$

where S is the area covered by the electrodes on the sample.

It is easy to see that all Landau coefficients can be determined by measuring the above-noted harmonics of the current. Here we shall discuss only the measurements of the third harmonic, which in accordance with the model is determined by the expression (10.1). A very important point here is that after a 90° shift of the reference signal used for synchronous detection (i.e., the reference signal should have the form $\sim\cos(3\omega t)$, and then the so-called Y component is detected), the sign of the third-harmonic signal in the paraelectric phase ($P_s = 0$) recorded by the synchronous detector should be determined by the sign of the coefficient β. This immediately permits drawing a conclusion about the order of the phase transition. Moreover, for a first-order phase transition $I_{3\omega}$ can vanish when

$$\beta + 10\gamma P_s^2 = 0. \tag{11}$$

Correspondingly, for sufficiently large P_s, the sign of $I_{3\omega}$ can change in the ferroelectric phase or in the region of coexistence of the phases.

The experimental data presented in Fig. 5 contain the features indicated. First, in the paraelectric phase the Y component of the signal is negative at $T = +40\,^\circ$C. Second, at $T = +15\,^\circ$C the signal reaches its minimum value and even changes sign (in the case of heating) in accordance with Eq. (11). Thus, in accordance with Eq. (10.1) the coefficient $\beta < 0$, and the phase transition is a first-order transition. As temperature decreases, the absolute value of the signal increases as a result of an increase in the electric susceptibility, to the fourth power of which the response is proportional. In a heating cycle the maximum absolute value of the signal with respect to temperature shifts (from $+8\,^\circ$C on heating to $+1\,^\circ$C on cooling), which also agrees with the first order nature of the phase transition. We note that the range $\{+1, +8\,^\circ\text{C}\}$ by no means determines the region of coexistence of the two phases. As noted above, on heating the condition (11) is realized near $T = 15\,^\circ$C, which falls below the upper limiting temperature of existence of the polar

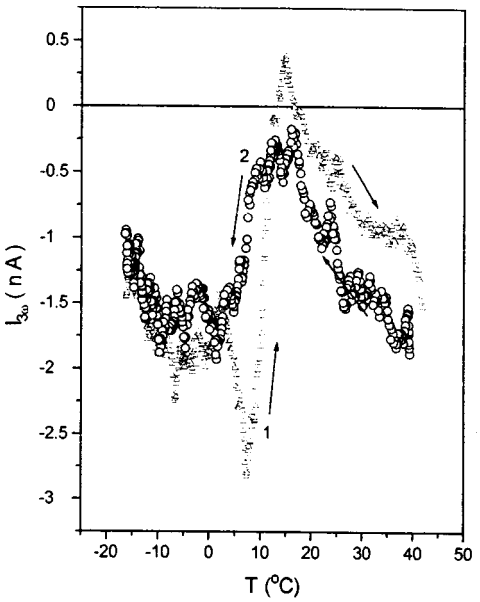

FIG. 5. *Y* component of the current response (effective value) on the third harmonic of the sinusoidal voltage applied to the sample ($U=U_0\sin(2\pi ft)$, $f=1000$ Hz, $U_0=500$ mV). The arrows show the direction of temperature variation. Curves: 1 — heating, 2 — cooling.

phase. For the present we place the Curie temperature in the range from $-10\,^{\circ}$C to $+5\,^{\circ}$C. As far as the mechanism of ferroelectricity is concerned, more detailed investigations are required to determine it. A substituted CPC molecule is large enough (volume $V_m \approx 3$ nm^3) to explain the possibility of proper ferroelectricity appearing as a result of dipole–dipole interactions, even it is assumed that the molecule possesses spontaneously broken D_4 symmetry. Indeed, a reliable estimate for the appearance of ferroelectricity is the inequality[11] $p^2/\epsilon_0 V_m \gg kT$, where ϵ_0 is the vacuum permittivity and p is the molecular dipole. In our system, at $T=300$ K ferroelectricity can arise spontaneously for a molecular dipole moment $p \gg 10^{-29}$ C·m (≈ 3 D), and the expected spontaneous polarization (dipole moment per unit volume p/V_m) should exceed 3.3×10^{-7} C/m^2. However, in the experiment we observe an order of magnitude lower polarization, and it is difficult to imagine a distortion of the structure of a CPC molecule, which has only nonpolar substituents, that is large enough to give $p \approx 3$ D.

An improper mechanism of ferroelectricity seems more realistic. It is known that similar substituted phthalocyanines form columnar phases with electronic conduction along the columns.[12] Columns of this type have also been observed in a monolayer of our material on a graphite substrate.[6] We infer that a phase transition from a structure with polar columns to a structure with nonpolar columns occurs in the range 5–20 °C. In the higher temperature (paraelectric) phase, molecules either retain their centrosymmetric shape or, acquiring a cup shape, they are packed in columns randomly, so that the dipole moments of the columns are zero. In the low temperature, ferroelectric phase the ''molecules-cups'' (formed, for example, as a result of deformation of alkyl tails) are nested, forming polar columns with a total dipole moment $\mathbf{P}=\mathbf{p}N$ (N is the number of

molecules in a column). The vector **P** plays the role of the spontaneous polarization, which is switched by an electric field, and we observe the ferroelectric effect. Such a model has been discussed previously[13] (see also the review Ref. 14), and it also seems to explain the recent observations of ferroelectric switching in a columnar phase of a liquid crystal.[15] In our case, $p \approx 0.3$ D, which does not give rise to any difficulties, is sufficient to explain the observed spontaneous polarization by an improper mechanism.

In summary, we have observed for the first time a ferroelectric phase transition in LB films obtained from substituted CPC molecules. The results obtained can be explained on the basis of the Landau–Ginzburg theory, based on the model of a first-order phase transition. The most likely molecular model is based on the idea of an improper ferroelectric phase transition into a columnar phase with cup-shaped dipolar molecules whose close-packing leads to spontaneous polarization.

We thank Professor J. Simon (ESPCI, Paris) for providing the copper phthalocyanine and M. De Santo (Calabria University) for determining the film thickness using an atomic force microscope. This work was supported by the Russian Fund for Fundamental Research (Grants 99-02-16484, 98-02-17071).

[1] S. Palto, L. Blinov, A. Bune *et al.*, Ferroelectrics **19**, 65 (1995).
[2] S. Palto, L. Blinov, E. Dubovik *et al.*, Europhys. Lett. **34**, 465 (1996).
[3] A. Bune, V. Fridkin, S. Ducharme *et al.*, Nature (London) **391**, 874 (1998).
[4] Th. Frauenheim, C. Hamann, and M. Mueller, Phys. Status Solidi A **86**, 735 (1984).
[5] L. M. Blinov, Usp. Fiz. Nauk **155**, 443 (1988) [Sov. Phys. Usp. **31**, 623 (1988)].
[6] A. Zlatkin, S. Yudin, J. Simon *et al.*, Adv. Mater. Opt. Electron. **5**, 259 (1995).
[7] S. G. Yudin, S. P. Palto, V. A. Khavrichev *et al.*, Thin Solid Films **210/211**, 46 (1992).
[8] L. M. Blinov, R. Barberi, G. Cipparrone *et al.*, Liq. Cryst. **26**, 427 (1999).
[9] S. P. Palto, *Molecular Field Effects in Langmuir–Blodgett Films: Optics and Stark Spectroscopy*, Doctoral Disssertation in Physico-Mathematical Sciences (Moscow, 1998).
[10] V. L. Ginzburg, Zh. Éksp. Teor. Fiz. **19**, 36 (1949).
[11] S. A. Pikin, *Structural Transformations in Liquid Crystals* (Nauka, Moscow, 1983).
[12] D. Adam, P. Schumacher, J. Simmerer *et al.*, Nature (London) **371**, 141 (1994).
[13] L. Lin, Mol. Cryst. Liq. Cryst. **146**, 41 (1987).
[14] L. M. Blinov, Liq. Cryst. **24**, 143 (1998).
[15] D. Kilian, D. Knawby, M. A. Athanassopoulou *et al.*, in *7th International Conference on Ferroelectric Liquid Crystals*, Darmstadt, September, Conference Summaries (1999).

Translated by M. E. Alferieff

Experimental observation of localization–delocalization of Cooper pairs in $Nd_{1.85}Ce_{0.15}CuO_4$

F. S. Nasredinov, N. P. Seregin, and P. P. Seregin
St. Petersburg State Technical University, 195251 St. Petersburg, Russia

(Submitted 16 September 1999; resubmitted 12 October 1999)
Pis'ma Zh. Éksp. Teor. Fiz. **70**, No. 9, 632–635 (10 November 1999)

Localization–delocalization of cooper pairs on ^{67}Zn impurity centers in the copper sublattice in the high-temperature superconductor $Nd_{1.85}Ce_{0.15}CuO_4$ was observed by emission Mössbauer spectroscopy on ^{67}Cu (^{67}Zn). © *1999 American Institute of Physics.* [S0021-3640(99)01421-8]

PACS numbers: 74.72.Jt, 74.62.Dh, 74.20.Fg, 61.18.Fs

Superconductivity is due to the appearance of Cooper pairs (the spatial scale of Cooper correlation is 10^7-10^{-4} cm) and the formation of a Bose condensate, described by a single coherent wave function. This means that the electron density distribution at the lattice sites of the superconductor should differ at temperatures above and below the superconducting transition temperature T_c.

Since the isomeric shift I of Mössbauer spectra is given by[1]

$$I=\alpha\Delta\rho(0) \tag{1}$$

(here $\Delta\rho(0)$ is the difference of the relativistic electronic states at the nuclei investigated in two samples and α is a constant that depends on the nuclear parameters of the isotope investigated), it is in principle possible to observe the formation of Cooper pairs by measuring the temperature dependence of the center of gravity S of the Mössbauer spectra of superconductors. The temperature dependence S at constant pressure P is determined by three terms[1]

$$(\delta S/\delta T)_p=(\delta I/\delta \ln V)_T(\delta \ln V/\delta T)_p+(\delta D/\delta T)_p+(\delta I/\delta T)_V. \tag{2}$$

The first term in this expression is the dependence of the isomeric shift I on the volume V. The second term describes the effect of the second-order Doppler shift D, and in the Debye approximation it has the form[2]

$$(\delta D/\delta T)_p=-(3kT/2Mc^2)F(T/\Theta), \tag{3}$$

where k is Boltzmann's constant, M is the mass of the probe nucleus, c is the speed of light in vacuum, Θ is the Debye temperature, and $F(T/\Theta)$ is the Debye function. Finally, the third term in the expression (2) describes the temperature dependence of the isomeric shift I at constant volume. The appearance of this term is due to the change in the electron density at Mössbauer nuclei, and this effect is expected with a transition of the matrix into the superconducting state.

However, attempts to observe the formation of Cooper pairs and a Bose condensate by measuring the temperature dependence of the center of gravity S of the Mössbauer spectra of ^{119}Sn for the classical superconductor Nb_3Sn were unsuccessful:[3] The observed temperature dependence of S was satisfactorily described by a second-order Doppler shift and no features were observed in the behavior of $S(T)$ near T_c that could be attributed to a change in the isomeric shift. This is explained by the small value of $\Delta I/2\Gamma_{nat}$ (here ΔI is the maximum achievable difference of the isomeric shifts of the Mössbauer spectra in the normal and superconducting phases, $\Gamma_{nat}=\hbar/\tau$ is the natural width of the nuclear level, and τ is the average lifetime of the nuclear level), which for ^{119}Sn Mössbauer spectroscopy does not exceed 6.

The conditions for observing Cooper pairs by Mössbauer spectroscopy should be more favorable for high-temperature superconductors (which have a minimal Cooper correlation scale), if a Mössbauer probe for which $\Delta I/2\Gamma_{nat} \gg 10$ is used. The choice of objects for investigation should also take account of the need to introduce a Mössbauer probe at the lattice sites. These conditions are satisfied for the Mössbauer probe ^{67}Zn in the lattices of copper metal oxides using the emission variant of Mössbauer spectroscopy on ^{67}Cu (^{67}Zn):[4] for ^{67}Zn $\Delta I/2\Gamma_{nat} \sim 200$ and the parent isotope can be introduced ^{67}Cu at the copper sites during synthesis, so that the daughter isotope ^{67}Zn likewise occupies copper sites in the lattice.

In the present work such investigations were performed for the probe ^{67}Zn in the lattice of the high-temperature superconductor $Nd_{1.85}Ce_{0.15}CuO_4$. The control object, for which a superconducting transition is not observed, was cuprous oxide Cu_2O. The samples were synthesized by the conventional ceramic technology.[5,6] The radioactive isotope ^{67}Cu was introduced into $Nd_{1.85}Ce_{0.15}CuO_4$ by diffusion doping at 900 °C in 1 h, and it was introduced into Cu_2O during synthesis. The samples were single-phase, and the transition temperature $T_c = 22$ K was obtained for $Nd_{1.85}Ce_{0.15}CuO_4$.

The Mössbauer spectra of ^{67}Cu (^{67}Zn) were obtained with the absorber ^{67}ZnS (the surface density is 1000 mg/cm^2 with respect to the ^{67}Zn isotope). The temperature of the absorber for all spectra was 10(2) K, while the source temperature could vary from 10(1) to 60(1) K.

In agreement with the data obtained in Refs. 5 and 6 at 4.2 K, the Mössbauer spectra of the ceramic $Nd_{1.85}Ce_{0.15}CuO_4$ in the chosen temperature range consists of well-resolved quadrupole triplets, whose isomeric shift corresponds to $^{67}Zn^{2+}$ ions at the copper sites. Figure 1 shows the temperature dependence of the quadrupole interaction constant $C=eQU_{zz}$ (here Q is the quadrupole moment of the ^{67}Zn nucleus and U_{zz} is the principal component of the electric field gradient tensor at the ^{67}Zn nucleus), and it is evident that C is essentially temperature-independent for $Nd_{1.85}Ce_{0.15}CuO_4$ and Cu_2O (the data obtained in Refs. 5 and 6 at 4.2 K are also plotted in the figure). Since for a Zn^{2+} probe the electric field gradient at the ^{67}Zn nuclei is produced only by the lattice atoms, taking account of the negligibly small variations of the lattice constants of $Nd_{1.85}Ce_{0.15}CuO_4$ in the temperature range 4.2–60 K,[7] the temperature independence of C is not surprising.

The temperature dependences of the center of gravity S of the spectrum, measured relative to its value at 22 K, differs substantially for $Nd_{1.85}Ce_{0.15}CuO_4$ and Cu_2O, though

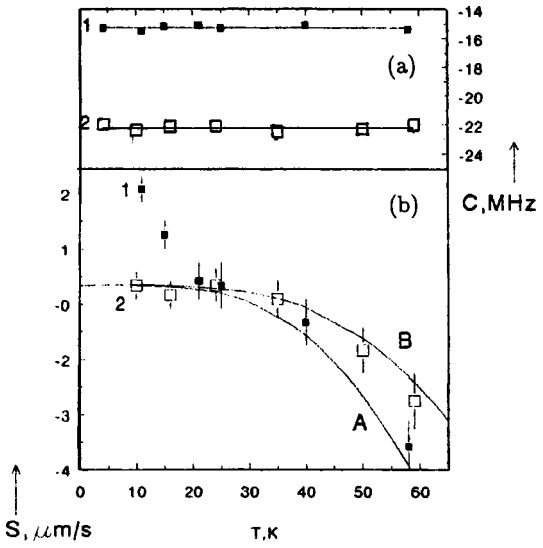

FIG. 1. a) Temperature dependence of the quadrupole interaction constant C of the probe ^{67}Zn for $Nd_{1.85}Ce_{0.15}CuO_4$ (*1*) and Cu_2O (*2*). b) Temperature dependences of the center of gravity S of the Mössbauer spectrum of ^{67}Zn, measured relative to its value at 22 K, for $Nd_{1.85}Ce_{0.15}CuO_4$ (*1*) and Cu_2O (*2*). The data for 4.2 K are taken from Refs. 3 and 4. The broken lines show the theoretical temperature dependences of S for the second-order Doppler shift with $\theta = 300$ K (A) and $\theta = 400$ K (B).

for $Nd_{1.85}Ce_{0.15}CuO_4$ no anomalous jumps are observed in S at the transition through T_c (Fig. 1b).

As noted, the temperature dependence of S is determined by the expression (2). As calculations show,[8] the first term in the expression (2) can be neglected for ^{67}Zn, since for the chosen temperature range it did not exceed 0.03 μm/s, and no structural phase transitions are observed for $Nd_{1.85}Ce_{0.15}CuO_4$ in the temperature range 10–60 K.[7]

The second term in the expression (2) describes the effect of the second-order Doppler shift and, as one can see from Fig. 1b, the experimental data for Cu_2O in the temperature range 10–60 K and for $Nd_{1.85}Ce_{0.15}CuO_4$ at temperatures $T > T_c$ are satisfactorily described by the dependence (3) with $\Theta = 300$ K and $\Theta = 400$ K (according to Ref. 9, $\Theta \sim 300$ K for $Nd_{1.85}Ce_{0.15}CuO_4$).

Finally, the third term in the expression (2) describes the temperature dependence of the isomeric shift I. This term appears as a result of the change in the *s*-electron density at the ^{67}Zn nuclei. The increase in S with decreasing temperature in the range $T < T_c$ attests to an increase in the electron density at the ^{67}Zn nuclei and therefore localization of electron pairs at the Mössbauer probe.

In summary, it has been established that for the superconductor $Nd_{1.85}Ce_{0.15}CuO_4$ the temperature dependence of S in the temperature range $T > T_c$ is determined by the second-order Doppler shift, while in the range $T < T_c$ localization of Cooper pairs on Mössbauer pairs on a Mössbauer probe predominantly influences S. As temperature decreases, the effect of the indicated process on the value of S increases, since the fraction of the Bose condensate increases with decreasing temperature. We note that the Möss-

bauer probe ^{67}Zn is a dielectronic center with a negative correlation energy — its charge state can change only as a result of the transfer of two electrons simultaneously, and the electron pair localized on the center possesses zero total angular momentum, orbital angular momentum and spin. At the same time, according to the BCS model, for $T < T_c$ electrons with opposite momenta are paired together, so that the total momentum, orbital angular momentum and spin of a Cooper pair are also zero. It is this combination of these factors that makes the conditions favorable for observing the localization–delocalization effect for a ^{67}Zn probe.

This work was supported by the Russian Fund for Fundamental Research (Grant 97-02-16216).

[1] G. M. Rothberg, S. Guimard, and N. Benczer-Koller, Phys. Rev. B **1**, 136 (1970).
[2] H. Wegener, *Der Mössbauer-Effect und seine Anwedung in Physik und Chemie* (Bibliographisches Institut AG, Mannheim, 1966).
[3] J. S. Shier and R. D. Taylor, Phys. Rev. **174**, 346 (1968).
[4] V. F. Masterov, F. S. Nasredinov, N. P. Seregin *et al.*, Zh. Éksp. Teor. Fiz. **114**, 1079 (1998) [JETP **87**, 588 (1998)].
[5] N. P. Seregin, F. S. Nasredinov, V. F. Masterov *et al.*, Solid State Commun. **87**, 345 (1993).
[6] F. S. Nasredinov, V. F. Masterov, N. P. Seregin *et al.*, Zh. Éksp. Teor. Fiz. **99**, 1027 (1991) [Sov. Phys. JETP **72**, 570 (1991)].
[7] W. Sadowski, H. Hagemann, M. Francois *et al.*, Physica C **170**, 103 (1990).
[8] M. Steiner, W. Potzel, C. Schafer *et al.*, Phys. Rev. B **41**, 1750 (1990).
[9] A. Tigheza, R. Kuentzler, G. Pourroy *et al.*, Physica B **165**, 1331 (1990).

Translated by M. E. Alferieff

Is control of the spontaneous decay of the long-lived state of the isotope ^{119m}Sn possible?

V. I. Vysotskiĭ*)
T. Shevchenko Kiev University, 252000 Kiev, Ukraine

(Submitted 30 September 1999)
Pis'ma Zh. Éksp. Teor. Fiz. **70**, No. 9, 636–637 (10 November 1999)
[S0021-3640(99)01521-2]
PACS numbers: 23.20.−g

Experiments on controlling the gamma decay of the isotope Sn^{119} by means of a resonant absorber (screen) were discussed in Ref. 1. Sn^{119} possesses energy levels $E_3 = 89.5\,\text{keV}$ ($\tau_3 = 245$ days, conversion coefficient $\alpha_3 \approx 5000$), $E_2 = 23.8\,\text{keV}$ ($\tau_2 = 1.85 \times 10^{-8}$ s, $\alpha_2 = 5.5$), and $E_1 = 0$. During the measurements, which lasted for six months, the author detected a slower dropoff of the radiation intensity of a source 1 (near which the resonant screen was located) on the transition $2 \to 1$ than for the control source 2. The author of Ref. 1 believes that this effect is caused by the inhibition of the decay of the level E_3 and occurs because the emitted photons with energy E_{21} are backscattered by the resonant screen and ''because of the relation $3E_{21} \approx E_{32}$ they synchronize the spontaneous decay on the transitions $3 \to 2$ and $2 \to 1$.'' In the opinion of the author, this effect corresponded to an increase in the lifetime by $\Delta\tau_3/\tau_3 \approx (0.1-0.5)$. The author also asserts that he has proposed a new method of influence.

In my opinion the basic assertions made by the author of Ref. 1 are incorrect.

1. The theory and experiments on the influence of a resonant screen on the rate of gamma decay (including on the isotope ^{119m}Sn) were examined in 1984–1998 (see, for example, Refs. 2–5).

2. A three-photon resonance is required for synchronization of the transition $2 \to 3$. Its cross section is always less than the cross section of the single-photon transition $2 \to 3$, equal to $\sigma_{23} \approx 10^{-58}\,\text{cm}^{-2}$ (taking account of the small width of the levels $\Gamma_2 \approx 10^{-7}$ eV, $\Gamma_3 \ll \Gamma_2$, and the large value of $\Delta E = 3E_{21} - E_{32} \approx 5.7\,\text{keV}$). The ineffectiveness of such synchronization is obvious. It is easy to determine the limit of the increase in τ_3. A distant screen can influence only the radiative (electromagnetic) decay channel of the level E_3 (its relative probability is $P_\gamma = 1/(1+\alpha_3)$) and it cannot affect the electron conversion. Even with complete suppression of the radiation channel τ_3 can change only by the amount $(\Delta\tau_3/\tau_3)_{\max} = P_\gamma = 2 \times 10^{-4}$. This is $10^3 - 10^4$ times less than the result declared in Ref. 1.

In my opinion the observed effect is not due to a change in τ_3 and could be due to the characteristic features of the process of detection of the radiation from high-activity sources ($Q_1 = 5$ Ci, $Q_2 = 2$ Ci). The number of excited nuclei N_1 and N_2 in the level 3 in

the sources 1 and 2 changes because of the spontaneous transition $3 \rightarrow 2$ according to the law

$$N_{1,2} = N_{01,02} \exp(-\lambda_3 t), \quad \lambda_3 \equiv (\ln 2)/\tau_3, \quad N_{01} \approx 3 \cdot 10^{18}, \quad N_{02} \approx 1.2 \cdot 10^{18}.$$

There are $N_{1,2}\tau_2/\tau_3$ nuclei in the level 2. This corresponds to source activities $Q_{1,2} = N_{1,2}\lambda_3/(1+\alpha_2)$. The number of photons from sources 1 and 2 detected by the detectors in time $\Delta t \ll \tau_3$ is $n_{1,2}(t) = \varepsilon Q_{1,2}[\Delta t - \delta t\, n_{1,2}(t)/g]$. It depends on the efficiency ε of the collimator and the detector, the resolution time δt in detecting a single photon, and the relative fraction g of the photons investigated with respect to all photons detected. The detection system is closed for the time $\delta t\, n_{1,2}(t)/g$. From the relation for $n_{1,2}(t)$ we find the equation

$$\log[n_1(t)/n_2(t)] \approx \log N_{01} - \log N_{02} - \Delta y,$$

$$\Delta y = [N_{01} - N_{02}] \exp(-\lambda_3 t) \varepsilon\, \delta t \lambda_3 / g(1+\alpha_2),$$

which is similar in form to the expression postulated in Ref. 1 assuming inhibited decay (in Ref. 1 $\Delta y = \lambda_3 t$). For sources with low or equal activity $n_1(t)/n_2(t) \approx N_{10}/N_{20}$, which corresponds to the same detected lifetime of both sources. The case $N_{10} > N_{20}$ corresponds to apparent inhibition of decay ($\Delta y > 0$, $\Delta\lambda_3 > 0$) of the more active source 1 with respect to the less active source. This is because the decrease of the photon flux from the high-activity source as a result of spontaneous decay is partially compensated by an increase in the photon detection efficiency. For typical parameters $\varepsilon \approx 10^{-2}$, $\delta t \approx 10^{-8}$ s, and $g \approx 0.03$ the apparent inhibition of decay $\Delta\tau_3/\tau_3 \approx \tau_3 \Delta y/t \approx 0.1$ is comparable to the result of Ref. 1. If the less active of the two sources had been investigated in Ref. 1 (and the control was the more active source), then speedup of the decay of the investigated source with respect to the control would have been ''detected.'' A large difference in the decay rates of the two sources was not detected in the additional experiment without a screen performed after six months.[1] This is due to the dropoff in the activity of both sources by this time.

*)e-mail: viv@vhome.kiev.ua

[1] S. K. Godovikov, JETP Lett. **68**, 629 (1998).
[2] V. I. Vysotskiĭ, V. I. Vorontsov, and R. N. Kuz'min, Pis'ma Zh. Tekh. Fiz. **10**, 300 (1984) [Sov. Tech. Phys. Lett. **10**, 126 (1984)].
[3] V. I. Vysotskii, A. A. Kornilova, R. N. Kuz'min *et al.*, in *International Conference ICAME-95*, Rimini, 1995, topic 13-19.
[4] V. I. Vysotskii, V. P. Bugrov, A. A. Kornilova *et al.*, Hyperfine Interact. **107**, 277 (1997).
[5] V. I. Vysotskii, Phys. Rev. C **58**, 337 (1998).

Translated by M. E. Alferieff

Inhibition of the radioactive decay of the isomer ^{119m}Sn

S. K. Godovikov
M. V. Lomonosov Moscow State University, 119899 Moscow, Russia

(Submitted 30 September 1999)
Pis'ma Zh. Éksp. Teor. Fiz. **70**, No. 9, 638 (10 November 1999)

[S0021-3640(99)01621-7]

PACS numbers: 23.20.−g

The remarks in Ref. 1, which attest to the author's interest in the results obtained in Ref. 2, unfortunately contain a number of misunderstandings and a fundamental error. These include the following:

1. In Ref. 2 there is a misprint in the nomination of the activities of the sources used, specifically, instead of 5 and 2 μCi, as in the original text, 5 and 2 Ci were given, i.e., a thousand times higher. This error does not occur in Refs. 3 and 4, which concern the same measurements. The author of Ref. 1 used incorrect values of the activities ($N_{01} \approx 3 \cdot 10^{18}$ corresponds to 5 Ci) and he also neglected the fact that a Pd filter,[3] which suppresses x-ray radiation (relative fraction $g \approx 1$), was used in the experiment. As a result, the parameter Δy from Ref. 1 must be decreased by at least four orders of magnitude ($\Delta y \approx 0$), which completely rules out the interpretation in terms of a ''high-activity source'' proposed by the author of Ref. 1 for the experiment.

2. At present, the criticism of the idea of dynamic synchronization of the oscillations of the nuclear levels can in no way be made quantitative, since the collective nucleon interaction processes in the field of resonant standing waves have not been worked out theoretically at all. For this reason, the qualitative interpretation in Refs. 2–4 is completely legitimate. Moreover, it should be noted that the experimental data given in Ref. 2 by no means uses the concept of a ''distant screen.'' This means that the estimate of the change in P_γ in Ref. 1 is invalid.

3. The claims of a priority nature are misunderstandings and have no relation to Ref. 2. This is due to the simple fact that in Ref. 2 the screen containing the stable nucleus ^{119}Sn($E_1 = 23.8$ keV) is in no way resonant, in the conventional sense of this word, for the 89.5 keV level, whose decay is being investigated. Moreover, there was no screen at all at the time of the measurements. This special and unique case has not been previously studied in the literature. The references presented in Ref. 1 refer to a somewhat different field of research, the declared achievements of which are far from being free of criticism.[5]

In conclusion, there exists a method for increasing sharply the effect of a screen on the decay of ^{119m}Sn. For this, the source must be surrounded by a screen in a 4π solid angle geometry, i.e., on all sides. Such an experiment with a 3 μCi source has been performed at the Scientific-Research Institute of Nuclear Physics at Moscow State Uni-

versity in 1999. As a result, it was found that $\Delta\lambda/\lambda = -(0.26 \pm 0.02)$, i.e., $T_{1/2} = 398 \pm 10$ days. In other words, the effect $\Delta\lambda/\lambda$ increased by more than a factor of 2, as expected.

[1] V. I. Vysotskiĭ, JETP Lett. **70** (1999), this issue.
[2] S. K. Godovikov, JETP Lett. **68**, 629 (1998).
[3] S. K. Godovikov, Laser Phys. **8**, 1100 (1998).
[4] S. K. Godovikov, Izv. Ross. Akad. Nauk, Ser. Fiz. **63**, 1396 (1999).
[5] A. V. Davydov, in *48th Conference on Nuclear Spectroscopy and Nuclear Structure* (1998).

Translated by M. E. Alferieff